NTNU
Norwegian University of
Science and Technology

Out of Plane Bending of Mooring Chains

Finite Element Analysis of a 7-link Model

Katarina Berthelsen

Marine Technology
Submission date: June 2017
Supervisor: Sigmund Kyrre Ås, IMT

Norwegian University of Science and Technology
Department of Marine Technology

Preface

The work with this thesis has been carried out at the Norwegian University of Science and Technology in Trondheim during the 2017 spring semester, and is part of a master's degree in the field of Marine Technology. The topic was chosen from gaining an interest in mooring systems after employment within Offshore Classification DNV GL summer 2016. This gave an insight in position mooring from a classification company's point of view and the topic for the thesis was later developed in collaboration with DNV GL. I would like to thank Erik Carlberg, Tomaz Kapella, and Dag-Børre Lillestøl with DNV GL for support and help throughout the semester.

The work with the thesis has been interesting and highlighted the importance of a well-functioning mooring system. The work process has been even and I managed to follow purposed schedule throughout the semester, although I might would have altered the plan in retrospect. Given the fact that I was rather inexperienced in ABAQUS CAE, building the model and running analysis took more time than I expected, even if warned, and the process was frustrating at times. If I could start the period over, I would have started modelling at the very beginning. Writing is easier for me and it would be more time efficient to write theory while waiting for completed analysis. However, the theoretic part was interesting and I learned a lot prior to making the non-linear FE-model. The thesis is written with an assumption that the reader has some foreknowledge within the field of marine, structural, or material engineering.

I would especially like to thank my supervisor Sigmund Kyrre Ås for support and help with the master's thesis work and for always keeping his office door open. I would also like to pass on my gratitude to Gro Maria Garborg from the Petroleum Safety Authorities for providing incident reports of mooring line failures in the period 2002-2014. In addition, I would like to thank the class of 2017 for support and great memories through five years at NTNU. Without that, this would simply not have been possible. At last, I want to thank my mother, Kjersti Myhre, for bringing back old FEM knowledge to join discussions and reading through the final report.

Trondheim, 07.06.2017

Katarina Berthelsen

Summary

This master's thesis is an investigation of out of plane bending (OPB) as a failure mode connected to the upper chain section of offshore mooring lines. A comprehensive literature study was done to present the OPB mechanism, findings from previous research, coverage of OPB within class rules and standards in the industry, as well as OPBs effect on offshore operations. For the latter purpose, eleven independent incident reports were reviewed where three listed OPB as main cause of line failure.

When offshore chain links are manufactured, a proof load representing 65 % to 80 % of minimum breaking load is applied to all links. This is done to prevent elongation during operation and creates a permanently deformed surface at the contact area between two adjacent links restricting interlink rotation, rolling, and sliding. Out of plane bending occurs when a chain link is bent out of its main plane because of resisted OPB-moments and transverse forces from link contact friction. If stresses are sufficient, crack propagation can occur at the first moving link leading to early failure. The interlink contact stiffness is studied by plotting the interlink angles between two adjacent links against the OPB moment appearing the link bent out of plane. In such plots, the three interlink motions can be identified. Sticking represents a linear increase of the OPB moment, whereas the moment remains constant when sliding motion has commenced. Rolling represents the increasingly nonlinear part of the curve. Investigation of out of plane bending is done by performing full-scale tests and supporting the results by FEA.

As offshore operations are moving further offshore, comprehensive mooring systems, larger chain links, higher pretensions, longer lines, and new operative environments are subsequently introduced. OPB is a failure mode that has received increased attention over the past decade, but the industry still suffers from gaps within scientific literature as well as safety standards.

The main part of the thesis was the development of an FE-model in ABAQUS CAE to investigate the OPB mechanism. The model was used to replicate full-scale tests recently done by DNV GL. These tests included seven chain links of R4 Ø = 175 mm, where chain links of this size have not been investigated previously. An OPB JIP completed in 2016 investigated R4 Ø 146 mm chain links and concluded with FEA being an effective method to study OPB and the interlink contact stiffness, but will continue to provide sub-conservative results. This conclusion was drawn from several sources of scatter

discovered in the result data. FE-software has difficulties reproducing the real conditions in the locking area, a factor dependent on friction and material properties as well as material hardening during loading and unloading of proof load. The interlink stiffness will further be dependent on if locking occurs within or outside the plastic mating area. The pretension in the line will also influence OPB, affecting the lines independently. This makes OPB a single line, single link problem for a mooring analysis.

The full-scale test results are confidential and DNV GL did their own comparison to validate obtained FEA results from the thesis. They concluded that the results were replicating the behavior of the chain during testing in a good way. The FE-model was further used in a parameter study, investigating the effect of friction coefficient (μ), operative tension (T), and proof loading (% of MBL). The sensitivity of the contact area was proven by a mesh convergence test, where a refinement of the element size at contact resulted in scatter of measured stress values, contact area size, and geometric deformation.

Obtained FEA results have proven that the model is behaving as expected when simulating submerged and dry conditions. The interlink stiffness curves are identical up until a certain angle, where the sliding threshold is reached more rapidly in water due to a lower friction coefficient. It was also proven that the operative pretension influenced the interlink stiffness, as an increase of tensile load lead to increased friction at the contact surface. By increasing the proof load, the length of the contact area at the link boundary was subsequently increased resulting in a stiffer interlink stiffness. An increase from 70 % to 73 % of MBL increased the interlink stiffness from 52 to 65.5 kNm per $^\circ$ angle at $+$ 0.5°. This represents a percentage increase of nearly 25 %.

OPB continues to be a complicated phenomenon in the maritime industry, related to difficulties when comparing results across geometries, size, material grade, manufactures, load, and boundary conditions. FEA is an effective tool to understand and investigate the influence of key parameters connected to the mooring systems, but will not provide conservative results yet. This conclusion also applies for the results obtained in the thesis due to simplifications and assumptions from modelling. An investigation of different parameter's influence is, however, useful as knowledge for future mooring analysis as well as for personnel operating the mooring systems offshore.

Sammendrag

Denne masteroppgaven er en utredelse av utmattingsfenomenet *out of plane bending* (OPB) tilknyttet fortøyningssystemer av offshoreenheter. Ved OPB blir kjettingløkken bøyd ut av plan som følge av friksjon mellom naboløkker og relativ bevegelse. Et litteraturstudie er gjort i sammenheng med oppgaven for å få en oppdatert status på OPB i den maritime industrien. Studiet inkluderte tidligere prosjekter, klassifiseringsregler og standarder, samt granskningsrapporter fra rapporterte hendelser hvor fortøyningslinen røk i de øverste kjekttingløkkene. OPB bør inkluderes i fortøyningsanalysene da brudd på fortøyningsliner utsetter liv og miljø for unødvendig risiko.

Ved produksjon av kjettingløkker blir hver løkke påført en testlast (proof load). Denne tilsvarer 65 - 80 % av maksimal strekkraft og etterlater en plastisk deformert kontaktflate som hindrer relativ kontaktbevegelse og rulling mellom naboløkker. OPB oppstår ofte ved innfestningspunktet til fortøyningsliner hvor den første frie løkken bøyes ut av plan ved et økende OPB moment fra friksjon i kontaktområdet. Hvis spenningene er høye nok, kan det føre til sprekkdannelse og tidlig brudd. Innvirkningen friksjon og krefter har på OPB studeres fra kontaktstivheten mellom to naboløkker. Kontaktstivheten finnes ved å plotte relativ vinkel mellom naboløkkene mot OPB momentet i løkken som bøyes ut av plan. De tre bevegelsene en løkke kan oppleve relativt til en naboløkke kan identifiseres ved slike plott; friksjonsheft, rulling og glidning. OPB mekanismen studeres ved fullskalatester og bekreftelse ved elementmetodeanalyse (FEA).

Ved å flytte offshore operasjoner lenger vekk fra kysten introduseres større kjettingløkker, høyere operasjonslast, lengre liner, kompliserte fortøyningssystemer og operasjoner i nye farvann. Oppmerksomheten rundt OPB har økt de siste ti årene, men industrien opplever fremdeles mangler når det gjelder vitenskapelig litteratur og standarder for klassifisering og sikkerhet.

Formålet med masteroppgaven var å utvikle en FE-modell i ABAQUS CAE som kunne brukes til å studere OPB. Modellen ble brukt til å reprodusere fullskalatester nylig gjennomført av DNV GL. Fullskalatestene inkluderte 7 løkker av stålgrad R4 Ø 175 mm, hvor løkker av denne størrelsesordenen ikke har blitt studert tidligere. En OPB JIP avsluttet i 2016 testet løkker av størrelse R4 Ø 146 mm og konkluderte med at FEA er et effektivt verktøy til å studere og forstå OPB og kontaktstivhet mellom løkkene, men vil fortsette å gi resultater som er underkonservative. Konklusjonen ble tatt på

bakgrunn av at det ble oppdaget mye spredning i resultatdata, da kontaktstivheten er avhengig om hefting skjer i eller utenfor det plastisk deformerte kontaktområdet. Elementmetode-programmer har vanskeligheter med å reprodusere virkelige egenskaper til materialer ved kontakt, noe som er avhengig av friksjon og plastisk herding av materialet under testlast. OPB vil også være avhengig av geometri og påført operasjonsstrekk, som gjør det til et fenomen avhengig av individuelle liner og løkker.

Kontaktstivheten fra FEA resultatene i masteroppgaven ble sammenlignet med resultater fra fullskalatestene av DNV GL. De konkluderte med at resultatene gjenskapte kjettingens oppførsel fra deres tester på en god måte. Modellen ble brukt videre i oppgaven til å teste effekten av friksjonskoeffisient (μ), operativ strekkraft (T) og test last (% av MBL). Sensitiviteten av kontaktområdet ble bekreftet ved konvergenstesting av elementstørrelse. Ved å endre elementstørrelsen i kontaktområdet resulterte det i en synlig endring av målt spenningsverdi i kontaktpunktet.

Oppgavens FEA resultater bekreftet at simuleringen av kjettingens oppførsel i vann og luft var som forventet. Kontaktstivhetene er identiske før kjettingbevegelsen for rulling og gliding starter ved en lavere vinkel for vann, grunnet en lavere friksjonskoeffisient. Det ble og bekreftet at en økning i operativ strekkraft gir en høyere kontaktstivhet, grunnet høyere friksjonskraft i kontaktområdet. Ved å øke testlasten blir det dannet et større deformert kontaktområde, som igjen resulterer i en stivere kontaktstivhet. En økning av testlast fra 70 % til 73 % av MBL økte kontaktstivheten fra 52 til 65.5 kNm/grad vinkel ved + 0.5 °. Dette er en prosentvis økning på nesten 25 %.

Som en konklusjon fra denne masteroppgaven vil OPB fortsette å være et komplisert fenomen i den maritime industrien. Grunnet manglende vitenskapelig dokumentasjon oppleves også vanskeligheter tilknyttet sammenligning av resultater på tvers av geometri, størrelse, materialgrad, produsent, last og grensebetingelser. FEA vil være et effektivt verktøy for forståelse og kan brukes for å teste endring av relevante operative parametere i systemet, men vil fortsette å gi underkonservative resultater. Dette gjelder også resultater fra oppgaven, grunnet forenklinger og antagelser tatt under modelleringen og beregning av kontaktstivhet. Det er derimot viktig at innvirkningen av ulike operasjonsparametere blir undersøkt, både for fremtidige fortøyningsanalyser og for de som opererer systemet offshore.

Contents

List of Figures

List of Tables

List of Abbreviations

ALLAE	Artificial Strain Energy
ALLIE	Internal Energy
ALLSD	Viscous Damping Energy
API	American Petroleum Institute
APL	Advanced Production and Loading
BC	Boundary Condition
BOMEL	Billington Osbourne-Moss Engineering Limited
BV	Bureau Veritas
CAE	Computer Aided Engineering
CBL	Chain Break Load
COV	Coefficient of Variation
DFF	Design Fatigue Factor
DNV GL	Det Norske Veritas - Germanischer Lloyd
FEA	Finite Element Analysis
FEM	Finite Element Modelling
FPSO	Floating Production and Storage and Offloading Unit
FSO	Floating Storage and Offloading Unit
GVI	General Visual Inspection
HAC	Hydrogen Assisted Cracking
ISO	The International Organization of Standardization
IPB	In Plane Bending
JIP	Joint Industry Projects
LF	Low-frequency
MBL	Minimum Break Load
MIC	Microbiological Influenced Corrosion
MIM	Mooring Integrity Management

MOU	Moving Offshore Unit
MPI	Magnetic Particle Inspection
NDT	Non-Destructive Testing
NMA	Norwegian Maritime Authorization, Sjøfartsdirektoratet
NORSOK	Norsk Sokkels Konkurranseposisjon
OLL	Oil Offloading Line
OPB	Out of plane bending
OSV	Offshore Supply Vessel
PL	Proof Load
PTIL	Petroleumstilsynet
PSA	Petroleum Safety Authorities
PSV	Platform Supply Vessel
ROV	Remotely Operated Vehicle
RP	Recommended Practice
SBM	Single Buoy Mooring
SCF	Stress Concentration Factor
SF	Safety Factor
SMYS	Specified Minimum Yield Strength
SPM	Single Point Mooring
STP	Submerged Turret Production
S33	Stress in tensile direction
T	Tension
TT	Tension-Tension
UTS	Ultimate Tensile Stress
WF	Wave-frequency
Ø	Nominal Diameter

Nomenclature

α	Interlink Angle
β	Angle
γ	Angle at Fairlead (BV)
δ	Shape Factor (BV)
d	Diameter
E	Elastic Modulus
ϵ	Strain
ϵ_{eng}	Engineering Strain
ϵ_{true}	True Strain
ϵ_P	Plastic Strain
H	Hardening Function
Hs	Significant Wave Height
L_d	Design Life
M_{OPB}	OPB Moment
μ	Friction Coefficient
σ	Stress
σ_{eng}	Engineering Stress
σ_{OPB}	Out of Plane Bending Stress
σ_P	Proportionality stress level
r	Radius
σ_{true}	True Stress
Tp	Peak Period

Chapter 1

Introduction

1.1 Mooring Integrity

To ensure safety at sea there are two major requirements that should be met at all times. The floating unit should remain floating, and a position moored unit should not move from its operating position regardless of weather, sea motion, and unexpected events. Any unintentional movement away from planned position exposes a potential threat to the crew, environment, adjacent units, and connection to wells and sub-sea equipment.

A position moored unit, typically an FPSO (Floating Production, Storage, and Offloading Unit), FSO (Floating Storage and Offloading Unit), flotel, or semi-submersible, have complex mooring systems. The system can be spread mooring, single point mooring such as turrets, or innovative designs used in more shallow waters e.g. a YOKE system. Spread and turret mooring systems can include from six to 24 mooring lines. The lines can be composed of chain links only or consist of a configuration of chain links, shackles, sockets, wire rope, and polyester rope. A mooring link can have a studless or stud geometry as illustrated in Figure 1.1.

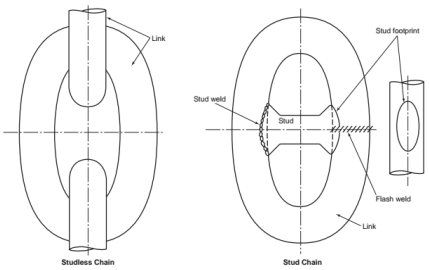

Figure 1.1: Studless and stud geometry configuration of chain links (API, 2015)

An offshore mooring line is usually designed for tension loads only as the exposed area is too small to experience forces from currents and waves directly. However, wave frequency induced loads apply cyclic motions and this can lead to fatigue damage of the lines. Fatigue and abrasion of the material can increase stresses in the material and reduce the overall component strength. This can lead to further crack growth and corrosion

in a marine environment, especially when operating in the slash zone, known to be a corrosion-aggressive area.

Authorities and classification companies around the world attempt to make the offshore industry safe and sustainable for personnel and environment. Keeping mooring integrity is essential for floating units as unintended incidents can have fatal consequences. A production field is a comprehensive cluster of production units, storing units, flotels, trafficking supply vessels, as well as expensive and complicated sub-sea installations where a position deviation can result in collision, failure of the drilling riser, and loss of the well.

Standards, recommended practices, and classification rules are frequently used within the industry. They are developed by world-wide classification companies such as DNV GL and Bureau Veritas, authorities of different countries like the Norwegian Maritime Authorities (NMA) and the Petroleum Safety Authorities (PSA) in Norway, and the American Petroleum Institute (API). The International Organization of Standardization (ISO) has standards for petroleum and natural gas industries and NORSOK has developed standards for the Norwegian continental shelf. To further collaboration and distribution of knowledge, Joint Industry Projects (JIP) around the world also addresses the issue of mooring line failures.

Following recommended practice, standards, and rules is the first step to ensure safe operations. When the system is in operation, inspection and maintenance should be in focus to prevent failures occurring, evaluating remaining life of the line, and give life extension. A functioning detection and alarm system is necessary as failure of a line should be discovered immediately. An acceptable and precise maintenance plan can relieve links of stress and loads by rotation of the links in contact with fairlead and chain stoppers (Akers, 2014).

Although the unit is moored to a fixed position there will be some relative motion between the lines and vessel introducing bending modes and other loads in the top chain section. To date, there are many uncertainties connected to inspections as well as current standard and recommended practice regarding out of plane bending and the impact corrosion plays on fatigue and lifetime of the mooring lines (Akers, 2014).

Mooring systems have existed for many years and are now tested in harsher environments and deeper waters. As no system or engineer can be prepared for every possible event, it is important to further distribution of knowledge and collaboration to limit mooring line failures. This applies to all aspects of the industry, from material properties, load predictions, finite element approaches, inspection, and maintenance.

1.2 Objectives and Thesis Structure

This master's thesis is a study investigating out of plane bending (OPB) of chain links in relation to fatigue calculations for offshore mooring lines. OPB has received increased attention as a failure mode over the past decade, but there is still a gap within existing scientific literature on how to address the problem. Failures of the upper section of a mooring line have occurred in spite of adherence to current DNV GL and API standards. These failures are extremely costly since production may have to be shut down. If spare chain is unavailable, mooring integrity may take several months to restore, involving costly replacement campaigns and a risk of damaging adjacent lines during the marine operations. A Guidance Note published by Bureau Veritas in 2014 attempt to address OPB, but is much dependent on a definition of a range of parameters.

Main objectives for the master's thesis is to develop a 7-Link FE-model in ABAQUS CAE. The model will be used to simulate and reproduce full-scale tests recently done by DNV GL. The FE-model is further to be used for a parameter study to investigate case-dependent parameter's influence on out of plane bending of the chain links. Obtained FEA results will be verified, discussed, and compared on background of previous projects and research studying OPB.

Part one of this thesis is a literature study with the purpose of documenting findings from previous tests and studies, in addition to getting an overview regarding class rules and standards set to cover OPB within the industry.

A Joint Industry Project (JIP) was completed in 2016 with OPB in focus. In addition to the main results from this JIP, MARINTEK performed an investigation on large sized chain links in 2014, highlighting the effect of pretension in the mooring lines. Both projects are relevant as the links used in DNV GL's full-scale tests are larger than what existing literature covers. The gathering of information serves as a good introduction to why it is interesting to perform an FE-analysis of the 7-link model in ABAQUS CAE for larger chain dimensions, serving as the second part of this thesis. A general script will also be developed in Python with the purpose of creating a simple script-based model where link diameter, applied loads, and operative environment are changeable parameters.

1.3 Method

The theory behind the master's thesis is gathered from literature search within NTNU's database Oria, suitable web pages, and relevant classification rules and standards available for the maritime industry. Information included in the thesis is carefully evaluated and considered before used. For a quality evaluation of found references, the following criteria were applied:

- Credibility
- Objectivity
- Preciseness
- Suitability (NTNU, 2010)

To meet the above stated criteria the credibility of the author is important, and sources of information is evaluated in terms of who wrote it, where, when, and why the source was published.

The FE-model in ABAQUS is built on the background of methods learned and practiced through the module course TMR4305 Advanced Static Analysis at NTNU fall 2016 and represents the full-scale test set-up. Result data is post-processes in Excel and MATLAB for presentation.

Chapter 2

Literature Study

2.1 Failure of the Upper Chain Section

Failure of a mooring line is seldom the result of a single event. It is caused by smaller, but significant factors applying stress to the system over time listing overload as the final failure mode. Today's current classification rules, standards, and recommended practice contribute to guarantee safe operations for systems and components. However, lines still break, and this due to operational and environmental factors as well as weaknesses in the material. Eleven incident reports where failure occurred in the top chain section are reviewed in relation to the thesis work. These are failures occurring from 2002-2014, and the reports were provided by The Petroleum Safety Authorities (PSA) in Norway. Investigations were performed by owner, manager, and sometimes the operator (Kvitrud A. for PSA, 2014). The following sections give a brief introduction to common failure modes of the upper chain section.

2.1.1 Interlink wear

Fatigue, corrosion, and mechanical issues are in general the reason for mooring line failures, while there are no design rules separating between interlink wear and corrosion (Yaghin and Melchers, 2015). Mooring lines are not equipped with cathodic protection and design is built on a sacrificial corrosion allowance. Lifetime is predicted from a uniform corrosion rate to foresee how the line strength is degrading. Corrosion of steel in water is further dependent on many factors such as temperature, water velocity, salinity, and surface roughness of the material.

Models used to predict corrosion rates does not include effects from abrasion or wear on the system induced by dynamics. It is therefore likely to believe that there will be greater material loss in the interlink zone than accounted for. Regular waves can generate repetitive wear to the system compared to an exposure to harsh environments. Corrosion can also be accelerated by microbiological influenced corrosion (MIC), requiring sufficient

availability of the critical nutrients for microbiological activity. To merge the discussed failure modes, hypothesis states that periodic wear in the interlink zones can trigger MIC at the edges of the contact area (Yaghin and Melchers, 2015).

2.1.2 Corrosion fatigue

From a perspective of safety as well as economics, corrosion is undesirable in operating life due to structural integrity and appearance of a unit. Corrosion can be prevented by selecting resistant material and applying correct surface protection, but this will not prevent components from fatigue damage. Cracks appearing from corrosion pits can further lead to sudden failure. A corrosive environment affects the fatigue life by creating a possibility for crack initiation at very low stress cycles, illustrated by SN-curves. When fatigue is occurring in a corrosive environment it is defined as *corrosion fatigue* (Schijve, 2009).

Another type of corrosion is *stress corrosion*. This is defined as crack initiation under repeated load and residual stress. Stress corrosion can be prevented in many technical developed materials, while fatigue corrosion can occur in most materials. It is important to distinguish between corrosion fatigue and fatigue of corroded materials. Corrosion fatigue is caused by a joint action of fatigue and corrosion interacting together. Both crack growth and crack initiation is affected by the operating environment. Crack initiation often occurs when a surface is damaged by corrosion, and the environment works as an accelerator for further crack growth (Schijve, 2009).

Corrosion fatigue is a time dependent phenomenon and thus related to the load history. If a crack has appeared, the liquid environment will enter the crack and wave loads attack like cyclic stress. The crack will then react like a pump, drawing the environment further into the crack opening and material, enhancing its growth. As a complex phenomenon, corrosion fatigue is the result of different variables within the material and environment, affecting fatigue limit, fatigue life, and crack growth. The area of origin is small and early observation extremely difficult. In a liquid environment, corrosion fatigue is usually seen as a reduction of the fatigue limit where damage from corrosion has entered from first part of fatigue life and contributes to further crack growth (Schijve, 2009).

Another concern related to corrosion is using mooring chains of high strength steel, leading to hydrogen embrittlement or hydrogen assisted cracking (HAC). This mode is mentioned as a possible cause of failure for the incidents regarding Transocean Spitsbergen in 2012 (Groven, 2012) and Deepsea Bergen in 2014 (DNV GL, 2014). HAC can lead to failure without warning as the crack growth is discontinuous. By the diffusion of

hydrogen into the metal, steels become brittle, and the hydrogen source can come from either self-corrosion or cathodic protection. Hydrogen atoms diffusing into the metal form molecules and increases the pressure within the material. As pressure increases, ductility and tensile strength of the metal is reduced leading to cracks opening and hydrogen-induced cracking (Solnørdal et al., 2009).

Fast fatigue crack growth in liquids can be explained by anodic dissolution at the crack tip or hydrogen embrittlement (Schijve, 2009). A plastic deformation of the crack tip can make the zone more anodic and thus more sensitive to corrosion. In salt water, the Cl-ions might weaken the strength of the material, whereas a weakened material an be the result of absorbed hydrogen form local surface corrosion. Increasing temperatures can increase the corrosive mechanism, and wave shape and load frequency might have an impact.

When corrosion is present, the surface is damaged and notches have appeared in the material. Even though the zone of the corrosion is small, pits are associated with high stress concentrations. Cracks appearing due to corrosion cannot always be avoided which makes awareness regarding its affect important. Applying safety factors and conservatism with respect to loads and environmental factors is essential when carrying out realistic crack growth predictions (Schijve, 2009).

2.1.3 Maintenance, Inspection, and Alarm Systems

Mooring lines are constantly in motion and should be considered as vulnerable primary structural components, classified as a category 1 safety critical system. If one mooring line were to fail, the possibility of multiple line failure is not that small as a mooring line in general have limited reserve capacity. This can lead to a consequential effect making the system "un-zip" itself when remaining lines fail due to overload. A JIP by Noble Denton addresses most failure modes connected to offshore mooring systems (Noble Denton, 2006).

Although this JIP was completed in 2006, and numbers may have improved, awareness was made concerning the alarm systems. Many FPSOs are unable to monitor the lines and thus not able to tell if a line has failed. In 2006, 78 % of the FPSOs included in the research did not have failure alarms and 50 % were unable to adjust the line length making inspection of the critical links difficult (Noble Denton, 2006). If a rotation is possible, it is achieved by ensuing a maintenance plan, either yearly or monthly. The maintenance plan is another area of concern, where there have been reported incidents where a plan was not ensued, listed as a possible contributor to final failure of the line (Kvitrud A.

for PSA, 2014). One example is the NORNE FPSO chain failure in 2012. The winch connected to the line was broken and the operating pretension had been wrongly adjusted for some time, potentially increasing the stress on the failed link (Statoil, 2013).

Inspections of in water of the upper chain sections can be done by ROV or divers, although submerged systems often are difficult to inspect because of marine growth coverage. Marine growth can be removed by the ROV, but this can also function as a corrosion accelerator as it leaves the steel directly exposed to salt water (Noble Denton, 2006).

2.1.4 Combined Tension and Bending Loads

Although failure modes are not always clear and assumptions often drawn from reviewing surrounding conditions, three of eleven reviewed incidents list out of plane bending as main cause of failure. This is the Girassol Buoy located outside the Angolan shore in 2002 (Jean et al., 2005) and Norne FPSO (Statoil, 2013) and Petrojarl Varg (Teekay Petrojarl, 2013) on the Norwegian continental shelf, both in 2012.

Out of plane bending was addressed as a failure mode in the 1990's in a JIP conducted by BOMEL (Billington Osborne-Moss Engineering Limited). Their study included tests of a five-pocket fairlead wheel to see the influence of tension and bending effects from gypsy wheel contact during operation, and its effect on mooring line fatigue. Even though standards, rules, and recommended practice have tried to address the issue of out of plane bending, fatigue calculations often only include tensile loads (Noble Denton, 2006).

OPB is a phenomenon where the chain link is bent out of its main plane, and occurs from resisted OPB moments and link contact friction under pretensions greater than 15% of the mean breaking load ratio (Vargas and Jean, 2005). If stresses are sufficient, crack propagation can occur at the first moving link. Figure 2.1 illustrates the OPB mechanism.

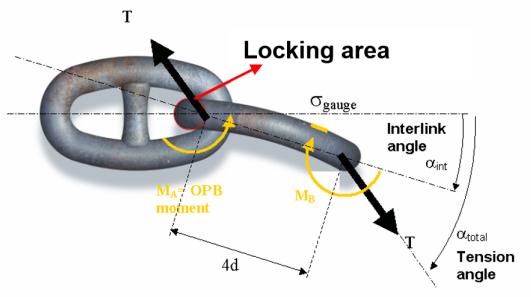

Figure 2.1: Out of Plane Bending mode of chain link (Jean et al., 2005)

2.1.5 Investigations of OPB after the Girassol Incident

After the Girassol incident in 2002, it was evident how great damage OPB could do in a short operating period. Three of a total of nine lines experienced failure at the same link after only eight months of service, for a system designed for a fatigue life of 20 years with a safety factor of 3.0 (Jean et al., 2005). The motions occurring for the off-loading buoy gave rise to interlink rotations which had previously been neglected. Combined with chain tension, large bending stress appeared in the link. The interlink rotations that can appear are defined as rolling, sliding and locking;

- Rolling: The link experiencing OPB is rolling inside the adjacent link. The rolling motion will continue until the tangential force balancing the tension load is exceeded by the friction force. When this happens the motion transfers to sliding. Rolling causes low OPB stresses.
- Locking: Due to high friction on the mating surfaces, the links appear to be locked static together. This condition continues until the moment from friction is lower than the applied moment, transferring into the sliding mechanism. These OPB stresses are high.
- Sliding: As the name implies, the bending link slides on the inside of the adjacent link. This mechanism can be developed by rolling or locking, which gives rise to respectively low and high OPB stresses (Vargas and Jean, 2005).

Calculations of stress caused by OPB is approximated by the following procedure for different interlink modes (Vargas, 2005). The dimensional properties for adjacent links are illustrated in Figure 2.2.

Rolling:

$$\alpha_0 = \beta\left(\frac{r_i}{r_0 - r_i}\right) \tag{2.1}$$

$$M_{OPB} = r_i(cos\beta sin\alpha_0 + cos\alpha_0 sin\beta)T \tag{2.2}$$

$$\sigma_{OPB} = M_{OPB}\frac{r_i}{I} \tag{2.3}$$

Sliding:

$$M_{OPB} = r_i \mu_{friction} T \tag{2.4}$$

$$\sigma_{OPB} = M_{OPB}\frac{r_i}{I} \tag{2.5}$$

Locking:

$$\sigma_{OPB} = kT^{0.75}(2r_i)^{-1}\beta \tag{2.6}$$

This in an empirical equation, where k is an empirical constant (Vargas, 2005).

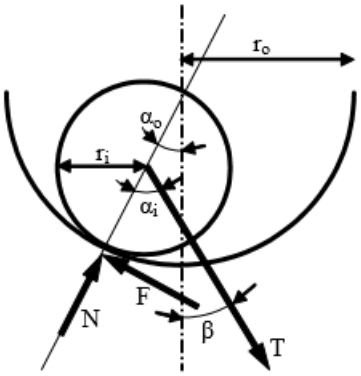

Figure 2.2: Dimensions for calculating OPB (Vargas and Jean, 2005)

Table 2.1: Approximation to calculate OPB moments (Vargas and Jean, 2005)

α_0	Angle
α_i	Angle
β	Interlink angle
r_0	Radius
r_i	Radius
M_{OPB}	Out of plane bending moment
T	Applied tension
$\mu_{friction}$	Coulomb friction coefficient
I	Moment of inertia
k	Empirical constant
σ_{OPB}	Out of plane bending stress

Crack growth from OPB

To make predictions of the applied loads, fatigue load is calculated from tension cycles. This includes low 2^{nd} order frequency motions and 1^{st} order wave frequency motions. The magnitude of these cycles will be dependent on the mean tension in the line, which is dependent on operative pretension and environmental loads affecting the system. The Miner-Palmgren procedure is used to calculate fatigue damage. Cracks appearing on a chain link are assumed to grow from the surface with a semi-elliptic shape. Using linear fracture mechanics and the two dimensional form of the Paris-Erdogan equation, crack growth can be modelled by Equation (2.7), where a is the crack depth, N number of applied tension cycles, m and C material parameters, and ΔK_A applied intensity range (Mathisen and Larsen, 2004).

$$\frac{da}{dN} = C(\Delta K_A)^m \tag{2.7}$$

Predicting when the link will fail is determined from critical crack depth a. This depth will lead to a rupture when the tension in the line is of the magnitude corresponding to a return period of 1 year, a value known from the mooring analysis. To find the critical crack length, level 2A failure assessment diagram from BS7910 is used. Fracture toughness is found from details from production by performing a Charpy V impact test (Mathisen and Larsen, 2004). FEA can be used to find the local stresses in a studless link

appearing from tension loads. Figure 2.3 illustrates where cracks are known to appear under tension load and out of plane bending.

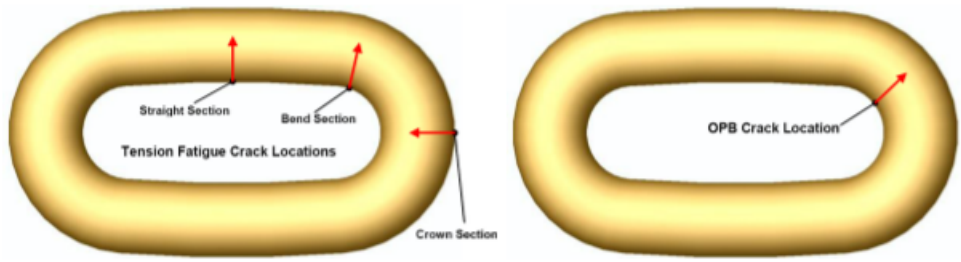

Figure 2.3: Location of cracks from tension and bending loads (Rampi et al., 2015)

Finite Element Analysis of OPB

The tension loads affecting mooring systems are usually low enough that adjacent links can rotate, roll and slide relatively to each other to account for dynamics. During manufacturing, the mooring links are tested by applying a proof load to all links. This load has a magnitude of 65 % to 80 % of the breaking load and will leave a permanently deformed surface area at the contact area between two adjacent links. The elliptically shaped contact area of size $\frac{D}{4}$ is proven by finite element analysis (FEA). When this surface is formed, the rolling motion is restricted and if a rotating motion is applied, the link will bend out of plane. Such bending moments appear every wave cycle and introduce cracks in the link until it fails (Jean et al., 2005).

Out of plane bending is examined through FEA. Different modes of the interlink rotations are investigated in addition to the proof loading. By using FEA, the hotspot location for OPB stress can be found in the bend part of the link, 45 ° from the main plane. The location of the OPB hotspot is illustrated in Figure 2.4, a result from the paper *"Failure of Chains by Bending on Deepwater Mooring Systems"* (Jean et al., 2005) investigating the Girassol 2002 incident. The found location is not identical to the tension stress hotspot, which makes it possible to distinguish cracks propagating from tension or pure bending.

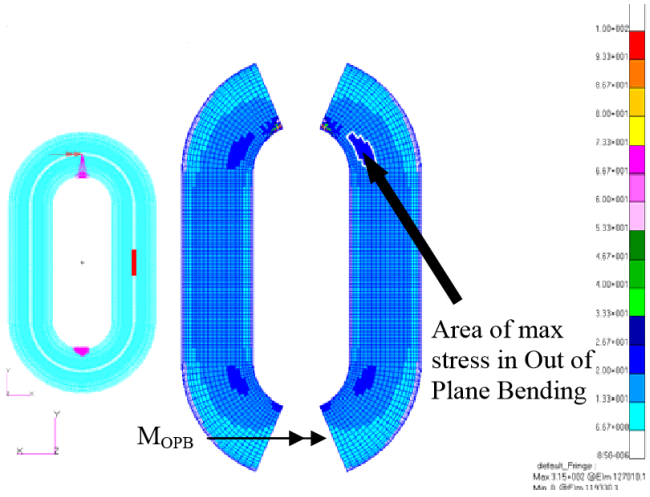

Figure 2.4: FEA location of hot spot stress in pure bending (Jean et al., 2005)

To investigate out of plane bending by FEA, one approach has been to use a *Three link FEA model* in ABAQUS. For this model, three types of contact are considered. Link-to-link contact, link to connector links contact, and rig-shoe contact. The contact surfaces should represent the correct surface conditions and coulomb friction. For the nonlinear material, a Ramberg-Osgood stress-strain curve was developed in the study by Pedro M. Vargas and Philippe Jean in 2005. The properties of the chain links were Vicinay R4 Ø 124 mm; SMYS = 580 MPa and UTS = 860 MPa. Isotropic hardening and a Von-Mises Yield material model was used for the analysis. A model of the *three link model* is shown in Figure 2.5, presented in the conference paper *"FEA of out-of-plane fatigue mechanism of chain links"* (Vargas and Jean, 2005).

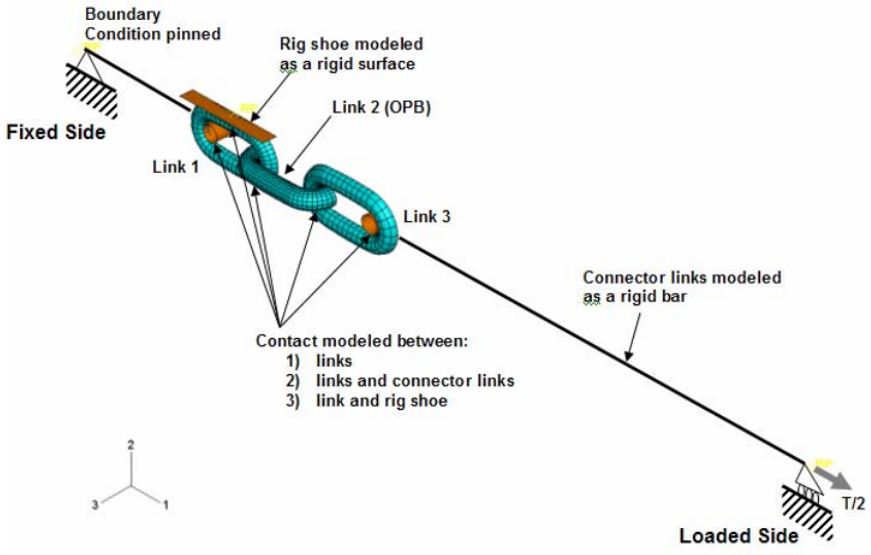

Figure 2.5: Three link model (Vargas and Jean, 2005)

A comparison of experimental results and FEA results for non-linear cases was included in the results from the above-mentioned conference paper. They represent modelling of the adjacent links with rolling motion in Figure 2.6, and locking motion in Figure 2.7. As illustrated, FEA stresses are lower than measured experimental stresses when interlink interaction is assumed to be of rolling mode. When the interaction is modelled as locking, stresses are similar for FEA and experimental results.

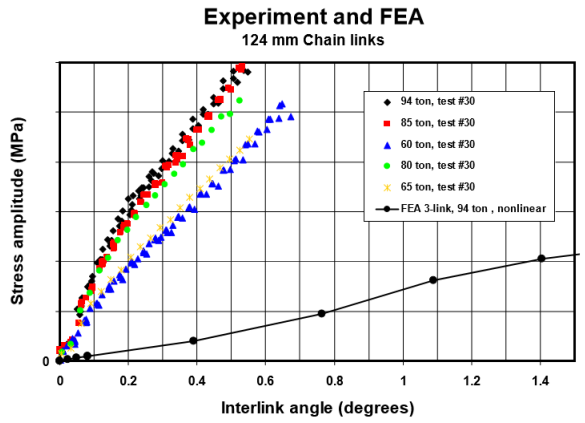

Figure 2.6: Three link model with Nonlinear material model. Interlink interaction: Rolling (Vargas and Jean, 2005)

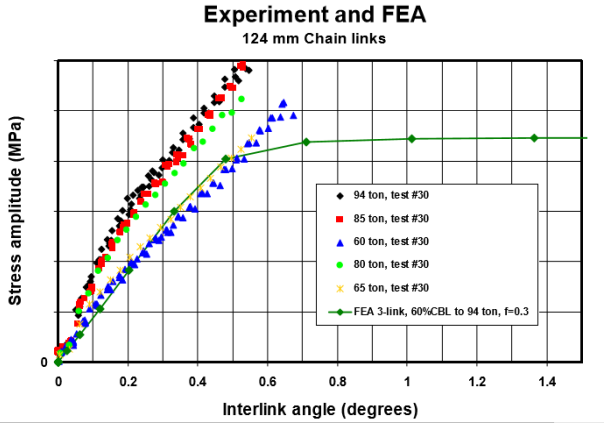

Figure 2.7: Three link model with Nonlinear material model. Interlink interaction: Locking (Vargas and Jean, 2005)

The difference between the two test results in Figure 2.6 and Figure 2.7 is the interlink interaction motion. When it is modelled as locking in Figure 2.7, the link has been applied an initial pre-load representing 60 % of CBL (Chain break load). This creates the mating surface allowing the links to appear as locked together generating high OPB stresses. The difference of residual stress at contact with and without an 80 % proof load is illustrated by Figure 2.8 (Vargas and Jean, 2005).

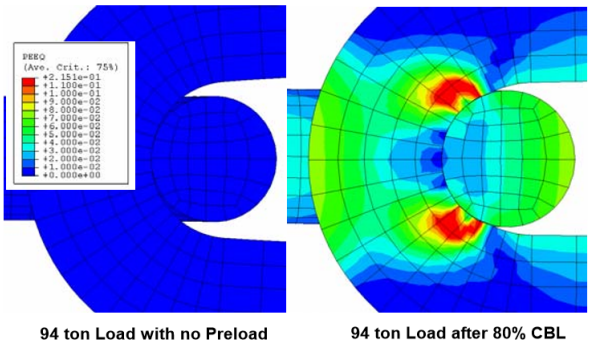

Figure 2.8: Plastic strains and interlink contact intimacy for no-Preload vs. 80 % CBL Preload (Vargas and Jean, 2005)

2.2 Chain Manufacturing and Operational Parameters

2.2.1 Residual Stresses in the Contact Area

Link size and steel grade are key parameters when choosing links for a mooring line design. Traditionally, the locations considered critical for fatigue of a chain link are found at the crown and the K_T point as illustrated in Figure 2.9. K_T is defined as the point where the straight and bend part meet. These regions are known for high stress ratios, indicating the difference between the local and nominal stress level (Bastid and Smith, 2013).

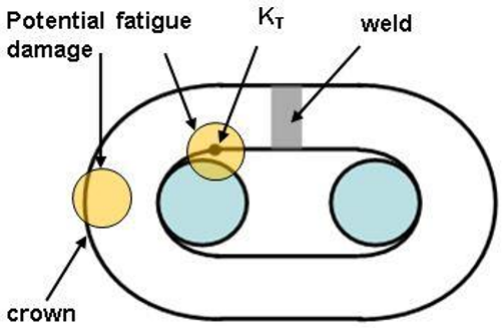

Figure 2.9: Regions where high stress ranges can cause fatigue damage (Bastid and Smith, 2013)

For studless links, the proof load corresponds to 70 % of MBL and is thus dependent on the link geometry and material. Proof load is applied to make sure the link does not elongate and safely sustain applied service loads. When a load of significant magnitude is applied, it causes yield and a shakedown that prevents elongation by ratchetting under cyclic loads. Tests have previously shown that the proof load improves resistance against fatigue damage, but that it also generates very high residual stresses in the interlink contact zone. Fatigue damage in this area is not covered by current standards, even if occurring from pure tension (Bastid and Smith, 2013).

The reviewed paper *"Numerical Analysis of Contact Stresses Between Mooring Chain Links and Potential Consequences for Fatigue Damage"* by Bastid and Smith (2013), performs a numerical investigation of the interlink zone. This was done with an idealized geometry of the links, as they were considered to be perfect cylinders. In reality, link geometry will be deformed when proof load is applied due to plastic deformation. The model used for their research is illustrated by Figure 2.10.

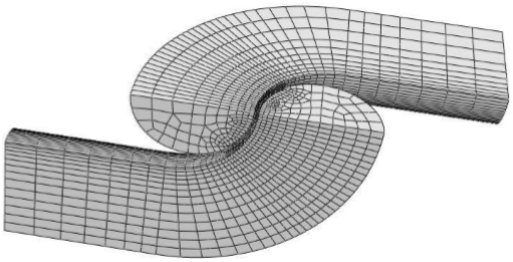

Figure 2.10: Geometry and mesh of the model (Bastid and Smith, 2013)

The steel grades investigated were R3S, R4, and R5, where R3S and R4 are frequently used for offshore mooring systems. The model material was elastic-plastic with linear isotropic hardening. The links were further subjected to a 70 % proof load, 20 % cyclic load, and 10 % static load, mainly arising from the chain's own dead weight, percentage taken from MBL. The friction contact coefficient was set to $\mu = 0.4$ (Bastid and Smith, 2013).

Although the investigation included different grades and link sizes, results showed a similar trend. The figures further included represents the results for an R4 Ø 124 mm link. As seen from Figure 2.11 the residual stress is compressive at the K_T point **(1)** and at the crown **(2)** in Figure 2.12, which has been proven to be beneficial to withstand fatigue loading in critical areas (Bastid and Smith, 2013).

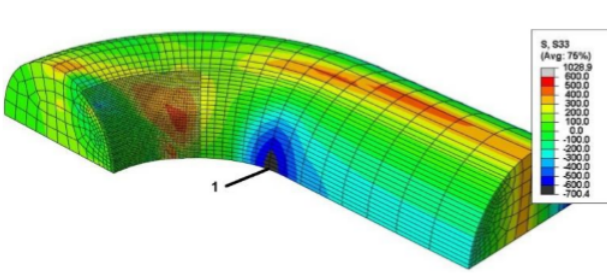

Figure 2.11: Unload from the proof load in K_T point (Bastid and Smith, 2013)

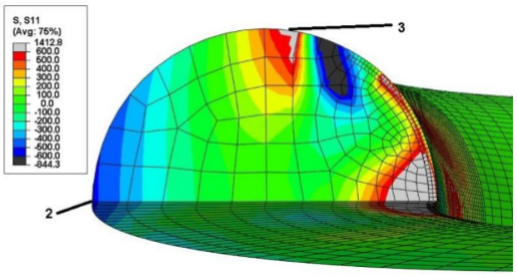

Figure 2.12: Unload from the proof load crown points (Bastid and Smith, 2013)

However, Figure 2.13 illustrates high and tensile stresses in the interlink contact zones, marked **(4)** and **(5)**. If a defect were to appear in these regions, the crack would be drawn open for the following load cycles. This local stress could possibly lead to crack propagation and impose a risk of further fatigue damage (Bastid and Smith, 2013).

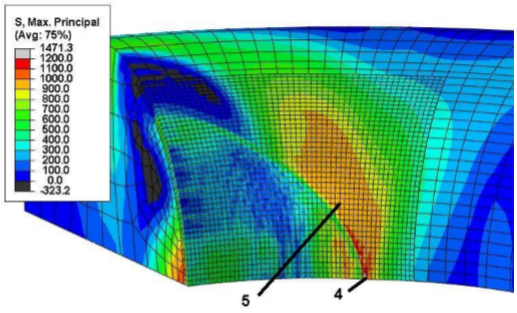

Figure 2.13: Unload from proof load interlink contact zone (Bastid and Smith, 2013)

While the plot contours in Figure 2.11 - 2.13 illustrated the stress state after proof load, Figure 2.14 and 2.15 illustrates the stress state after tensile operational loading. The residual stress after proof load remains, and the figures indicate a continuation of tensile stresses in the edge of the contact zone. It is worth mentioning that for many FEA tests, links are assumed to be stress free before subjected to a proof load. In reality, the links have had numerous manufacturing stages during production such as heat treatments, quenching, bending, and shot peening (Bastid and Smith, 2013).

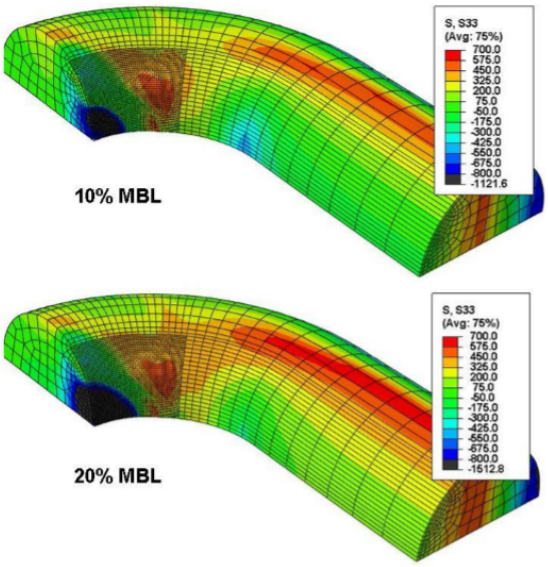

Figure 2.14: Axial load in K_T point (Bastid and Smith, 2013)

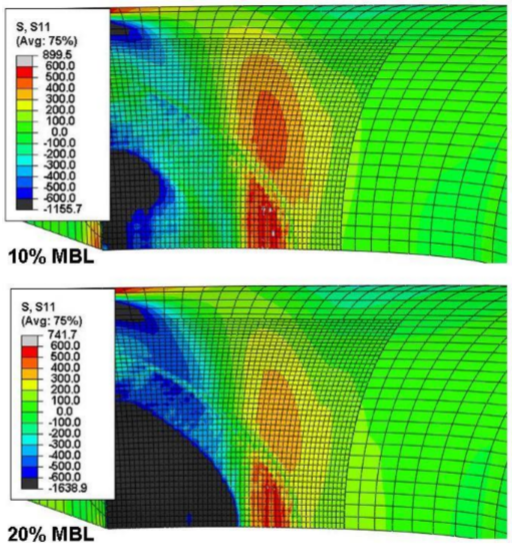

Figure 2.15: Stress in X-direction in contact zone edge (Bastid and Smith, 2013)

Applying proof load results in a variety of remaining compressive and tensile stresses in the critical regions of a chain link. For some locations, those feared to experience fatigue damage, the stress is compressive and hence beneficial. For the interlink contact zones, an area of interest when it comes to OPB, the residual stress is tensile and thus a threat for further crack propagation. This was proven to be one cause of the Girassol accident

in 2002. Illustrated by Figure 2.16 is the deformed geometry of the mating area from one of the failed links. Failure location is seen in Figure 2.17, corresponding to the edge of the contact zone and not the critical K_T point.

Figure 2.16: Contact zone of the Girassol link (Jean et al., 2005)

Figure 2.17: Link failure on a deep water buoy due to OPB (Rampi, Dewi, Francois, Gerthoffert and Vargas, 2016)

Another interesting finding from the paper by Bastid and Smith in 2013, is how stress measured at the edge of the contact zone increases with increased chain sizes. The links of steel grade R5, representing the largest links used in the industry, are not frequently used and existing fatigue curves and standards may be non-conservative for this purpose. For lower service loads, the interlink edge zone will be the most critical location for cracking of larger chains. If the tensile service stress is high and exceeding the compressive stresses in the crown or K_T point, these areas will be the locations first exposed to fatigue cracking (Bastid and Smith, 2013).

2.2.2 Effect of Pretension

MARINTEK Experiments on Large Chain Links 2014

Research done by MARINTEK (now SINTEF Ocean) in 2014 investigates and proposes a fatigue design methodology for large mooring chains subjected to out of plane bending (Lassen et al., 2014). The investigation included testing of high strength R5 steel links with diameter Ø 165 mm. Such links have a predicted service life of 30 years with a Design Fatigue Factor (DFF) equal to 10.0. Full-scale testing was done to test different hang off configurations, and they concluded that having a chain connected to a longer stopper arm with bearing had a better response regarding stresses arising from OPB. This compared to having a direct connection with the chain to the fairlead. The tests were done with varying pretension and Figure 2.18 illustrates how the strain is increased when the pretension T is increased. By altering the tension from 1500 kN to 2000 kN, the strain increased with 81% and if the pretension increases, as will the friction and sliding threshold. The bending moment can thus continue to increase for a longer period applying higher stress to the links of interest (Lassen et al., 2014).

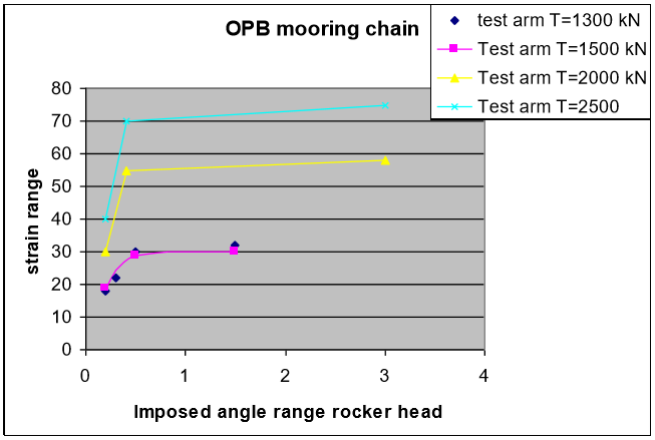

Figure 2.18: Adjusted nominal strain range in first free flat link as a function of imposed angle and chain tension. $\mu = 0.3$ (Lassen et al., 2014)

It was noticed an increase of the friction in the bearing between the two phases of this experiment as the links had been stored for two months. This had a detrimental effect on the contact surfaces of the chains and increased the friction coefficient from 0.11 to 0.14. Results were thus adjusted by multiplying the measured strains with the ratio between the friction coefficients from Phase 1 and Phase 2, 0.79 (Lassen et al., 2014).

FEA modelling of the chain stopper and chain links verified measured OPB stresses from the experiments. This was done by including 9-10 links in a non-linear analysis to

include larger global deflections and to include the non-linearity occurring from coupling between bending and axial forces. The latter is modelled by stiffness in combination to friction. Relevant parameters are adjusted to find a good fit to the experimental material properties. To simulate the result from Phase 2, the friction coefficient was given the value 0.14 (Lassen et al., 2014).

Maximum bending moments are measured for the two first flat links, link 1 and link 3. Figure 2.19 illustrates how the bending moments differs for increased pretension. As seen, the increase is almost linear for Link 1, whereas there is almost no change for Link 3. This defines Link 1 as the most critical when subjected to OPB as the bending moment is by far lower for Link 3 (Lassen et al., 2014).

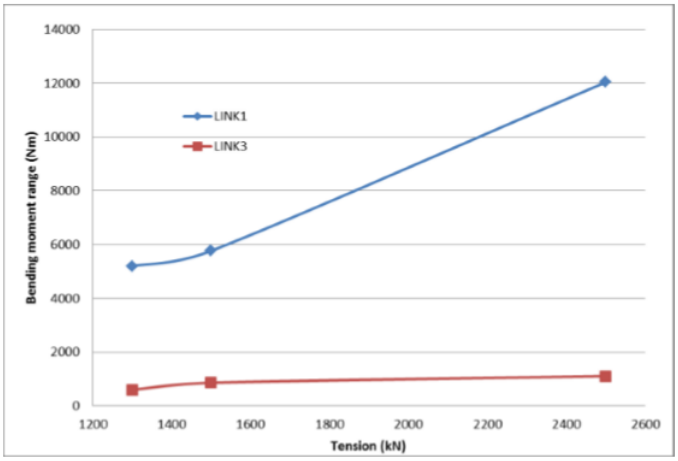

Figure 2.19: Bending moment range in mid-section of critical links as a function of chain tension (Lassen et al., 2014)

For tension equal to 2500 kN, calculations give an OPB moment equal to 12 kNm, or a bending stress of 13.6 MPa. These values are equal to a calculated strain of 66 μs, whereas the measured strain was 75 μs from testing (Lassen et al., 2014). Thus, the results from FEA provide a 14 % underestimation of stress values. At the hot spot location, stress is calculated to be 23.9 MPa, while the measurements indicated a value of 24.9 MPa corresponding to a 4 % underestimation. The non-corresponding percentages comes from FEA, predicting higher shear forces in the link than measured in the bent area (Lassen et al., 2014).

The research from 2014 found the following parameters relevant in influencing the problem of combined tension and bending stresses:

- Nominal link diameter
- Proof load from production
- Hang-off configuration
- Stopper arm and bearing friction
- Pretension in the mooring line

MARINTEK concluded that an in-service simulation in combination with FEA modelling is sufficient for life predictions of the mooring lines. A long stopper arm with low friction bearing was also found beneficial in the project as a hang-off configuration resulting in lower stresses (Lassen et al., 2014).

Life prediction based on simulation of in-service chain behavior

Mooring lines are grouped together to ensure redundancy if one line were to fail. Spread mooring systems are typically grouped in four clusters, whereas turret mooring systems include lines in three groups. If the pretension in a group is inaccurate, lines can be unevenly loaded and experience more fatigue damage. If the system uses an offloading buoy like the Girassol did, a directional load towards the oil offloading line (OLL) is created, generating an asymmetrical mooring system to resist the loads from the OLL (Bhattacharjee, 2015).

The applied pretension in each mooring line will be adjusted due to the predicted forces of the independent line. Load predictions are dependent on several parameters such as the weather, including wave, current, and wind direction. Time series simulations for short term sea states of tension and imposed interlink angles are used to find accumulated impact on the hot spot location of the chain links.

MARINTEKs investigation included a case study of a cylindrical shaped FPSO in the Barents Sea. The FPSO has a typical mooring configuration as illustrated in Figure 2.20, using thee clusters of mooring lines with different pretension dependent on direction and weather predictions. Cluster 1 in direction North and Cluster 3 in direction West has the lowest pretension and the shortest fatigue life when only considering the tensile loads. Cluster 2 in direction South-East has a pretension of 2700 kN and a subsequent high fatigue life for tension. Further, the weather is not predicted to be too harsh including a maximum Hs = 7 m. However, the latter line will be critically affected by OPB due to

higher pretension. The case study illustrates how the effect of OPB is highest for lower sea states, and for this case Line 5 in the South-East cluster. This line does not achieve desired DFF exceeding 10.0, and the direction of the line position should be changed to reduce the local OPB phenomenon for Link 1 in Line 5 (Lassen et al., 2014).

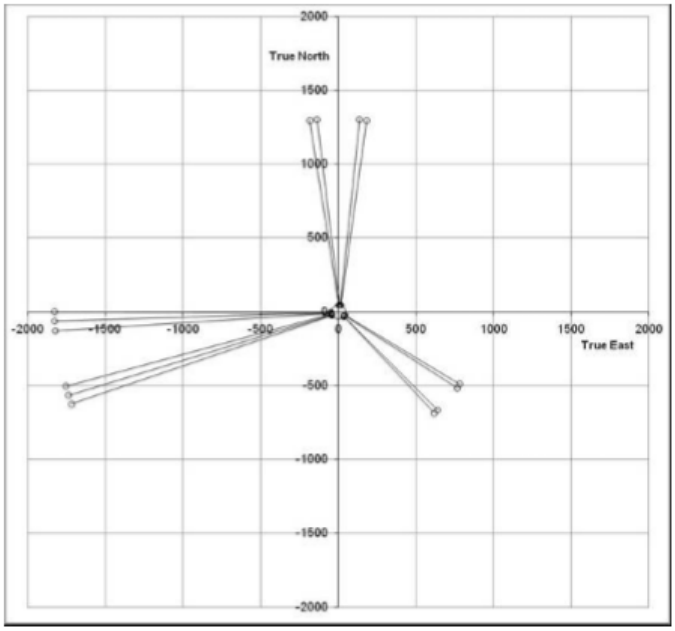

Figure 2.20: Typical Mooring Configuration for FPSOs (Lassen et al., 2014)

A maintenance plan is used to solve problem as the tension in the line probably will be adjusted and increased during service life to avoid slack from bedding-in of the polyester rope. This operation is typically done a couple times during a desired 30-year service life. The position of the critical chain link will thus change, and Link 3 becomes the new Link 1. It is further assumed that Link 3 has escaped from any accumulated previous OPB damage, and starts from zero bending stresses. This increases the DFF for the line and if a tightening is done every 10th year, its new DFF value is 15.0 (Lassen et al., 2014).

The effect and influence of pretension was also addressed in 2007, in a paper by ter Brake et al. called "Calculation methodology of out of plane bending of mooring chains" (ter Brake et al., 2007). Results are illustrated in Figure 2.21, and proves how the OPB moment is increased from increased tension in the mooring line. As also proven by MARINTEK, lines operating with higher tensile loads will have a higher risk of OPB damage (Lassen et al., 2014).

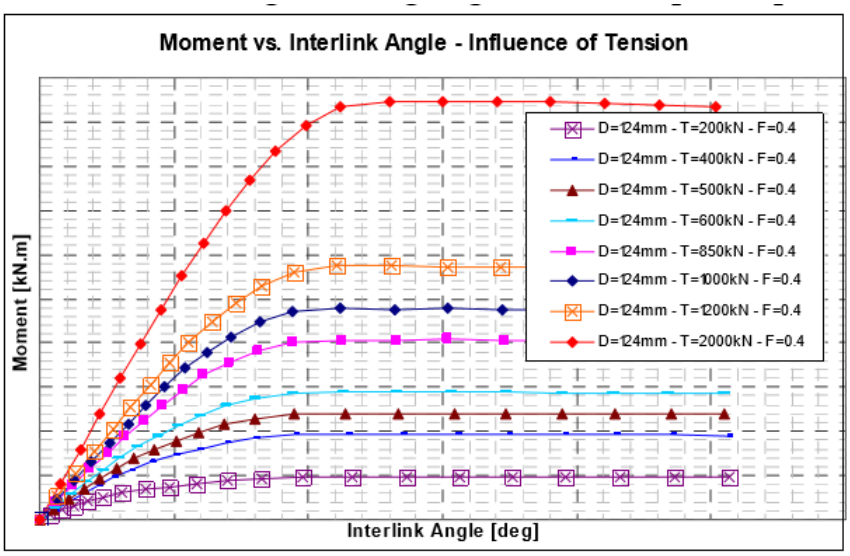

Figure 2.21: Influence of Tension (ter Brake et al., 2007)

2.3 JIP Research 2007 - 2016

To get a better understanding of out of plane bending, a JIP was commenced in 2007. It included 28 different companies and took more than six years to complete. Its aim was to understand, and to make further recommendations on chain fatigue design when OPB is considered. This was done by full scale testing, FEA works, and testing on smaller samples to see the environmental influence on fatigue initiation and crack propagation (Rampi et al., 2015). This section will summarize some of their findings to highlight what has been done as research for OPB in the past, and to get some insight in what to expect from a non-linear FEA.

2.3.1 Fatigue Life Prediction of Mooring Chains subjected to OPB

Out of plane bending must be included in the fatigue calculations to reduce its effect on the mooring line's service life. The paper *"Fatigue Life Prediction of Mooring Chains subjected to tension and out of plane bending"* (Lassen et al., 2009) was included in the JIP and results propose using an appropriate hot spot S-N curve for further fatigue calculations. This has previously been done by traction experiments to establish S-N curves by including only the nominal stress range in the link's straight part, neglecting stress concentrations. Out of plane bending results in high stress concentrations and S-N curves developed by pure traction can hence not be used for a good representation.

The problem of OPB occurs for situations where the chain links are in direct contact with the bilge area of the floater, and it has been debated if it is necessary to use chains for this location. Some new designs have been considered, such as the Advanced Production and Loading's (APL) Submerged Turret Production (STP), that uses wire instead of chains for connecting points. This does, however, impose some difficulty to the adjustment of the line length, an operation easier achieved by using chain links.

Figure 2.22 illustrates the stress concentrations for a link subjected to pure traction. They are located at the outside of the crown, inside at the bend, and along the straight part. The point located at the crown has an SCF of 4.2 and the point in the bend an SCF close to 3.7. Figure 2.23 illustrates the stress distribution for a link subjected to combined tension and OPB bending, and it is visible how the bend location hot spot has been relocated further towards the bend (Lassen et al., 2009).

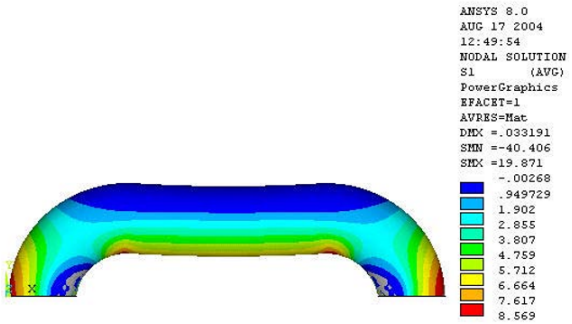

Figure 2.22: Stress at pure traction (Lassen et al., 2009)

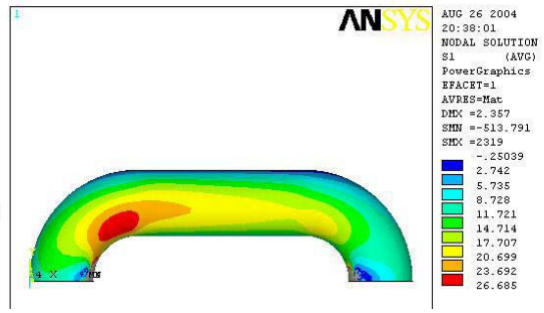

Figure 2.23: Stress at combined tension and OPB (Lassen et al., 2009)

With small specimen testing in sea water with free corrosion of an R4 grade link, an SN curve was developed. A curve that predicted a fatigue life better than the ones used for pure traction. However, for a small-scale test several aspects of early ignition fatigue life might get lost, such as corrosion pits and defects from manufacturing (Lassen et al., 2009).

To make good fatigue life predictions, maximum stress in the bend area should be addressed by FEA. Fatigue life can then be predicted by DNV B1 S-N curves. Local cathodic protection can be applied for fully submerged critical links. The included article by Lassen et al., recommend using long connecting arms with articulation about two axes and have low friction in the bearings for the connecting point. If possible, the diameter of the chain should be large and the steel grade lower. An example of a hang-off arm configuration is illustrated in Figure 2.24. For this configuration rotation is possible about horizontal and vertical planes, and the angles are to some degree determined by the choice of material for the bearing at hang-off (Lassen et al., 2009).

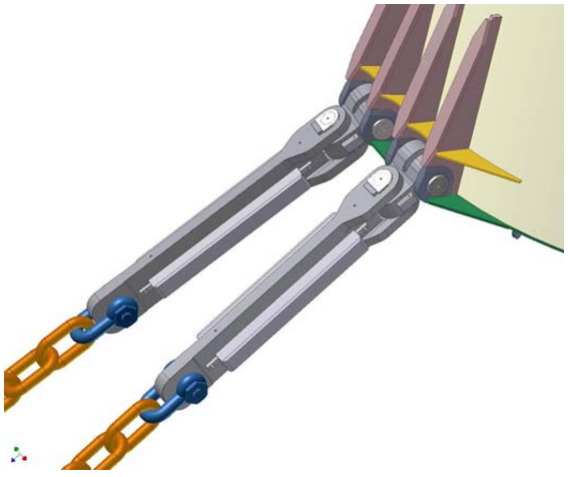

Figure 2.24: Connecting arm hang-off configuration (Lassen et al., 2009)

2.3.2 Static OPB Testing

To derive the OPB interlink stiffness, a quasi-static OPB stiffness measurement campaign was commenced. It tested four different chain sizes, two different chain grades (R3 and R4), studlink and studless links, in addition to the effect of proof loads, manufacturer, and a salt water or air-filled environment. The test consisted of 15 links with a constant horizontal tension applied as illustrated in Figure 2.25. The middle link was subjected to a vertical displacement implementing OPB on both adjacent links, and in plane bending (IPB) to the following links.

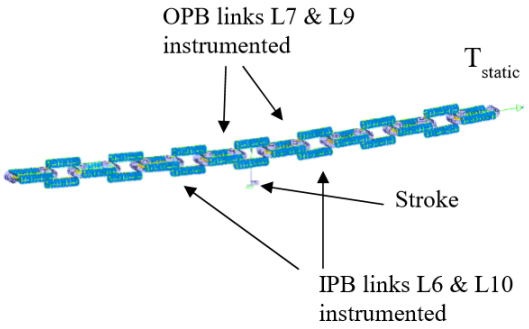

Figure 2.25: Test principle (Rampi, Dewi, Francois, Gerthoffert and Vargas, 2016)

Strain gauges were used to measure the stress and displacement transductors were placed on all links to measure angles along the chain. The stress and various angles were used to find a correlation and derive a local interlink stiffness by Equation (2.8).

$$M_{OPB} = K(T, d, \alpha_{int}, ProofLoad)\alpha_{int} \tag{2.8}$$

OPB bending stress from the straight part of the link was found as a function of the angles by data from four gauges to display an image of the average OPB moment. This made it possible to create an average plot for bending stress versus angle illustrated by Figure 2.26. The three different interlink motions, mentioned in Section (2.1.5), can be recognized from these plots. The *Sticking mode* represents the steepest part of the stress slope, and *rolling* is represented when the slope is portrayed as non-linear. When the *sliding mode* is reached, the stress more or less remains the same.

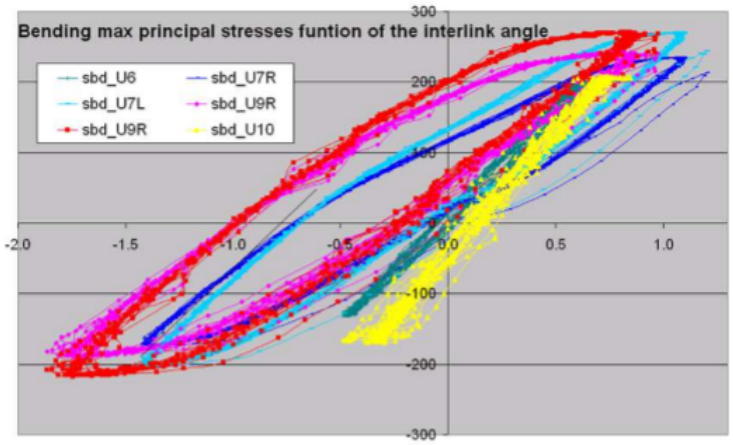

Figure 2.26: Typical hysterisis curve from static tests. OPB bending stress versus interlink angle (Rampi, Dewi, Francois, Gerthoffert and Vargas, 2016)

One out of 14 tests were performed in seawater. By comparing results, it is proved that the sticking modes are almost equal for both environments for lower interlink angles as illustrated in Figure 2.27. However, sliding mode is reached more rapidly in seawater, coinciding with a lower friction contact coefficient which also lowers the stress. Figure 2.27 represents averaged curves for two samples, S1 in air and S2 in seawater (Rampi, Dewi, Francois, Gerthoffert and Vargas, 2016).

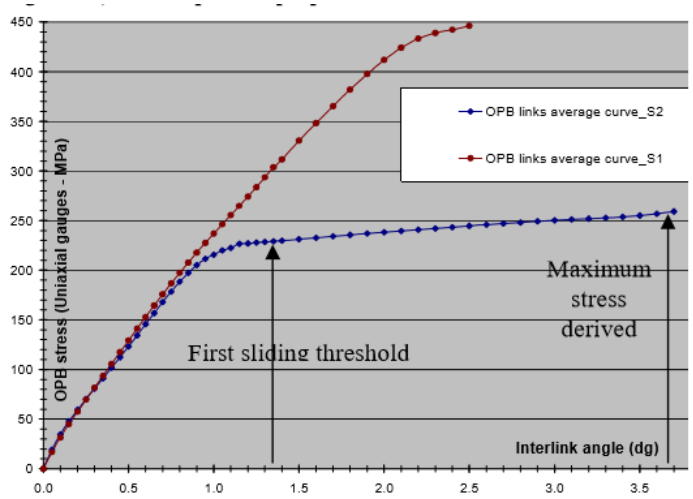

Figure 2.27: Averaged translated OPB stresses for S1 and S2 at 500 kps (Rampi, Dewi, Francois, Gerthoffert and Vargas, 2016)

The friction coefficient influences the phases locking and rolling as well as the sliding threshold, defined as the OPB angle when sliding occurs (Rampi, Bignonnet, Cunff, Bourgin and Vargas, 2016). The static tests made it possible to derive a friction factor from the assumed sliding threshold. In air, the value was an average of 0.54, whereas

in seawater it was 0.29. A friction factor of 0.3 was then used for further calculations as a conservative choice for the nonlinear part of the curve (Rampi, Dewi, Francois, Gerthoffert and Vargas, 2016).

When the sliding threshold is reached, the OPB moment is defined as Equation (2.9)

$$\Delta M_{OPB_{sliding}} = \mu T d \tag{2.9}$$

They noticed some scatter in the measurements. Main sources for scatter are listed below.

- The same link can provide different up and down curves in the hysteresis curve.
- The sticking mode can occur inside or outside of the mating area, which will result in different interlink contact stiffness.
- The rolling mode can start at different interlink angle ranges for the different links.

In addition to these sources, scatter can occur from differences in material, link geometry, and proof load mating area, but it was concluded that the main source for the scatter came from the different locations of the contact point. The locking stiffness is higher inside the mating area and the contact stiffness will therefore alter dependent on contact location. This will also happen during service and as the location is random, the interlink stiffness will to some degree be a random variable (Rampi, Dewi, Francois, Gerthoffert and Vargas, 2016).

2.3.3 FEA Results of OPB

The FEA works done for this JIP had the intention of further understanding of the OPB locking mechanism, performing a sensitivity study to different parameters, and assessing the stress state at different locations. A proof load of 70 % MBL was first applied to the links. They were later exposed to constant tension and bending to simulate real operating conditions (Rampi, Bignonnet, Cunff, Bourgin and Vargas, 2016).

To identify the different modes of motion, the vertical displacement of two adjacent nodes in the contact area was tracked. This is illustrated by the FE-model in Figure 2.28. In locking mode, node 1 and node 2 stick together and the OPB moment increases. When the nodes start to separate, the link experiences rolling, while the OPB moment remains. When the nodes are separated, sliding motion is reached and the OPB moment ceases to increase. The non-linearity of the stiffness curve increases when the nodes

start to separate and rolling occurs. The relative displacement and interlink stiffness in submerged conditions are illustrated by the graphs in Figure 2.29.

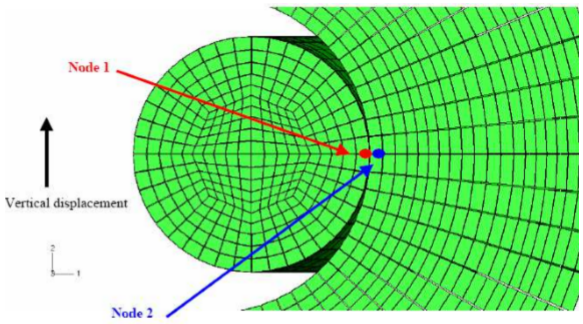

Figure 2.28: Adjacent nodes for relative vertical displacement (Rampi, Bignonnet, Cunff, Bourgin and Vargas, 2016)

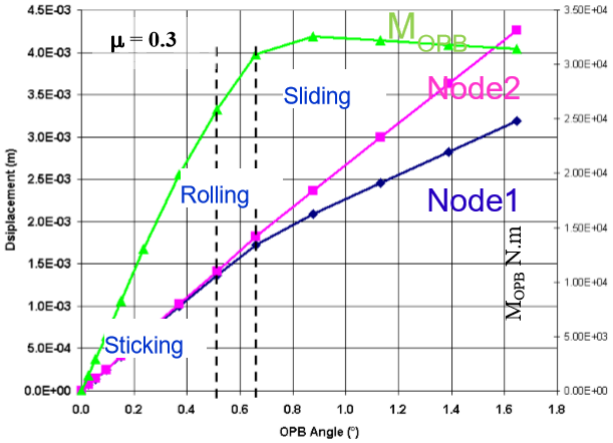

Figure 2.29: Relative displacement by angle (Rampi, Bignonnet, Cunff, Bourgin and Vargas, 2016)

As from static testing, it was also proven by FEA that the interlink stiffness will alter dependent on whether the locking appears inside or outside the mating area. This illustrated by the curves in Figure 2.30, where the initial slope is stiffer that the final slope when the locking point has shifted from inside to outside by the third cycle.

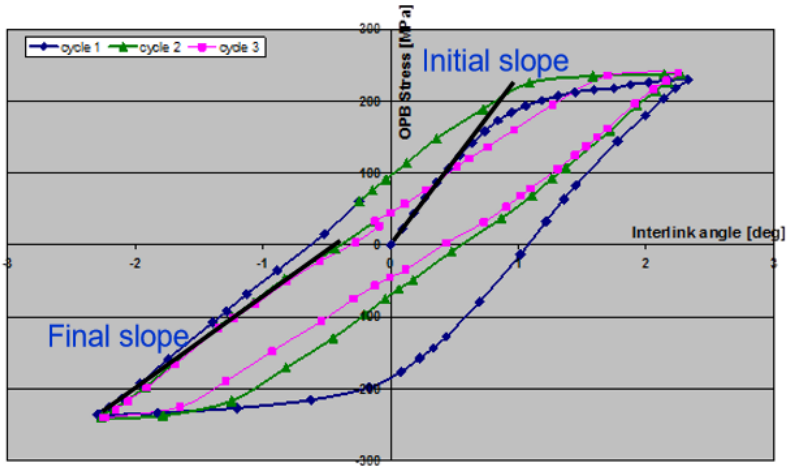

Figure 2.30: Relative displacement by angle (Rampi, Bignonnet, Cunff, Bourgin and Vargas, 2016)

The static tests mentioned in the previous section were addressed and modelled by FEA, illustrated by the model in Figure 2.31. A constant horizontal tension was applied and the middle link experienced vertical displacement in a symmetric up and down motion.

The elements applied in ABAQUS CAE can accurately take the contact friction into account, an elasto-plastic material behavior, and large strain and displacement laws. The element type was ABAQUS C3D8I, elements known to behave well when subjected to bending loads. It was anyways concluded from the FEA works that FE-results in general underestimate the interlink contact stiffness (Rampi, Bignonnet, Cunff, Bourgin and Vargas, 2016).

Figure 2.31: Static FE model (Rampi, Bignonnet, Cunff, Bourgin and Vargas, 2016)

A Ramberg-Osgood elastic-plastic material type was used for most of the FEA works. By performing a sensitivity study on different parameters, they further found how the material property is an influencing parameter. The material law has a significant impact on the interlink stiffness as the OPB stiffness decreases with a tougher hardening law (Rampi, Bignonnet, Cunff, Bourgin and Vargas, 2016).

The JIP proposed a new material model, where plasticity is described by a Von Mises yield surface and associated plastic flow rule. A combined nonlinear kinematic and isotropic model described the hardening model. This new model can model cyclic hardening or softening, ratchetting, and shakedowns. Young's modulus is sat to 206.6 GPa and the Poisson's ratio equal to 0.3. The new material law could reproduce the interlink stiffness found from the static tests, but it was still not a conservative solution (Rampi, Bignonnet, Cunff, Bourgin and Vargas, 2016).

The stress concentration factor for OPB is dependent on the link shape and is therefore deemed to change after the proof load is applied and geometry is altered by plastic deformation in the contact surface area. The ratio between the OPB stress at a node and the nominal OPB stress is defined as the OPB SCF. It has been found by various analysis that the maximum principal stress from OPB is occurring between location B and B' as illustrated by Figure 2.32 corresponding to the beginning of the bend part of the link. The principle stress and shear stress during a cycle is multiaxial in the curved part, and location C is correspondent to the maximum shear stress location. It was concluded that a multiaxial fatigue criterion is more suitable to address the SCFs connected to OPB (Rampi, Bignonnet, Cunff, Bourgin and Vargas, 2016).

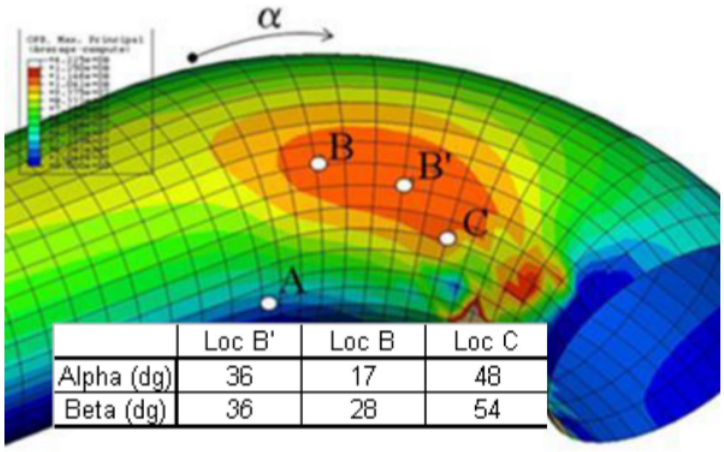

Figure 2.32: Location of SCF (Rampi et al., 2015)

The location of the OPB hotspot was verified by running full scale fatigue tests, predicting how most OPB fatigue cracks appeared at location C (Rampi et al., 2015). This location is defined as approximately 50 ° from the top (or bottom) as illustrated by the parameter β in Figure 2.33.

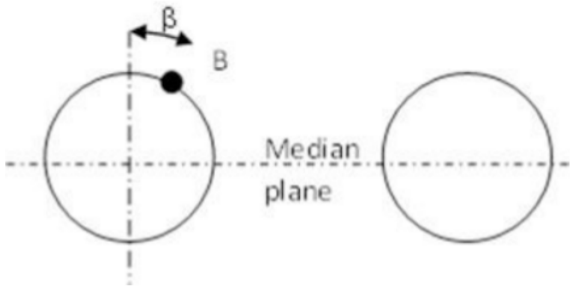

Figure 2.33: Location of OPB hotspot (Rampi et al., 2015)

The JIP project was a success in the search for answers connected to the OPB interlink stiffness and connected fatigue problems. It proposed a multiaxial OPB SCF as a breakthrough, and highlighted a need to perform more high cycle fatigue testing in corrosive environments (Rampi et al., 2015).

As a conclusion drawn from the JIP research, FEA is an effective way to understand OPB locking and the interlink contact stiffness. It was also proven that a multiaxial fatigue criterion is a better fit to address the maximum principal stress. The research proposed multiaxial OPB SCFs for different locations, but further recommended that the contact stiffness laws found from full scale testing is used, as it is a better fit for the uncertainties connected to the real chain links in operation (Rampi, Bignonnet, Cunff, Bourgin and Vargas, 2016).

Chapter 3

Classification Rules and Standards

To get an overview of what measures the industry has taken to prevent failures, standards, classification rules, and recommended practices are reviewed with a focus on out of plane bending and fatigue. This includes the safety standards by ISO and NORSOK, codes for permanent position mooring by the classification societies DNV GL and Bureau Veritas, as well as recommended practice (RP) by the American Petroleum Institute (API). An RP is defined by DNV GL as: *"publications which cover proven technology solutions found by DNV to represent good practice, and represents an alternative to the safety requirements by DNV offshore standards"* (DNV GL, 2013). This chapter sums up the findings related to OPB.

3.1 Classification rules by DNV GL

DNV GL has developed their class rules for position mooring to address mooring integrity. They offer a possibility to obtain the class notation *POSMOOR* for a position moored unit (DNV GL, 2013). The requirements are given for long term mooring, defined as a unit located at the same location for more than 5 years. The class rules contain the technical requirements as well as guidelines for design and construction of mooring systems. Configuration components such as chain links, different types of shackles, windlasses, winches, chain stoppers, fairleads, and turrets are included in the mooring scope.

There are no general guidelines in the POSMOOR rules regarding out of plane bending. It is, however, mentioned that it should be considered as the SN-curves only include tension-tension fatigue. The following is taken from their classification rules (DNV GL, 2013). OPB must be considered for interlink rotation and occurs in the first link free to rotational movement. These are chain links located in a chain wheel, in addition to any link passing over a chain stopper or bending shoe. OPB contributions can be established by calculations or testing, and it is important to define the friction factor in the bearings at location for connection with fairlead, chain pipe, or connecting rod. SCF due to OPB

must be included in the fatigue analysis for long term mooring systems. The DNV GL rules refer further to a paper called *"Stress concentration factors for stud-less mooring chain links in fairleads"* (Vargas et al., 2004). This paper describes tests of studless chain located in a 7-pocket fairlead wheel. If this is the case, the chain links in contact should be added a SCF of 1.15 to account for the bending stresses. If the configuration is different, additional studies should be carried out regarding the increased SCF. The study shows that the minimum magnification factor for stresses on a fairlead should be $\frac{1}{cos\alpha}$, where α is the interlink angle (Vargas et al., 2004). The configuration of the 7-pocket fairlead wheel from the study is illustrated by Figure 3.1 and the angle α is defined as in Figure 3.2.

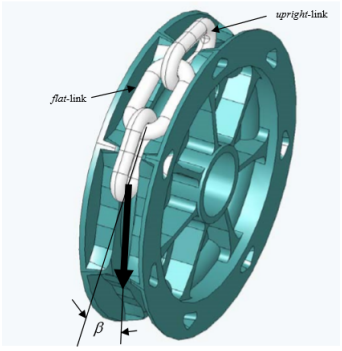

Figure 3.1: Chain links in a 7-pocket fairlead wheel (Vargas et al., 2004)

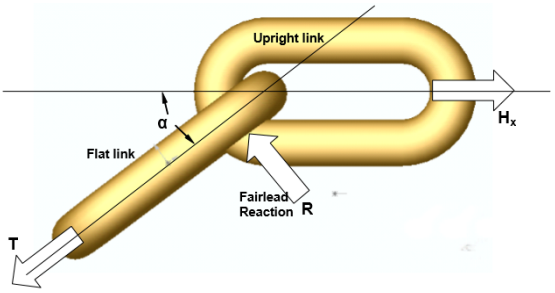

Figure 3.2: Angle between flat and upright link in fairlead wheel (Vargas et al., 2004)

It should be noted that the bending problem mainly occurs as the chain links fail to run smoothly over the wheel, and bending stresses arise when the links are twisted back into place. A 7-pocket fairlead wheel will be larger in size, include more pockets, and thus the angle between the adjacent links will be smaller. The difference in stresses for a 5- and 7-pocket fairlead wheel is not that significant if the links were to run smoothly over the wheels (DNV GL, 2013).

3.2 International Standards

International Organization of Standardization (ISO)

The international standards for permanent mooring is called 19901-7 *"Stationkeeping systems for floating offshore structures and mobile offshore units"*. ISO has no direct guidelines for OPB, but recommend using SCF as an additional safety factor. They encourage the use of inspection and adjustment of lines as a temporary solution to relieve the links in contact areas of permanent stress (ISO, 2013).

NORSOK

The NORSOK standards, developed mainly to increase values for developments and operations within the petroleum industry at the Norwegian Continental Shelf, refers to the ISO 19901-7 standards regarding safety of mooring systems (NORSOK, 2010). To avoid fatigue damage under combined tension and bending, there should exist an operating plan combining regular inspection and alteration of the mooring lines by winches to avoid constant stress at one link (ISO, 2013).

3.3 Recommended Practice by API

API provides recommended practice for the maritime industry, mainly in America, but now also internationally. Their recommended practice (RP) for mooring systems is called API-RP-2SK, "Design and Analysis of Stationkeeping Systems for Floating Structures" (API, 2015). It is a guidance for analysis, design, and evaluation of mooring systems for floating units. API also emphasizes on inspection and planned to give out a new RP for mooring integrity management (MIM) in 2016 (C. Carra and A. Phadke and D. Laskowski and K.-T. Ma and R. Gordon and G. Kusinski, 2015). Regarding the phenomenon of combined tension and bending loads, there exists no design curves for this per date due to lack of data. API does not provide any specifications for OPB calculations, but add some additional ideas about the geometry of the fairlead diameter (D) and link diameter (d) at contact point. This sets an upper requirement for the ratio D/d to resist excessive bending. API also proposes a shift of the links located in the chain stopper and prefers a 7-pocket fairlead wheel. They refer to the use of FEA, but no direct guidelines on how to do this.

Fatigue T-N tests of chain in a 5-pocket fairlead indicates a 5 - 20 % Bending-Tension fatigue life in terms of Tension-Tension fatigue life. A 7-pocket wheel have proven to give better fatigue life regarding combined bending-tension. The stress concentrations experienced at contact points with fairlead, chain stoppers, bending shoes, hawser pipes, or other components should be addressed and evaluated through FEA. The stress concentrations in these areas should further be included in the fatigue analysis and the predicted fatigue life should be at least three times the design service life of the system (API, 2015).

3.4 Guidance on OPB by Bureau Veritas

Bureau Veritas is the only classification company that offers guidelines on how to handle OPB. Their guidance note *"Fatigue of top chain of mooring lines due to in-plane and out-of-plane bending"* was created in 2014, where the top chain is defined as the first 20 chain links after chain stopper or fairlead. Combined tension and bending loads should be considered when the pretension is above 10 % MBL (Bureau Veritas, 2014).

Previous methodology has been to neglect any other loads than tension between adjacent chain links which is correct in locations far from connection points. At connection points, high bending loads will be introduced and additional fatigue damage generated due to angular difference between fairlead and chain link. The rolling motion between adjacent links are to some degree prevented and the links will either appear to stick together by friction, or experience a sliding mode. The latter occurs when the interlink moment exceeds the friction limit. This summary is developed from Guidance Note NI 604 DT R00 E (Bureau Veritas, 2014).

Mooring analysis for combined fatigue estimation for OPB

Three bending modes can occur for a link segment; in plane, out of plane, and torsion, whereas torsion generally is neglected for combined fatigue evaluation. The methodology for calculating OPB is done in the following steps;

1. **Fatigue mooring simulations.** This provides the time series of tensions and angles at fairlead for damage calculations, as well as the maximum angles and tensions at fairlead. It includes the mooring patterns, hydrodynamics, and the meteocean data. An analysis is done in time domain for each possible sea state for each line producing time series for the following:

   - Tension at fairlead **T**
   - In and out of plane angles of the line α
   - Vessel rotations at fairlead connection β

   Thus, maximum and minimum tension at fairlead is calculated for all sea states and all lines. This is also applied for the actual angles at fairlead for all sea states and all lines for both in and out of plane bending, a parameter called γ. Figure 3.3 is taken from the BV guidelines to illustrate the parameters α, β, and γ.

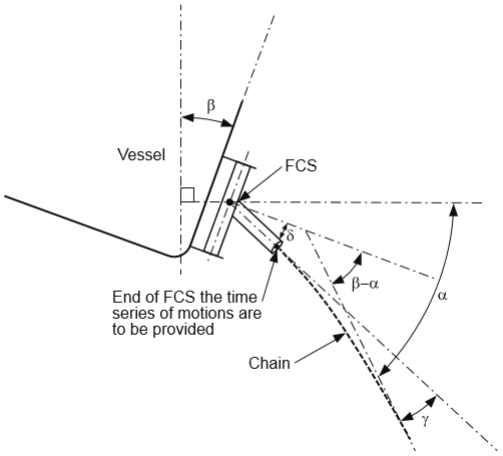

Figure 3.3: Chain Relative angles at Fairlead/Chain Stopper (FCS) (Bureau Veritas, 2014)

2. **Interlink stiffness analysis.** Provides the relationship for damage calculation between chains at fairlead, tension at fairlead, OPB/IPB interlink moments, and angles for first two links. It is calculated by the following method:

   A FEM beam model or a non-linear stiffness model is created of the top chain links. Each mooring link is considered to appear as a single beam. A point load at fairlead connection imposes tension and an angle in the first link. The boundary condition at the end is fixed. The beam model will be loaded with every possible combination of tension at fairlead between T_{max} and T_{min} and all angles at fairlead in and out of plane between γ_{max} and γ_{min}. Each link in every mooring line should be evaluated with respect to tension and in and out of plane bending angles and moments.

3. **Fatigue damage evaluation.** A combined top chain fatigue damage in time domain is done by time series of tension, in and out of plane angles, and interlink moments. Time series of nominal TT stress, OPB stress, and IPB stress for each line and link is gathered. Diameter and pretension effects are considered with applying SCF in combination with TT, OPB, and IPB stresses. SN-curves and Rainflow counting are used to find the damage and a long-term distribution of stresses. All results must be verified.

(Bureau Veritas, 2014)

Friction limiting moment

Relative angle between fairlead/chain stopper and chain link will be a factor dependent on fairlead characteristics and chain and vessel motion. To reduce the bending moments,

the fairlead/chain stoppers must be able to rotate around vertical and horizontal axis, an ability restricted by friction.

The introduced bending moments should be investigated by testing. The behavior of sticking and sliding is tested in full scale from fixed axial loads. If the connecting points are submerged, tests are done in seawater. Thickness and surface roughness measurements should be taken before and after each test for wear assessment. The static friction coefficients from the bushing material is measured from prototypes. The range of applied loads are to coincide with values from the mooring simulations.

The limiting moment is calculated by Equation (3.1), where F is the axial load and D is the diameter of the axis in the bearing. The friction coefficient μ is generally between 0.5 and 0.6 in air and 0.25 and 0.3 in seawater. If the fairlead is unable to rotate, or the sliding limit is higher than for the chain's sliding limit, sensitivity parameters of the friction parameters should be considered.

$$M_{lim} = 0.55\mu DF \tag{3.1}$$

(Bureau Veritas, 2014)

Interlink Stiffness

The interlink stiffness is defined by Bureau Veritas as ″the range of moment at interlink for a given tension and given range of interlink angle". FE analysis are not sufficient to provide the true interlink stiffness. The reason for this is that the effective contact area and material properties cannot be accurately modelled. FEM calculations provide sub-conservative results, and full-scale tests must be performed. The results of the test should provide a global best-fit interlink stiffness law.

To measure interlink stiffness, full-scale tests are performed by the manufacturer with chains of equal size as the designed system. Attachment points and other configurations should be able to represent the loading phenomena occurring at site. They reproduce cycling for different tension and angles that occurs during operation. The chain must sustain a satisfactory number for cycles to assess non-linear bending moments and stresses due to the hysteresis of the bending moment during a loading range. The chain links are equipped with measuring instruments and strain gauges to validate results from FEM calculations.

The same bending stiffness curve can be applied for air and seawater. Due to a sliding threshold in fluids, there will be a limitation to the bending moments in seawater. This

is implemented in the interlink stiffness law and reached when the angle is increasing, while the moment remains constant. The link sticks back when the angle reaches a local extreme, creating a hysteresis loop of moment versus angle as shown in Figure 3.4.

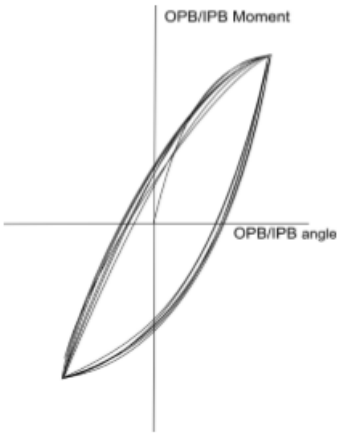

Figure 3.4: OPB/IPB moment hysteresis loop (Bureau Veritas, 2014)

The sliding threshold is defined by Equation (3.2), where T is the working tension, μ the friction coefficient, and d is the chain nominal diameter.

$$M_{threshold} = \mu T \frac{d}{2} \tag{3.2}$$

The interlink stiffness will vary as the contact area between links is varying under sliding motion. This variation is considered statistically independent of the other parameters of the stiffness law. It can be considered to be a log normal distribution, linking the shape factor δ to the coefficient of variation (COV).

$$ln(1 + COV^2) = \delta^2 \tag{3.3}$$

The coefficient of variation is the ratio between standard deviation and mean value of stiffness. The independent variation of contact area is defined by a constant factor Z_s, depending only on the shape factor δ, and SN-curve exponent m.

$$lnZ_s = \frac{m\delta^2}{2} \tag{3.4}$$

Z_s is further used to calculate combined fatigue stress in Equation (3.13) (Bureau Veritas, 2014).

FEM modelling

Results from full-scale tests are measured from strain gauges, load cells, inclinometers etc. All results from full scale tests are to be compared with the similar calculations from FEA. If any differences occur between tests and FEM results, they must be justified for further verification. FEM loading of the model must represent all possible axial tension loads as well as possible interlink moments appearing on site and in full scale tests. Loading the FEM model should be done by the following procedure:

1. Load the model up until proof load (Chain dimensions should still be within rule requirements after the proof loading)
2. Unload
3. Apply axial load to a predetermined line tension from mooring analysis
4. Apply a predetermined range of angles and displacements/moments

SCF from TT loads, OPB and IPB moments are evaluated from FEM calculations to obtain the stresses.

Tension at fairlead form interlink stiffness and relative angle of chain/fairleads determines the interlink angle. This angle will be reduced to the following links and is assumed to be negligible after 20 links. The dependent parameters from the interlink stiffness are chain diameter, stiffness grade, and manufacturer.

There are no dynamics or memory effects and calculations can be done statically. This is done by a static non-linear FE-analysis of the 20 first links where each link is represented as a beam with equal stiffness. Interlink stiffness with bending moment threshold is implemented between links and the last link has a pinned boundary condition. The model is loaded with tension and in and out of plane relative angles at fairlead, in combinations that cover the whole range obtained from the mooring analysis. Angles and moments in and out of plane are to be evaluated at each link for each load case. An example of a beam model is taken from the BV guidelines in Figure 3.5 (Bureau Veritas, 2014).

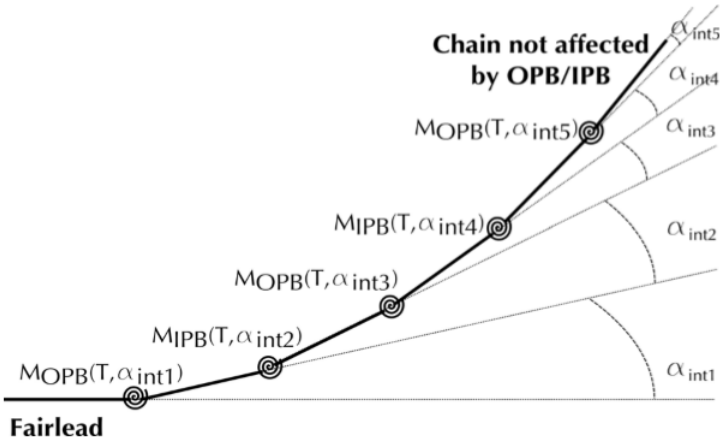

Figure 3.5: Beam model of chain and inderlink angles (Bureau Veritas, 2014)

Requirements for FEM software

The software program used for FEM calculations must be qualified for elastic-plastic calculation with contact. The model must consider at least one complete chain link connected with two adjacent half links. One of the half links is fully constrained at mid-link plane and loading is done by applying tension and moments/displacements on the other half-link. The contact behavior should be realistic, coinciding with the full-scale test regarding friction and material behavior. The geometry should represent the chain as from manufacturing at the end of heat treatment. The material stress-strain (hardening) law should represent the true material properties (Bureau Veritas, 2014).

Chain link hotspots

Fatigue failure location will vary as the hotspot stress is located at different parts of the chain link for TT, OPB and IPB. The hotspot stress connected to OPB is spread over a wide area, and the location for maximum combination with IPB and TT stress will be the area for fatigue failure.

Another critical hotspot location is defined from the occurring multiaxiality stresses in the interlink contact area, and should be addressed by appropriate multiaxial fatigue methods (Dang Van) (Bureau Veritas, 2014). The most critical hotspots are the following:

- Hotspot A: Pure TT hotspot.
- Hotspot B: Uniaxial OPB hotspot, maximum T, OPB and IPB effects.
- Hotspot C: Multiaxial OPB hotspot (closer to contact area, multiaxial effects).

When disregarding the effects of corrosion, the following stress concentration factors are found for tension-tension and out of plane bending stresses:

$$SCF_{TT} = \frac{\Delta\sigma_{TT}}{\Delta\sigma_{TT,nom}} \tag{3.5}$$

$$\Delta\sigma_{TT,nom} = \frac{2\Delta T}{\pi d^2} \tag{3.6}$$

$$SCF_{OPB} = \frac{\Delta\sigma_{OPB}}{\Delta\sigma_{OPB,nom}} \tag{3.7}$$

$$\Delta\sigma_{OPB,nom} = \frac{16\Delta M_{OPB}}{\pi d^2 3} \tag{3.8}$$

In plane bending stresses are dependent on chain geometry (studless or stud chain).

$$SCF_{IPB} = \frac{\Delta\sigma_{IPB}}{\Delta\sigma_{IPB,nom}} \tag{3.9}$$

$$\Delta\sigma_{IPB,nom} = \frac{2.33\Delta M_{IPB}}{\pi d^2 3} \tag{3.10}$$

$$\Delta\sigma_{IPB,nom} = \frac{2.06\Delta M_{IPB}}{\pi d^2 3} \tag{3.11}$$

The stress concentration factors are estimated through FEM calculations and calibrated through full scale model tests of chain links (Bureau Veritas, 2014).

Corrosion

Material loss during unit life must be considered for fatigue damage calculations. In the top chain, it is valid to consider uniform or hypothesis corrosion, where the corroded diameter is calculated from Equation (3.12). L_d is the design life of the unit, and r_{corr} is the loss of diameter due to corrosion per year.

$$d_{corroded} = d_{uncorroded} - \frac{L_d}{2} r_{corr} \tag{3.12}$$

A geometrical corrosion factor, Z_{corr}, should be applied to the SCF in the FE-model to account for the material loss which results in a varying chain geometry. The SCF is to be

based on a mid-life corroded FE-model if the chain reduction at mid-life is predicted to be more than a 5 % diameter loss. If the material loss is less than 5 %, the geometrical corrosion factor Z_{corr} can be set to 1.08 times a SCF for a new chain.

Stresses should be combined by a summation of time series and fatigue calculations done in four possible locations for fatigue crack initiation, appearing due to the chain link's two symmetry planes. The loads in these locations are anti-symmetric. Figure 3.6 illustrates the four stress locations.

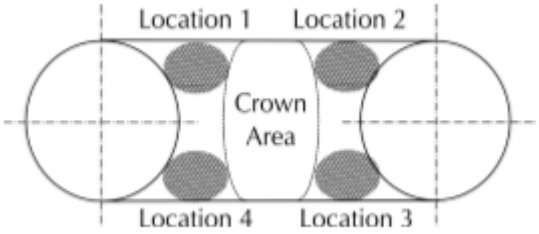

Figure 3.6: Location of fatigue failure (Bureau Veritas, 2014)

Combined stress is calculated by Equation (3.13). Z_{corr} is the geometrical corrosion factor and Z_s is a stiffness variation factor (Bureau Veritas, 2014).

$$\Delta\sigma_{combined} = Z_{corr}(\Delta\sigma_{TT} \pm Z_s\Delta\sigma_{OPB} \pm Z_s\Delta\sigma_{IPB}) \tag{3.13}$$

Considering environmental conditions

SN-curves for free corrosion in sea water are to be used for OPB calculations. An SN-curve for air can be used if the fairlead location is far from splash zone, either 5 meters above free surface, or 110 % off relative wave elevation at mooring line location with a probability of occurrence of 5 %. The most critical situation is to be chosen.

If cathodic protection is utilized, which is generally not considered for OPB, a detailed plan for inspection and maintenance for the first six links must be made for approval. The SN curve characteristics used for the combined fatigue calculations are included in Figure 3.7.

Environmental Case	First slope		Second slope		
	$\log K_1$	m_1	$\log K_2$	m_2	$\Delta\sigma$ at $N = 10^7$ cycles
Seawater free corrosion	12,436	3	No second slope		
Seawater under cathodic protection	14,917	4	17,146	5	106,97
Air	15,117	4			
Note 1: Other SN curves may be defined by the designer provided they are documented by a sufficient amount of fatigue tests.					

Figure 3.7: SN curves (Bureau Veritas, 2014)

Rainflow counting is used to find the fatigue stress cycles for each sea state from combined stress time series. The fatigue damage is then obtained by Miner sum of individual cycle damage d_i.

$$d_i = \frac{\Delta\sigma^m_{combined}}{K} \tag{3.14}$$

Damage from one sea state is defined as Equation (3.15).

$$d_{ss} = \sum_{cycles} \frac{\Delta\sigma^m_{combined}}{K} \tag{3.15}$$

K is calculated as in equation (3.16).

$$K = N\Delta\sigma^m_{combined} \tag{3.16}$$

The total fatigue damage during the design life L_D is calculated by Equation (3.17). This includes all set of sea states with the probability of occurrence p_{ss}. N_{SY} is defined as the number of sea states per year, equal to 2922 sea states for 3 hours (Bureau Veritas, 2014).

$$D_{total} = \sum_{SeaStates} = p_{ss}N_{SY}L_D d_i \tag{3.17}$$

The Guidance Note by Bureau Veritas, addressing combined loading from bending and tension, is comprehensive and depends on defining a big range of variables. However, they are the only specific OPB guidelines available today.

3.5 Industry Developement

Investigating out of plane bending has previously been done by performing full-scale tests and supporting the results by FEA. It is, however, difficult to form an FE-model that represents the real conditions of the material regarding corrosion and surface defects. The problem is related to the FE-model and -software, unable to reproduce the true interlink stiffness as the effective contact area cannot be modelled. As there are many factors affecting mooring integrity, there are also many factors affecting out of plane bending. Some of these needs further investigation to fully understand and consider OPB for a mooring analysis and fatigue calculations.

Fatigue is usually calculated from SN-curves, but there are no standard SN-curves for OPB due to lack of data. To account for OPB it is proposed to use additional SCF, but there are no general SCF available as they are case-dependent (API, 2015).

FEA should be able to give some predictions of how the upper chain section is responding to out of plane bending. If this is to be done, there must be a certainty that the FE-software predicts and reproduces the same material responses as on site. This includes a realistic contact behavior and friction as well as material loss from corrosion. FEA could also be used to study fatigue and crack initiation and propagation from OPB due to the friction and interlink stiffness, as well as using FEA to find a general approach to include SCF in fatigue calculations.

Regarding mooring systems, it is important to be aware of all elements influencing the system in a negative way. The dynamics of the system must be understood and not just by the ones doing the mooring analysis, but also the ones operating it offshore. Precautions must be taken with respect to the unknown, but predicted influence of corrosion and wear, and extra safety factors added where the system is exposed to bending stresses.

Incidents related to the failure of a mooring line have had a high rate over the past decade often occurring at interfaces or discontinuities of the line, such as at the vessel connection, chain stoppers, connected buoyancy elements, and clump weights. While some of these events could have been prevented through a quality increase of inspection and monitoring, links subjected to OPB are often hidden inside trumpets or hawse pipes at the vessel interface making detection through GVI (general visual inspection) difficult. Offshore units are also moved further offshore introducing a subsequent increase in chain size, material grade, and line pretension (Ma et al., 2013).

In addition to having units located onto deeper waters, operations are commenced in new environments. This can introduce more severe weather conditions such as in the cyclonic areas, or more environmental sensitive areas such as the Arctic's. Any failure resulting in a release of hydrocarbons in sensitive areas would be unacceptable, and an update in design criteria is thus required. As a review of historic failures has illustrated, a mooring failure is typically the result of fatigue, manufacturing, installation and OPB, not pure overload. Increasing the design criteria and introducing stronger lines for more severe sea states is therefore not the simple solution. Investigating the previously-mentioned failure modes is important for a development of new and better mooring designs (Ma et al., 2013).

Another critical and debated challenge within the industry is life extension. This is usually done by an approval from class, requiring an up-to-date status of the line to estimate remaining life. For systems operating deep water the total line length to be inspected can be up to 75 km (Ma et al., 2013). In addition to great lengths and numerous components comes the complication of poor vision due to darkness and marine growth.

Chain and shackle components estimate life from measuring key components of remaining material. The estimation of links subjected to OPB can be difficult. They are often unreachable during inspection and the sensitivity of an operative parameter change is not well investigated or documented. There are no general standards, SN curves are non-existing, and values for calculations are case-dependent (Ma et al., 2013). An interest in how existing values will fit to new cases is the background for the second and following part of this thesis.

Chapter 4

Finite Element Modelling

4.1 Full-Scale Tests

DNV GL has recently performed full-scale tests of chain links to investigate the effect of out of plane bending. The links included in the tests had a nominal diameter Ø = 175 mm, which exceeds dimensions previously investigated and covered by existing literature. It is of interest to see if values provided from scientific literature is a fit also for the project. During testing, the effect of varying the proof load and pretension was also investigated (Carlberg E., DNV GL, 2017).

Seven links were used for the test, all studless of steel grade R4. Link 1 is fixed and restrained from any movement. This should represent actual operating conditions where this link is represented by the link fastened by the chain stopper or similar locking equipment. The next link, Link 2, and the interlink contact area is the area of interest as this is the first moving link and the link subjected to out of plane bending. This link was equipped with measuring instruments to measure local strains and inclination. Constant tension and a vertical displacement was applied to Link 7. The tension was 300 tons and was always in line with the link's original horizontal plane. Vertical movement was ±290 mm and the first two links were tested in both air and seawater. Maximum interlink angle achieved by this test rig illustrated in Figure 4.1 was ± 3 °.

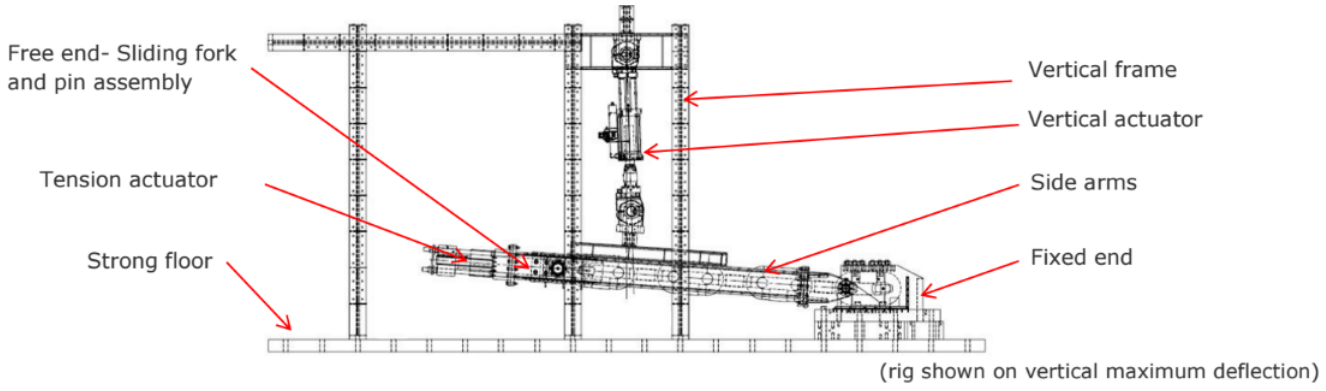

Figure 4.1: Testing configuration DNV GL (Carlberg E., DNV GL, 2017)

Large diameter links are making an entrance to the industry, but there is still an existing gap in literature when it comes to OPB, wear, and effect of different surface treatments. As found in the literature study in Chapter 2, OPB represents an area of uncertainty. By gathering high quality data for larger chain sizes, higher steel grades, and surface conditions, it should be possible to optimize the mooring system design and reduce the overall cost of the system in addition to finding life-extension solutions. This could possibly be achieved by full scale testing of larger chains and further development of the FEA methodology for OPB (Carlberg E., DNV GL, 2017).

The links investigated by DNV GL are manufactured by Vicinay with geometry as illustrated in Figure 4.2. Table 4.1 represents data for the test links, studless R4 Ø 175 mm chain corresponding to DNV OS-E302 (Vicinay, 2016).

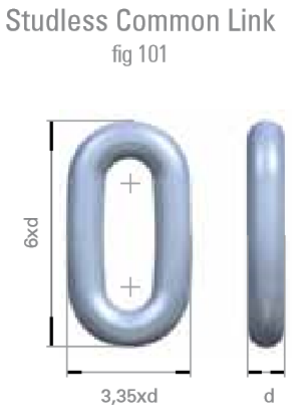

Figure 4.2: Chain Link Geometry Vicinay (Vicinay, 2016)

Table 4.1: Chain Link Parameters (Vicinay, 2016)

Parameter	**Definition [Unit]**	**Value**
Diameter	Ø [mm]	175
Straight Part	L [mm]	463.75
Z	D^2(44-0.08d)	918750
Proof Load	0.0192*Z [kN]	17640
BreakLoad	0.0274*Z [kN]	25173.75

4.2 Finite Element Modelling of a 7-link Model

4.2.1 Non-Linear Analysis

Non-linear effects in models and structures can occur within the geometry, material, or boundary conditions. Geometric non-linearity will affect equilibrium and kinematic compatibility of the model as it experiences larger geometric changes which will alter structure stiffness. Material non-linearity affects the stress-strain relationship. When applied load exceeds a limit called the proportionality limit σ_P, the relationship between stress and strain can no longer be assumed to follow the linear Hooke's relationship in (4.1).

$$\sigma = \epsilon E \tag{4.1}$$

Any load resulting in a stress increase above the proportionality level σ_P, leads to an elastic-plastic non-linear response within the material. Increasing the load further, the material will reach the yield stress. For brittle material, this stress corresponds to a pop-in event, while for ductile alloys a smooth transition occurs. The yield stress for ductile materials is usually defined at 0.2 % plastic strain, expressed as $R_{p0.2}$. Unloading form a condition where the stress has reached σ_P, follow a straight line as illustrated by the dashed line in Figure 4.3, parallel to the linear relationship (Moan, 2003). Thus, applying loads of great magnitude leaves behind residual plastic strain ϵ_P, and a deformed surface at material boundaries. Regarding offshore chain links, the applied proof load is large enough to exceed σ_P and create the damaged mating surface. The material behavior for a nonlinear material is defined as in (4.2) where ϵ^P is the plastic contribution to the strain increment. H is the hardening function of the yield surface as it is modified under plastic flow (Moan, 2003).

$$\sigma = H(\epsilon^P) \tag{4.2}$$

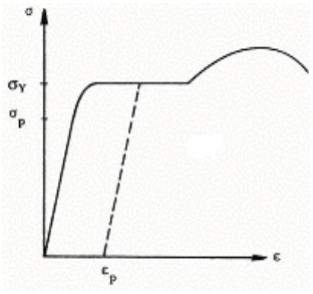

Figure 4.3: Stress-Strain curves for metals (Moan, 2003)

Non-Linear FEA

A finite element analysis represents a simplified model of an actual structural behavior and sensitivity studies should be included in the work process to verify achieved results. Many parameters are decided by the engineers during the process of creating an FE-model and it is important that the choices are both conservative and realistic compared to the real life behavior of the structure. Parameters for consideration are element types, mesh size, material curves, imperfections, and residual stresses from manufacturing (DNV GL, 2016).

When it comes to mesh size, it is important that final mesh has reached a converged solution before starting to extract values for results and analysis. For this FEA, the residual stresses in the material are only the ones left by the proof load, introducing the assumption of neglecting stresses from bending and different heat treatments from production.

Elastic - Plastic Material Models

The material model for the FEA must reproduce the non-linear behavior of steel grade R4. The time independent elastic-plastic model used for a non-linear analysis contains the following main components (DNV GL, 2016):

- A yield surface defining where the plastic strains are generated. Commonly used for steel materials is the Von Mises plasticity. This model assumes that the yield surface is unaffected by the level of hydrostatic stress (Moan, 2003).
- A hardening model defining how the yield surface is altered by the plastic strains. This can be defined as isotropic hardening, kinematic hardening, or a combination of both. The hardening rule is of importance for analysis including reversed load such as the proof load applied for chain links. This is due to something called the Bauschinger effect, where a material model using a combined isotropic and kinematic hardening rule should be applied. This is relevant if the yield strength will increase in one direction of plastic flow and decrease in the other from plastic deformation (Moan, 2003).
- A flow rule where the flow potential defines the relation between the plastic strain increment and the stress increment. The yield surface is often utilized as a flow potential or an associated flow (DNV GL, 2016).

The difference between kinematic and isotopic hardening is illustrated by Figure 4.4. When isotropic hardening is applied, the yield surface expands evenly in tension and compression even if the load is pure tensile. This implies that the material properties are equal in all directions. The yield surface will keep its shape, but expand in size. Kinematic hardening includes a softening in compression due to a hardening in tension. The yield surface shape will remain constant and only translate in the stress-space (Moan, 2003). The difference of the yield surface modification under hardening is illustrated by Figure 4.5.

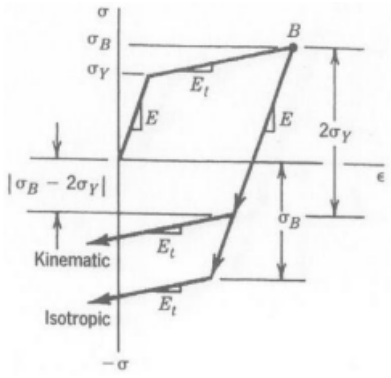

Figure 4.4: Kinematic and isotropic hardening rules (Moan, 2003)

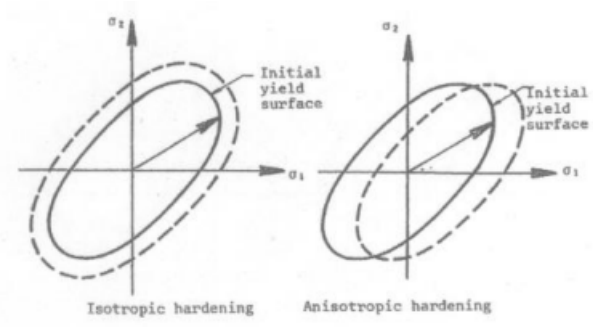

Figure 4.5: Kinematic and isotropic hardening yield surface (Moan, 2003)

Reasons for applying proof load to the chain links are not only related to testing of material strength, but also done to reach a state and a plastic phenomenon called *Elastic Shakedown*. This is reached after hardening of the material is commenced and the unloading behavior occurs with a linear elastic behavior that results in no further yielding of the material. The material has reached shakedown when the stress-strain relation from load and unload will continue to follow a stabilized linear constant line. This is an assumed settled elastic state, where the high magnitude of the previously applied load prevents further elongation during regular operation of the material. Illustrated by Figure 4.6, shakedown is seen by the stable motion between point B and C. This is desirable to prevent another plastic phenomenon to take place called ratchetting, also known as cyclic creep. If this were to occur, increments of plastic strain would continue to grow and lead to final failure (Moan, 2003).

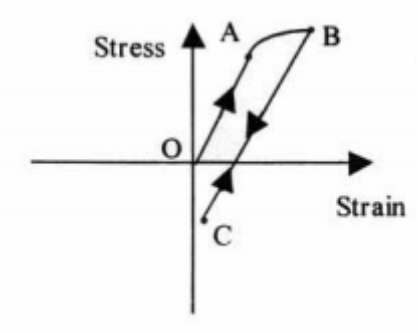

Figure 4.6: Elsatic shakedown (Moan, 2003)

The FE software utilize the true stress strain relation which is updated continuously due to plastic change of the material under loading. The relationship between the engineering strain and stress and the true strain and stress are defined in Equations (4.3) and (4.4).

$$\sigma_{true} = \sigma_{eng}(1 + \epsilon_{eng}) \tag{4.3}$$

$$\epsilon_{true} = ln(1 + \epsilon_{eng}) \tag{4.4}$$

Strain values in the FE-model are discrete values, and depend on the element size, element type, and material model. The mesh must therefore be validated and re-meshed to provide a converged and correct solution. Strain values collected from element integration points are calculated based on the element deformations, and nodal averaged value might be lower than at the element if the intersecting points are loaded. The boundary conditions applied for a non-linear analysis are supposed to represent the real conditions, such that they provide a safe and accurate solution. Sensitivity studies are used to find the best ones (DNV GL, 2016).

4.2.2 Developing an FE-Model

The second part of this thesis is the development of a 7-link FE-model in ABAQUS CAE to replicate DNV GL's full-scale tests. If the FEA results are a good fit to the full-scale test results, findings can be used to offer suggestions for further work regarding guidelines for out of plane bending.

Model Geometry

The links modelled in ABAQUS CAE have a nominal diameter Ø = 175 mm and the link dimensions are illustrated in Figure 4.7, representing the links manufactured by Vicinay (Vicinay, 2016).

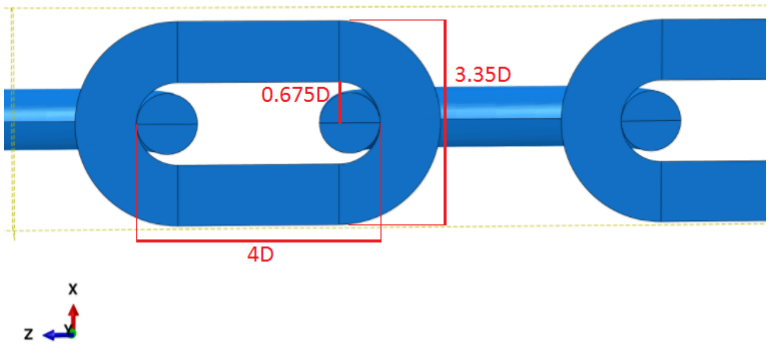

Figure 4.7: ABAQUS CAE Model - Chain Link Geometry

Three or four independent parts are used to build one half link, symmetric around the y-axis to save computational time. The parts are merged together by surface to surface tie constraints. Independent parts are meshed independently, beneficial as it allows the interesting contact area between Link 1 and 2 to have a finer mesh grid. The tie constraint offers the ability to use a non-matching mesh between merged parts.

R4 Material Model

Chain links used for mooring of offshore units are divided into five grades; R3, R3S, R4, R4S, and R5. The given grade is dependent on the nominal tensile strength of steels for manufacturing. Each grade must be approved individually prior to operational use, where tests for approval include different fracture mechanics tests in addition to break and proof load. After successful testing, approval is given by the society (IACS, 2009).

The steel used for the full-scale test had the grade R4. This is a higher strength steel, which also requires testing for hydrogen embrittlement. As mentioned in Section 2.1.2, the increased use of higher strength steel for structures moving further offshore also increases the risk of hydrogen induced cracking (HIC). This is a factor that can lead to sudden and unforeseen cracking of the links (IACS, 2009).

The values for the elastic and plastic part of the material model are provided and developed by DNV GL based on the Ramberg-Osgood relation in Equation (4.5) where K is a grade-dependent value (DNV GL, 2016). The stress strain relationship for the plastic part is illustrated by Figure 4.8 and values are included in A.1 (DNV GL and Kapella, 2017).

$$\epsilon = \frac{\sigma}{E} + (\frac{\sigma}{K})^{10}. \tag{4.5}$$

E modulus: 206600 MPa
Poissons ratio: 0.29-0.33

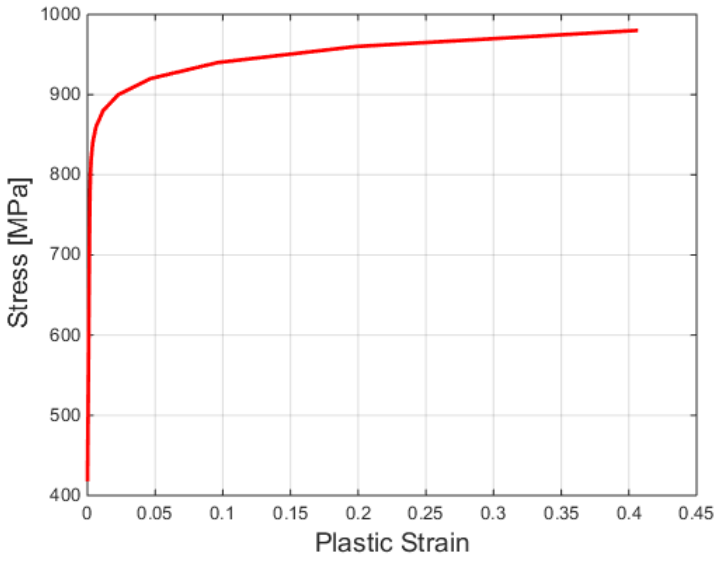

Figure 4.8: Material Model R4 - Steel

All parts of the model consist of the same material and hardening is defined as isotropic. The Poisson ratio was given the value 0.3 for the analysis.

Contact and Interaction

When modelling with contact surfaces, a master surface and a slave surface is chosen defining the slave surface as the one with the finest mesh. The Master Slave Technique is a way to reduce the degrees of freedoms present in a model, and this way reduce computational time and storage space (Langen and Sigbjörnsson, 1980). Contact is modelled as surface to surface.

The contact property settings consist of a tangential and a normal part. The tangential part is defined by a penalty based friction formulation with isotropic directionality. The normal behavior is defined as hard contact, which will minimize the penetration of contact nodes (Moan, 2003). Contact is further defined by a finite-sliding tracking approach, which allows arbitrary movements between the contacting surfaces. Friction coefficients are dependent on the operative environment and sat to be the same as for the 2016 JIP, respectively μ=0.3 for seawater and μ=0.5 for air (Rampi, Bignonnet, Cunff, Bourgin and Vargas, 2016).

Boundary Conditions and Loading

Developing a non-linear model in ABAQUS CAE can be challenging due to convergence problems at the contact areas. Applying the load through an MPC reference point (Multi Point Constraint) connected to Link 7 is a functioning solution, although an MPC introduces additional degrees of freedom to the system. Tension force is transferred through the final link and will follow nodal rotation when the vertical displacement is applied through the same reference point. Only half of the cross-sectional area is modelled due to symmetry, and thus is half of the original load magnitude applied. This represents proof load of 8820 kN and operational pretension of 1500 kN. The MPC reference point utilized for pretension and displacement is illustrated in Figure 4.9. The load sequence is illustrated by Figure 4.10 and the step sequence is done in the following order:

1. Apply proof load: 17640 kN / 8820 kN
2. Apply constant tension: 3000 kN / 1500 kN
3. Apply displacement of link 7 + 290 mm, or until sliding motion is reached.

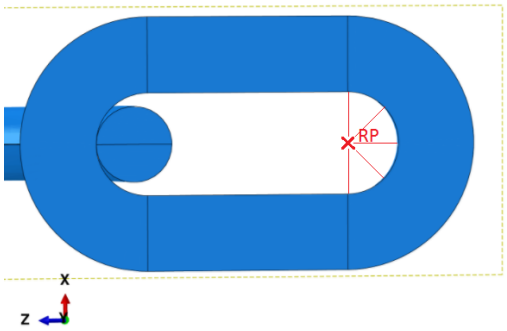

Figure 4.9: Load applied through MPC reference point connected to end of Link 7

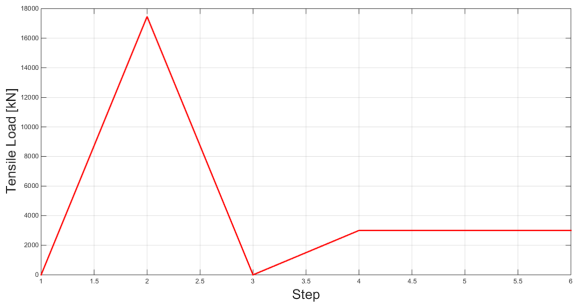

Figure 4.10: Illustration of Load Sequence

Boundary Conditions

To save computational time, only half of the link's cross-sectional area is included in the FE-model. Symmetrical boundary conditions are therefore applied to the symmetry plane in y-direction. Link 1 must be fixed against rotation and translation in the displacement step to replicate the full-scale test. This does not apply for the step where the proof load is applied, as Link 1 should experience the same plastic deformation as the other links. Proof load of the full-scale links was not done during the full-scale tests by DNV GL, but is included in the simulation to replicate this stage of the chain manufacturing process. For the first step, only part of the first crown of Link 1 is fixed against translation as illustrated in Figure 4.11. Two different boundary conditions (BC) are further investigated to simulate the locking equipment.

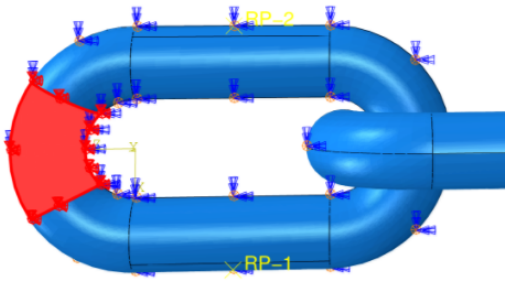

Figure 4.11: Boundary Conditions for Proof Load

Boundary Condition 1 - Clamped Boundary conditions (BC1)

This model has clamped sections applied to Link 1 as rigid bodies. A rigid body is defined in ABAQUS CAE as a collection of nodes and elements whose motions is governed by the motion of a single node, a rigid body reference node. The shape of the rigid bodies will not change during the analysis and will only experience rigid body motions by applying boundary conditions to the rigid body reference node (Abaqus Analysis User's Manual, 2016). A concentrated load is applied to the rigid bodies through the reference point and further distributed to the elements included in the rigid parts. A rigid body is used to model very stiff and fixed components, a fit to represent the frame that held the first link in place during the full-scale test. Figure 4.12 illustrates how in the visualization, the rigid parts are unaffected and not at all deformed.

One advantage of using rigid bodies as part of the boundary conditions, is decreased computational time as element-level computations are not performed for elements part of the rigid body. The motion is solely defined by the motion of the reference node and the six degrees of freedom appearing in that area (Abaqus Analysis User's Manual, 2016). The reference node is restrained from motion in five degrees of freedom, all but translation in the x-direction where it is applied a small load to clamp the parts to the straight part of Link 1. The clamps are modelled as shells and will further be locked in the current position for the displacement step.

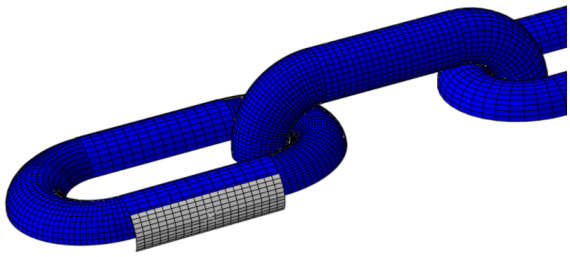

Figure 4.12: BC1 - Clamped Boundary Conditions

Boundary Condition 2 - Constrained Boundary conditions (BC2)

This boundary condition does not include clamps and the straight parts of Link 1 are fixed in the current position to keep the link from experiencing any rigid body motion in Step 3. The boundary condition is illustrated by Figure 4.13. Step 1 and 2 has boundary conditions as illustrated in Figure 4.11.

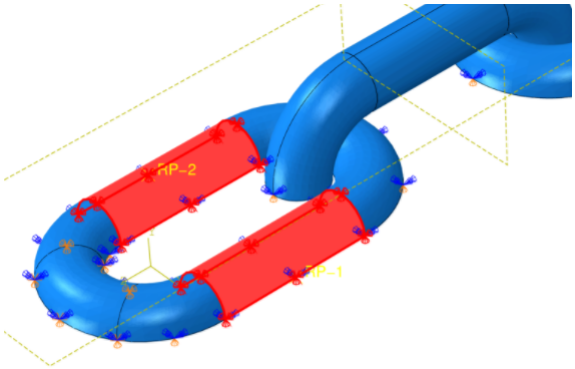

Figure 4.13: BC2 - Constrained Boundary Conditions

Comparison of Clamped and Constrained Boundary Condition

A comparison of the interlink stiffness for Boundary Conditions 1 and 2 is included in Figure 4.14. From consulting with DNV GL, it is clear that the clamped boundary condition (BC1), representing the stiffer interlink stiffness, replicated the behavior from the full-scale test set-up best. This boundary condition was implemented onto the final FE-model.

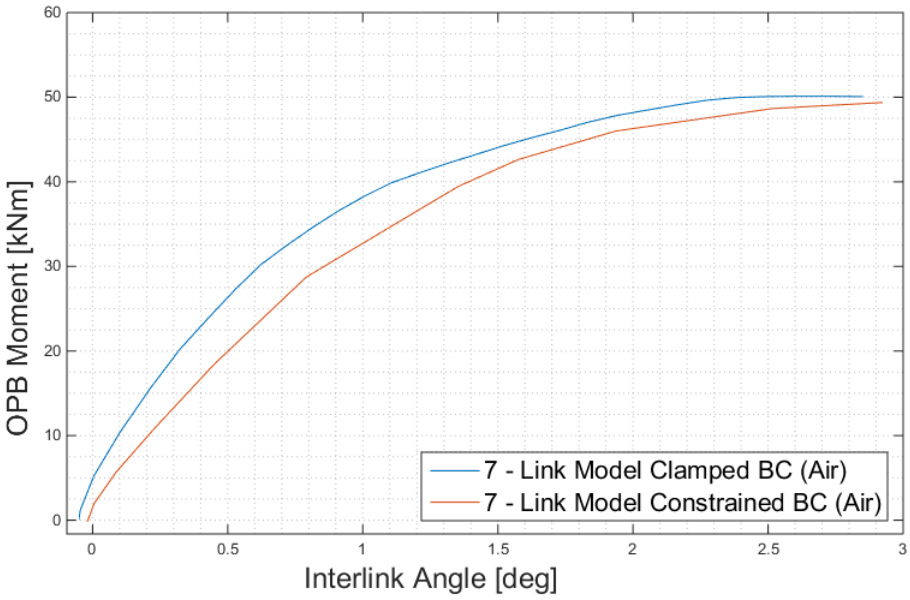

Figure 4.14: Comparison of Boundary Conditions 7-link Model

It is noticed that the simulated interlink angles have a small negative start angle of -0.05°. Figure 4.15 compares the vertical displacement in Link 2 for BC1 and BC2. The results are similar, but the negative start angle is still more evident for the clamped boundary condition (BC1).

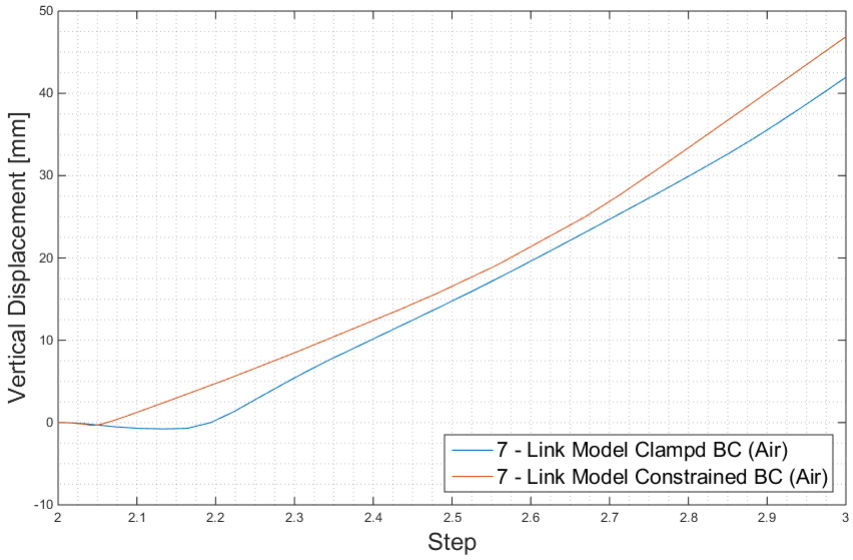

Figure 4.15: Comparison of Displacement of Link 2 for Clamped and Constrained BC for a 7-link Model

Boundary conditions and loads applied to the final model are listed in Table 4.2.

Table 4.2: Boundary Conditions applied per simulation step

Step	Boundary Conditions Link 1	Boundary Conditions Link 7
1	Crown fixed	T = 17640 kN
2	Link Fixed by Clamps	T = 3000 kN
3	Link Fixed by Clamps	T = 3000 kN Vertical Displacement = + 290 mm

Comparing a 3-link Model and a 7-link Model

A 7-link FEA requires much computational time, but it has previously been proven that the interlink stiffness is different for models with three and seven links. A master's thesis investigating OPB by Nilakesh Das in 2016 concluded that if more than seven links are included, the reactions between Link 1 and Link 2 is independent of additional links and boundary conditions (Das, 2016). A comparison of the interlink stiffness of a 7-link model and a 3-link model is included in Figure 4.16, where it is seen that the 7-link model provides a stiffer interlink stiffness.

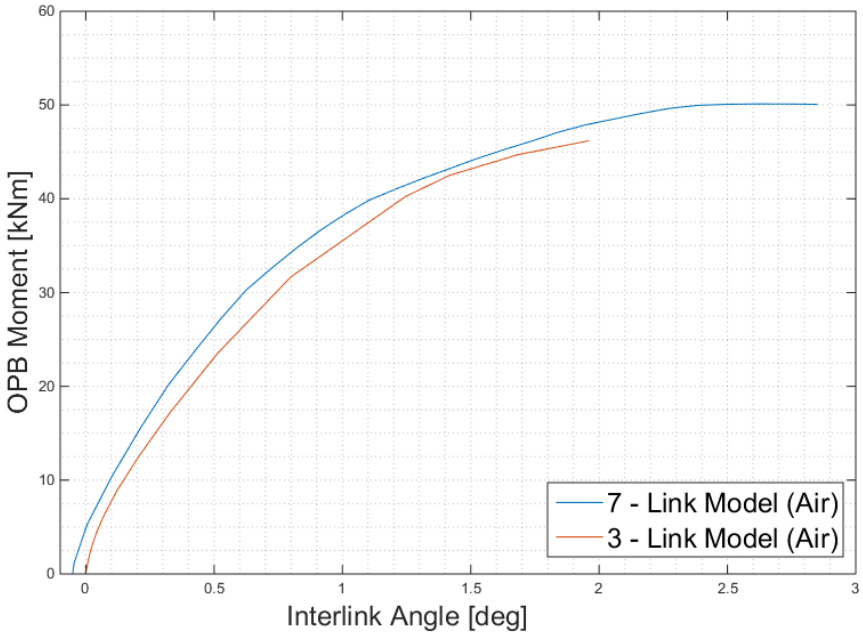

Figure 4.16: Comparison of a 7-link Model and a 3-link Model with Clamped Boundary Conditions

Also seen from the comparison in Figure 4.16 is the negative start angle of -0.05° for the 7-link model, whereas the 3-link model has a start angle closer to 0.0°. This is further investigated by plotting the vertical displacement of Link 2 in Figure 4.17 for both models. For a 3-link model the vertical displacement is steadily in positive direction. This indicates some retarded motion by the addition of multiple links, not representing straight beam element behavior.

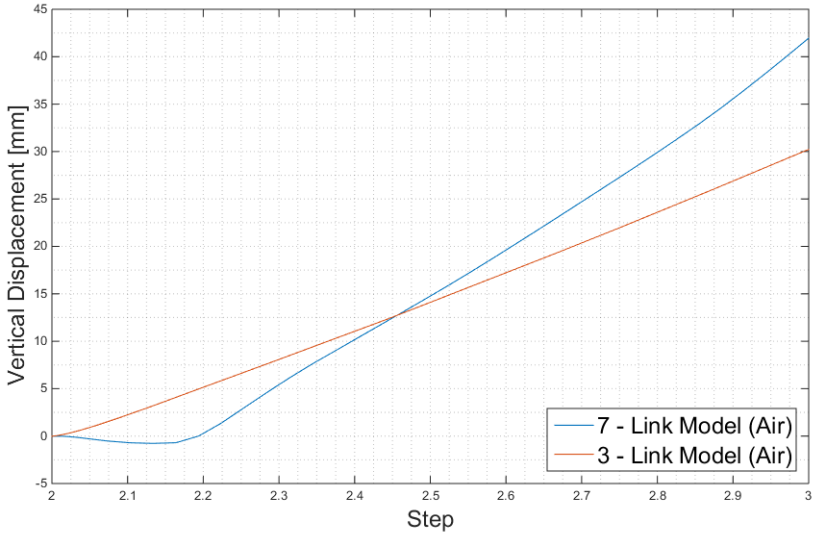

Figure 4.17: Comparison of a 7-link Model and a 3-link Model - Displacement of Link 2

4.2.3 Verification

Mesh and Convergence test

Convergence testing is done to verify that the obtained solution is converged. Due to some complications, the test is performed in two phases. Phase one is a test on a 3-link model to save computational time. As for the 7-link model, the load is applied through an MPC-point. Four tests are run, respectively with coarse, medium, and fine mesh, in addition to one test where the mesh is refined in the areas of contact and coarser at the edges. The contact area between Link 1-2 has the finest mesh also for this model, and the mesh sizes in test 1-4 are illustrated by Figure 4.18 through Figure 4.21. Applied elements are linear C3D8R elements. This is an 8-node brick element with reduced integration, hourglass control, and one integration point.

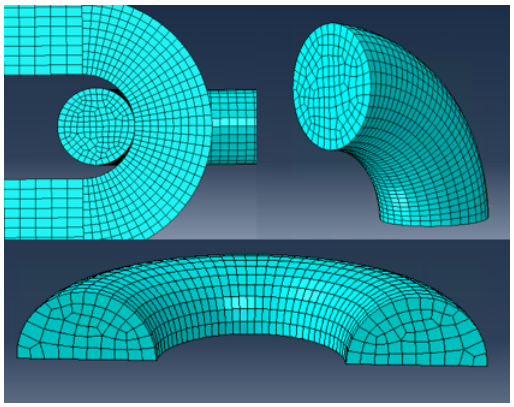

Figure 4.18: Test 1 - Coarse Mesh

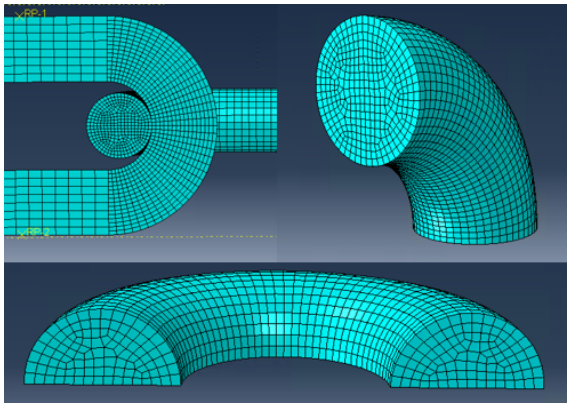

Figure 4.19: Test 2 - Medium Mesh

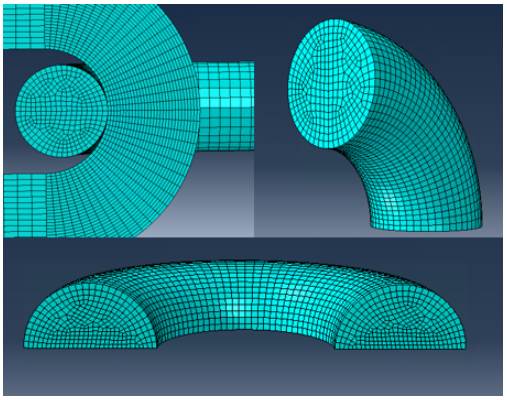

Figure 4.20: Test 3 - Fine Mesh

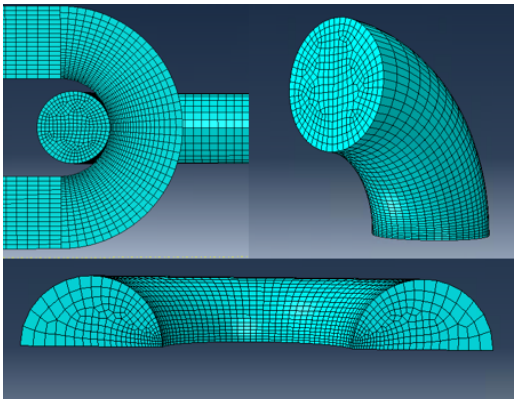

Figure 4.21: Test 4 - Refined Mesh at contact

Figure 4.22 illustrates the stress in the direction of the applied tensile proof load, 3 being Z-direction. The stress is measured over the final crown of Link 1 in contact area 1-2.

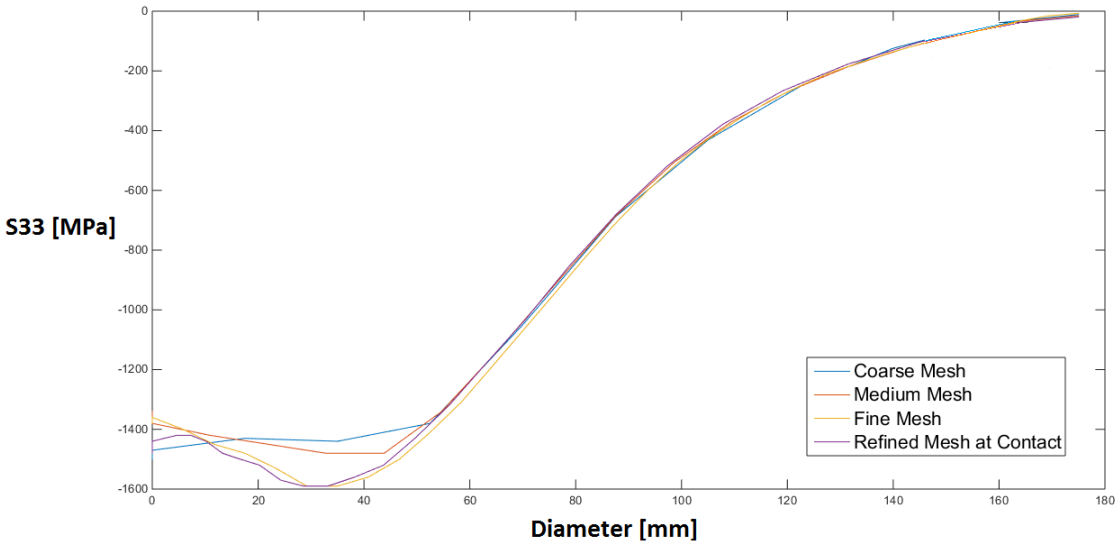

Figure 4.22: Results form the Mesh Convergence Test

Test 1-4 provide a converged solution after 50 mm as illustrated in Figure 4.22, while the measured stress varies in the contact area. This verifies previous statements regarding how the contact area represent a complex region where stresses easily can be wrongly estimated. The result from Test 3 and 4 show a similar trend after 5 mm, but also for these tests, a visible gap in stress values at point of contact.

Using a refined mesh grid at the contact area can result in more accurate simulations and provide a better geometrical fit for the mating area between the links. Figure 4.23 and 4.24 illustrates the size of the contact surface between Link 1 and Link 2 after proof load for Test 1 and Test 3. This comparison shows a slight increase of mating area when using a finer mesh.

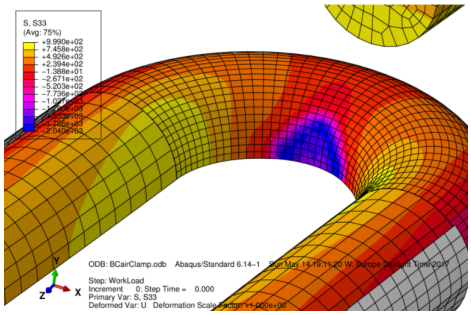

Figure 4.23: Mating Area after proof load - Coarse Mesh

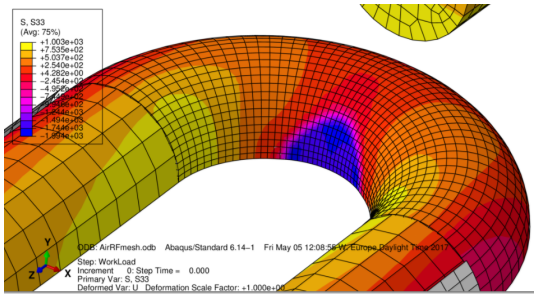

Figure 4.24: Mating Area after proof load - Fine Mesh

Source of Error

The mesh tests from phase one were done with a friction coefficient representing seawater μ=0.3. When this parameter is altered to μ=0.5, the model from Test 3 and 4 does not complete the analysis due to convergence issues. Proof load is applied in dry conditions, and the previous tests are not a representation of real manufacturing conditions. The decision to include the previous figures, representing Figure 4.18 through Figure 4.24, was taken to illustrate the sensitivity of the mating area when simulating OPB behavior. Mesh corresponding to the coarse grid (Figure 4.18) and slightly finer grid than the medium mesh grid (Figure 4.19) is further implemented on a 7-link model for phase two. The resulting stress in Z- and tensile direction is plotted in Figure 4.25 over the same diameter as in 4.22 showing a similar trend for both curves, but some differences in the contact area.

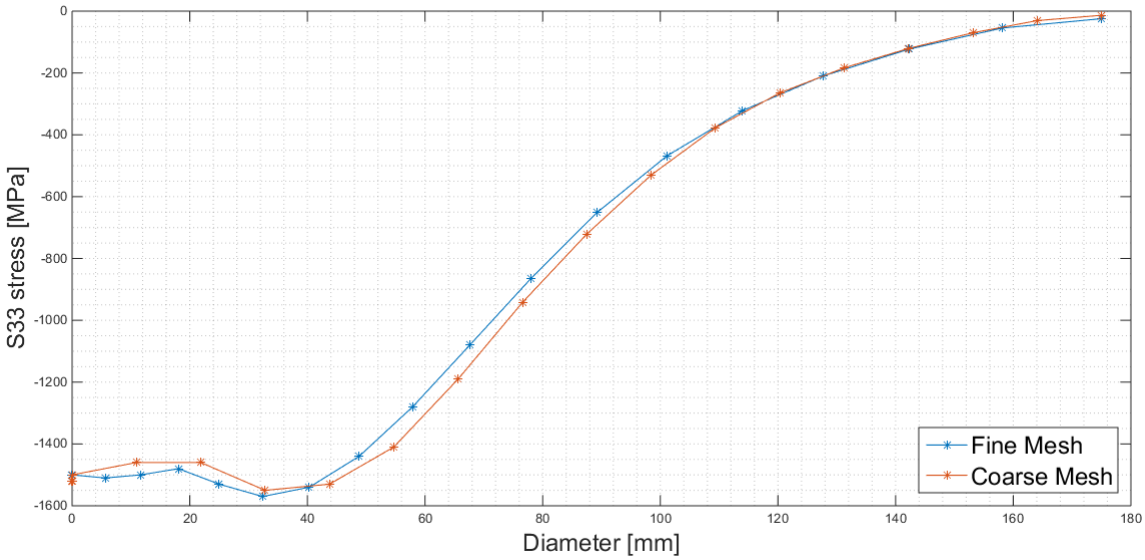

Figure 4.25: S33 stress in a 7-Link Model after proof load - Coarse and Fine mesh

As a conclusion from the convergence tests, the mesh size at the contact area is highlighted as a source of error when using FEA to produce the interlink stiffness. The contact area is dependent on mesh size, element type, and contact properties at surface. As the solution has converged, the coarse mesh is used for the final model to reduce computational time.

Energy Verification

The lack of information and literature for large chain links and load scales makes it difficult to verify results along the way. Verification of obtained FEA results is done by consulting DNV GL.

Static dissipation and stabilization is applied to achieve convergence at contact areas. Viscous damping help reaching a solution by automatically applying damping forces to local regions where sudden instabilities and severe discontinuities can occur. When stabilization is applied, the energy balance within the model must be verified to make sure the solution for the non-linear analysis is conservative and not applied excessive damping leading to a possible poor response within the structure. The total internal energy (ALLIE) is compared to the viscous damping energy (ALLSD) for this purpose in Figure 4.26, where ALLSD should be less than 5 % of ALLIE (OPTIMEC Consultants, 2017).

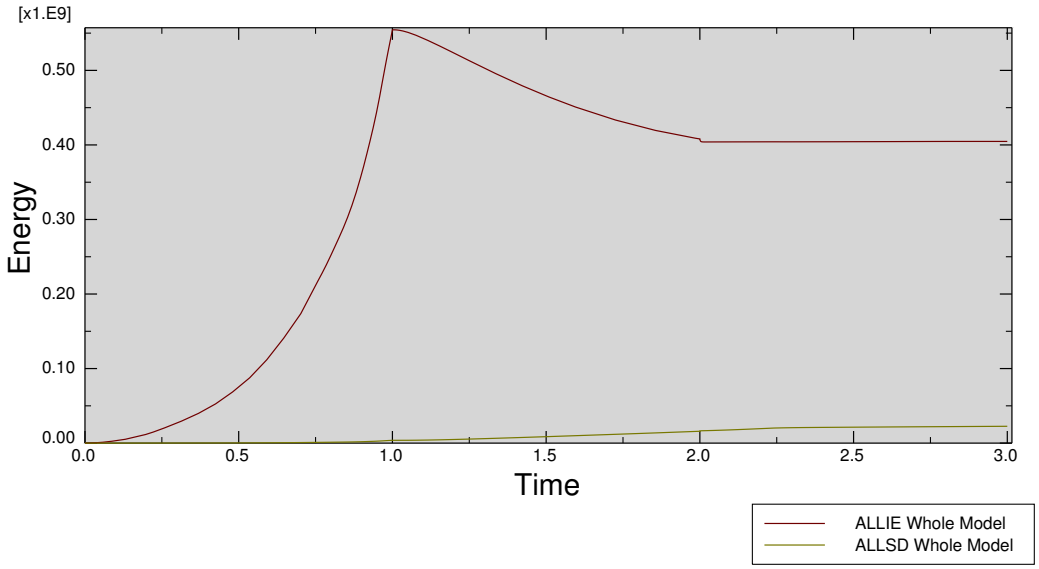

Figure 4.26: Comparison of Internal Strain Energy and Viscous Damping Energy

As illustrated in Figure 4.26, the level of damping is well within the criteria for the first two steps, but increases to approximately 5 % for the final phase of the displacement step. This is close to the acceptable limit.

Hourglass Control

Linear first order elements of type C3D8R are used for the simulations, whereas some sources state that these elements tend not be stiff enough when exposed to bending. This would lead to a poor representation of measured displacements, arising from zero energy modes connected to the elements (Dhondt, 2014). Response from zero energy modes are non-physical and connected to use of coarse mesh and a phenomenon called hourglassing. First order reduced integration elements like C3D8R can respond too flexible due to hourglassing, and the elements are deformed under bending moments leading to zero magnitude of shear and normal stresses in the integration points. This results in zero strain energy related to bending and deformation, propagating into to poor results (Sun, 2006).

To avoid hourglassing, C3D8R elements are applied hourglass control. This can be verified by comparing the artificial strain energy (ALLAE) against the internal energy (ALLIE), where ALLAE must be less than 1 % of ALLIE. This verification is illustrated in Figure 4.27 and is seen to be within acceptable limit. Applied elements are kept for further simulations, but its use should be discussed when verifying obtained results.

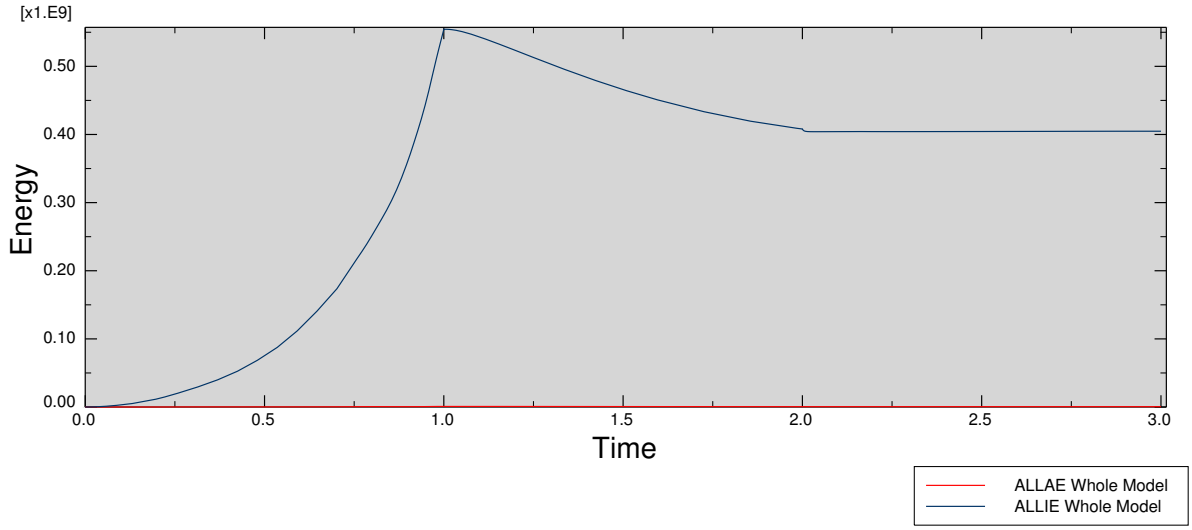

Figure 4.27: Comparison of internal energy and artificial strain energy for original conditions and model

4.2.4 Calculations and Post-Processing

ABAQUS CAE does not have units and consistency is thus important. Table 4.3 lists the ones used in the finite element modelling for input and output parameters.

Table 4.3: Consistency Units

Parameter	Unit
Length	[mm]
Force	[N]
Stress	[MPa]

Some areas are highlighted in Figure 4.28 for collecting data for post-processing of results. The mid node of crown 1 and 2 of Link 2 collects vertical and horizontal displacement for interlink angle calculations. An assumption of no excessive geometric bending in the straight part of Link 2 is introduced. Stress and strains are gathered throughout all steps from pre-selected elements in the straight part of Link 2 and further used to calculate the OPB moments.

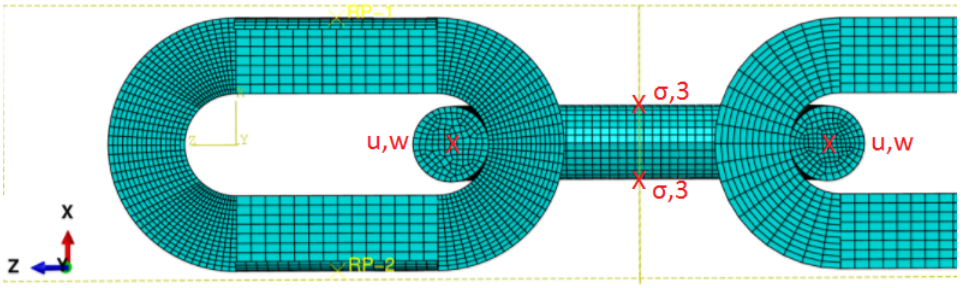

Figure 4.28: Nodes and Elements of interest for Post-Processing ABAQUS CAE

To investigate the interlink stiffness, the OPB Moment in the first free link is plotted against the interlink angles between two adjacent links. The following procedure is used to present the results of the 7-link FEA.

Interlink Angle

The interlink angle is defined as the angle between two chain links, located between Link 1 and Link 2 for this model. The interlink angle is defined as illustrated by Figure 4.29.

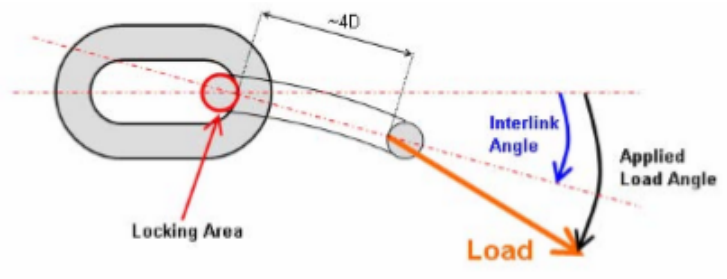

Figure 4.29: Definition of the Interlink Angle (ter Brake et al., 2007)

By monitoring the deflection in vertical direction of the midpoint in the crown of Link 2, the interlink angle is calculated by Equation (4.6) illustrated in Figure 4.30. The calculations take elongation of the link from tension forces into account.

$$\alpha = sin^{-1}\left(\frac{x}{5D}\right) \tag{4.6}$$

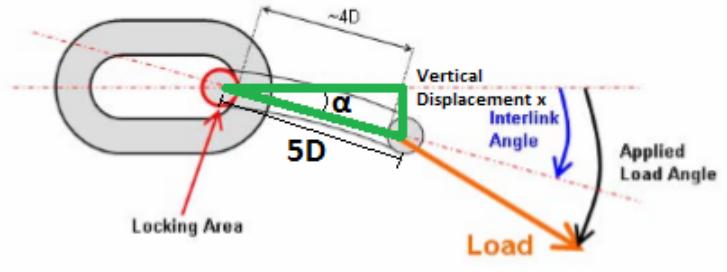

Figure 4.30: Interlink Angle (ter Brake et al., 2007) (modified by the author for illustration of calculation procedure)

OPB moment

Stress from bending in Link 2 is calculated by the Equation (4.7), extracting the OPB stress from tension stress when the bending curvature in the link is assumed to be small.

$$\sigma_{OPB,FE} = \frac{\sigma_{zz,A} - \sigma_{zz,B}}{2} \tag{4.7}$$

σ_{zz} is the normal stress along the z-axis gathered from elements in point A and B located diametrically opposite of each other on the straight part of Link 2 visualized in Figure 4.31.

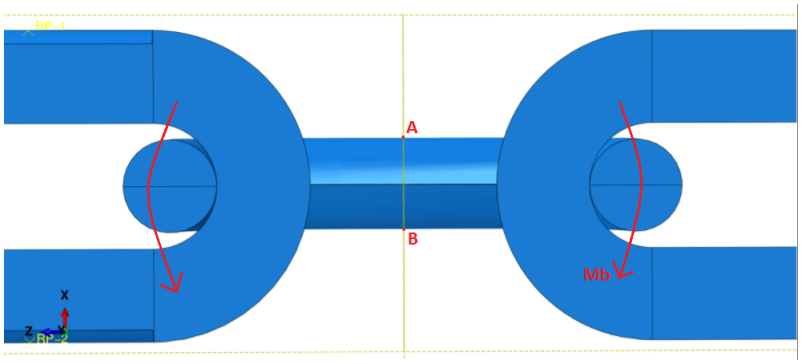

Figure 4.31: OPB Moment ABAQUS CAE

The OPB moment is further calculated from beam theory by the section modulus of Link 2, where the value **y** is defined as the radius of the link.

$$M_{OPB} = \sigma_{OPB}\frac{I}{y} \tag{4.8}$$

$$I = \frac{\pi D^4}{64} \tag{4.9}$$

$$M_{OPB} = 2\sigma_{OPB}\frac{I}{D} = \sigma_{OPB}\frac{\pi D^3}{32} \tag{4.10}$$

The variations of OPB moments inside Link 2 are assumed small and will be ignored for the calculations.

Comments

Linear C3D8R elements have only one integration point, located in the middle of the element. This introduces some insecurities related to the calculations of the OPB moment. A new model with a refined mesh on the straight part of Link 2 is used to locate the integration further towards the boundary. The results are nearly identical as illustrated by Figure 4.32, assuming that the stress variations inside the elements are small and that the solution is converged.

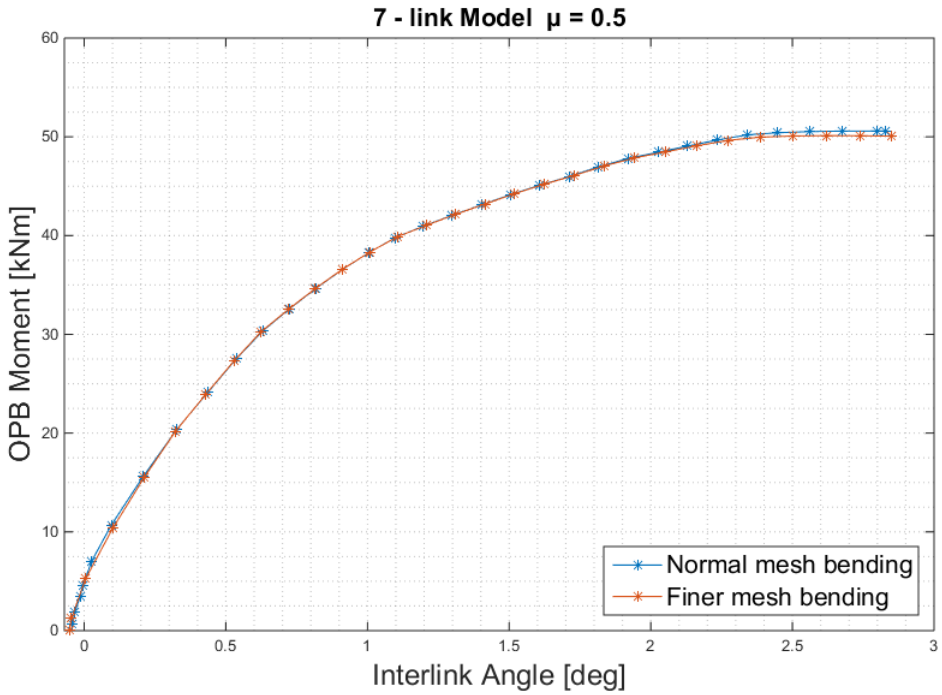

Figure 4.32: Refined mesh of Link 2 straight part

Full 7-link FE-model

The FE-model developed in ABAQUS CAE is illustrated by Figure 4.33, numerated as further referred to in the thesis.

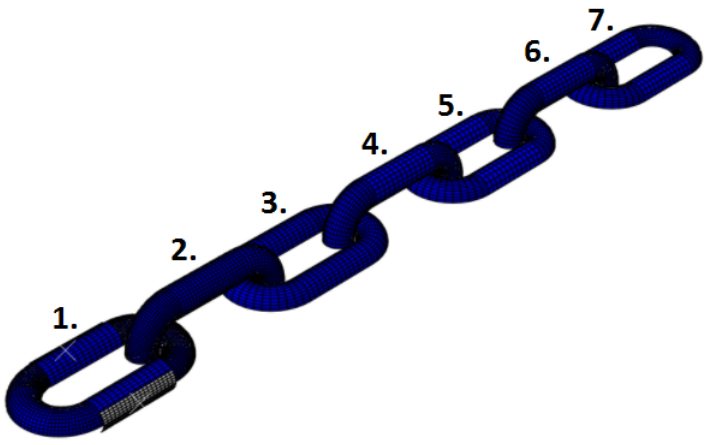

Figure 4.33: Full 7-link Model

4.3 Parameter Study

When a functioning model is developed, three parameters will be altered to investigate their influence on the interlink stiffness.

- **Test 1** - Friction coefficient (μ)
- **Test 2** - Pretension (T)
- **Test 3** - Proof Load (% of MBL)

The parameter study is done partly as validation to confirm that the model is behaving as expected, and because these parameters are dependent on the mooring system, environment, and manufacturer.

Test 1 - Friction coefficient

The friction coefficient (μ) is interesting to investigate as the mooring hang off location can either be fully submerged or located above the sea surface. μ also represents a complex parameter assumed to be linear for the analysis and thus representing a simplification. The influence of the friction coefficient is investigated by two sub-tests, representing environmental conditions of air and seawater defined in Table 4.4. The following tests, investigating pretension and proof load, are also tested for both environmental conditions.

Table 4.4: Test 1 - Environmental Effects

Test	**Friction coefficient μ [-]**	**Environment**
Test A	0.5	Air
Test B	0.3	Seawater

Test 2 - Pretension

Operative pretension is interesting to investigate as this is an individual parameter for individual mooring lines determined from the mooring analysis. It is also a parameter that can be altered during operation and has proven to have consequences when wrongly adjusted (Kvitrud A. for PSA, 2014). Three sub-tests are run for dry and submerged conditions defined in Table 4.5.

Table 4.5: Test 2 - Effect of Pretension

Test	Pretension [kN]	Percentage of MBL [%]
Test A	3000.00	12
Test B	3776.06	15
Test C	5538.22	22

Test 3 - Proof Load

The magnitude of the proof load is interesting to investigate as this is a process done by the manufacturer and is defined by level of obtained elongation of the independent link. The magnitude of the proof load is usually between 65 - 80 % of MBL, and the original value specified in the Vicinay catalogue represents 70 % MBL (Vicinay, 2016). Four sub-tests are run for dry and submerged conditions defined in Table 4.6.

Table 4.6: Test 3 - Effect of Proof Load

Test	Proof Load [kN]	Percentage of MBL [%]
Test A	16362.94	65
Test B	17640.00	70
Test C	18000.00	71.5
Test D	18376.84	73

Chapter 5

Results

The results from Test 1, 2, and 3 described in Section 4.3 are presented in this chapter. The results will further be discussed and explained in Chapter 6.

5.1 Test 1 - Environmental Effects

Figure 5.1 illustrates the interlink stiffness for the original 7-link test set-up. DNV GL compared them to the full-scale test measurements and concluded that the FEA results were replicating the behavior of the chain during testing in a good way. Test 1 proves that the model behaves as expected when simulating tests for dry and submerged conditions.

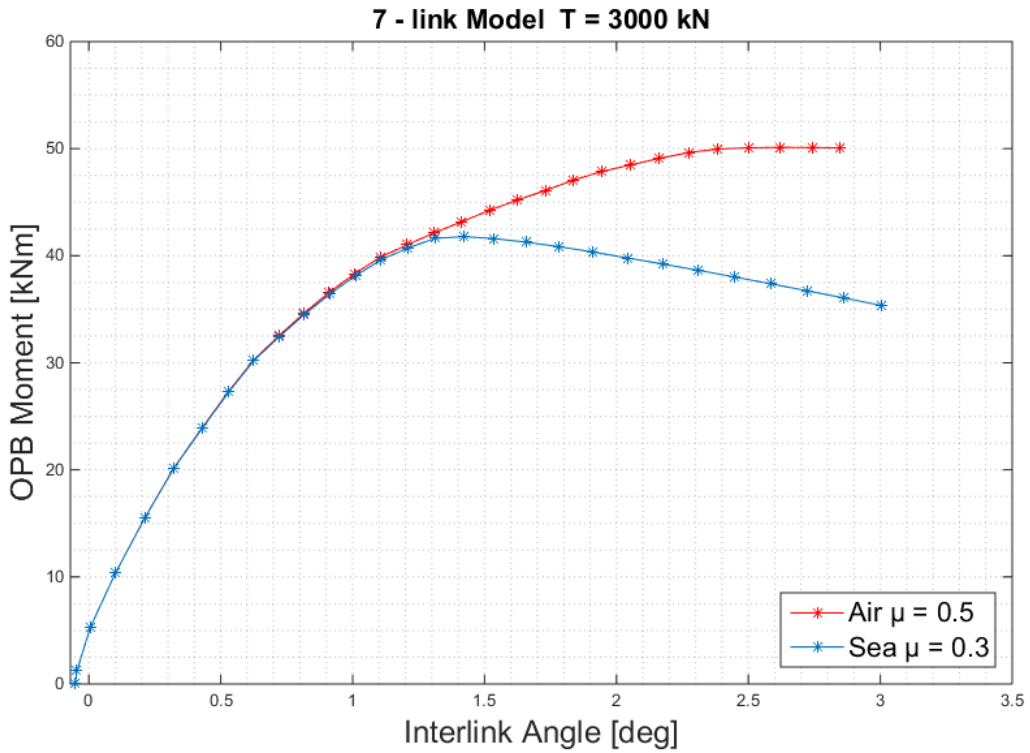

Figure 5.1: Interlink stiffness 7-link Model, original operative conditions

Figure 5.2 illustrates the interlink stiffness for submerged conditions compared to the vertical displacement of the node at the contact point between Link 1-2. The three interlink motions are identified in this figure.

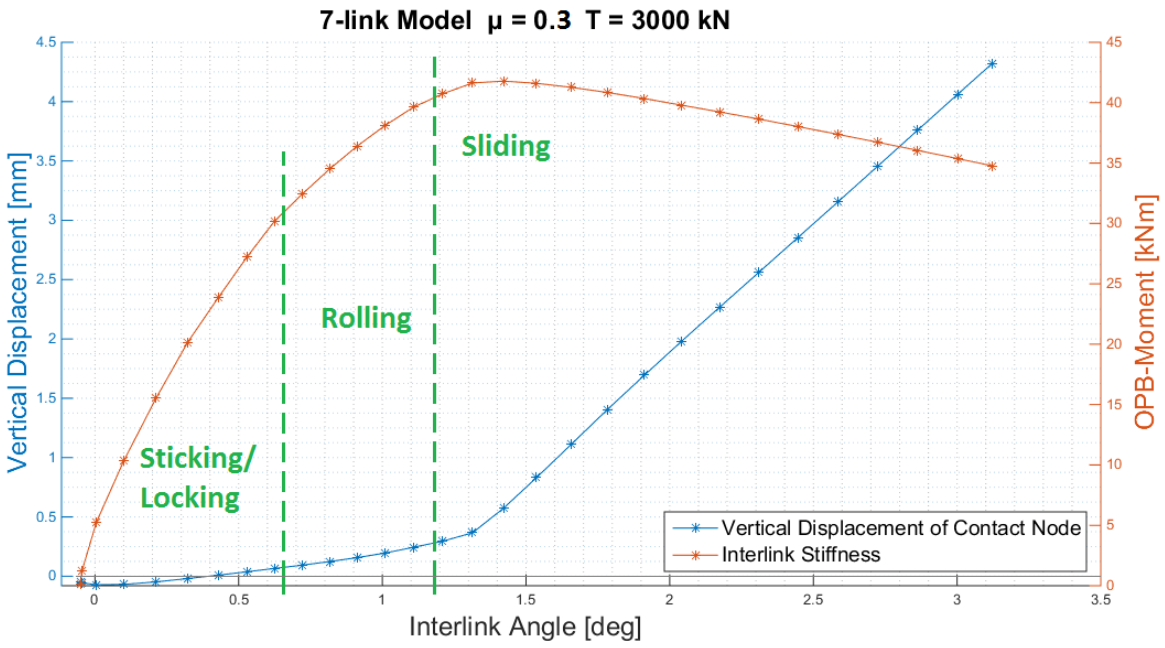

Figure 5.2: Interlink stiffness and vertical displacement of contact node

5.2 Test 2 - Effect of Pretension

Test 2 proves that the operative pretension has an influence on the interlink stiffness in both operative conditions. Figure 5.3 illustrates the influence of pretension in dry conditions.

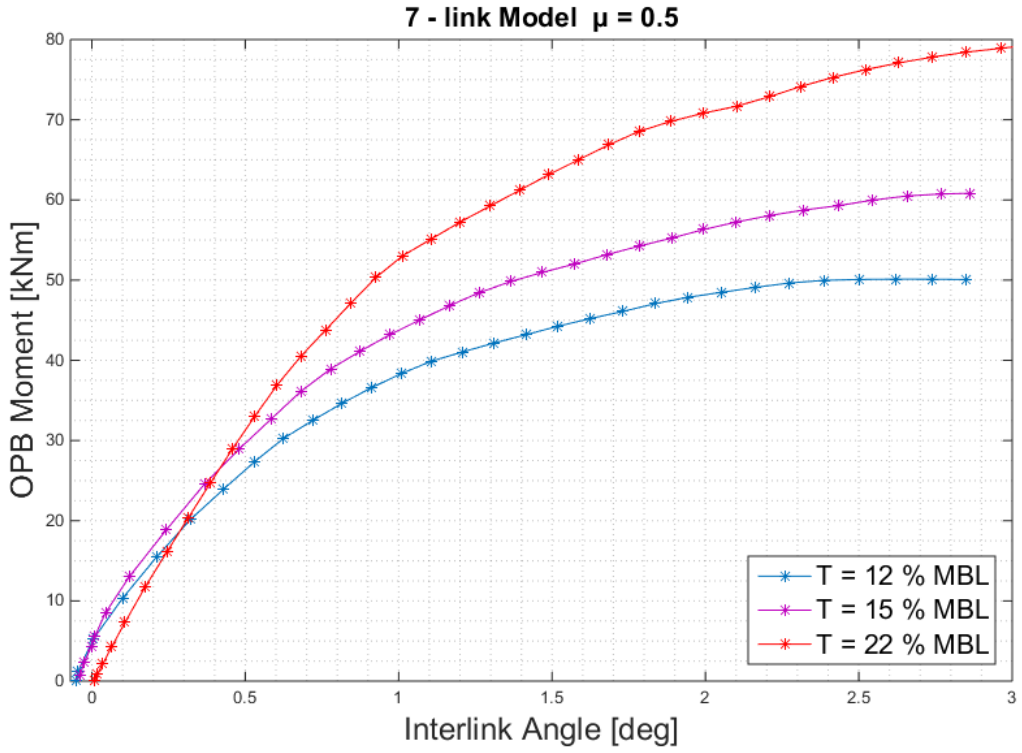

Figure 5.3: Interlink Stiffness when operative tension is increased in an air-filled environment

Figure 5.4 illustrates the influence of pretension in submerged conditions.

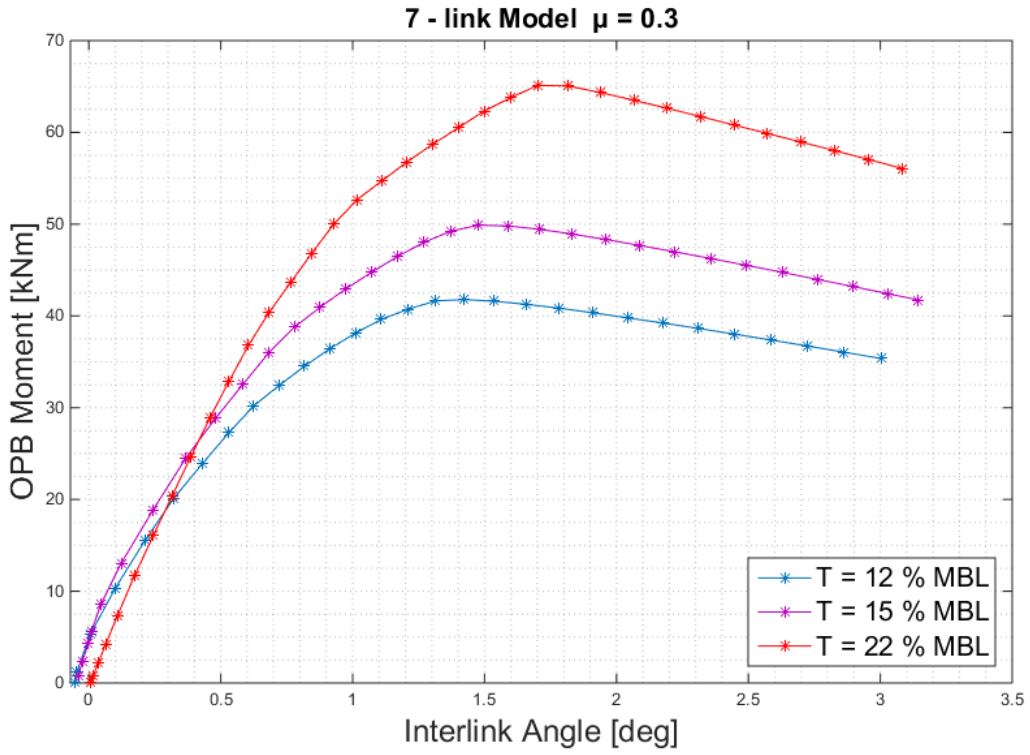

Figure 5.4: Interlink Stiffness when operative tension is increased in seawater

5.3 Test 3 - Effect of Proof Load

Test 3 proves that the proof load has an influence on the interlink stiffness in both environmental conditions.
Figure 5.5 illustrates the influence of proof load in dry conditions.

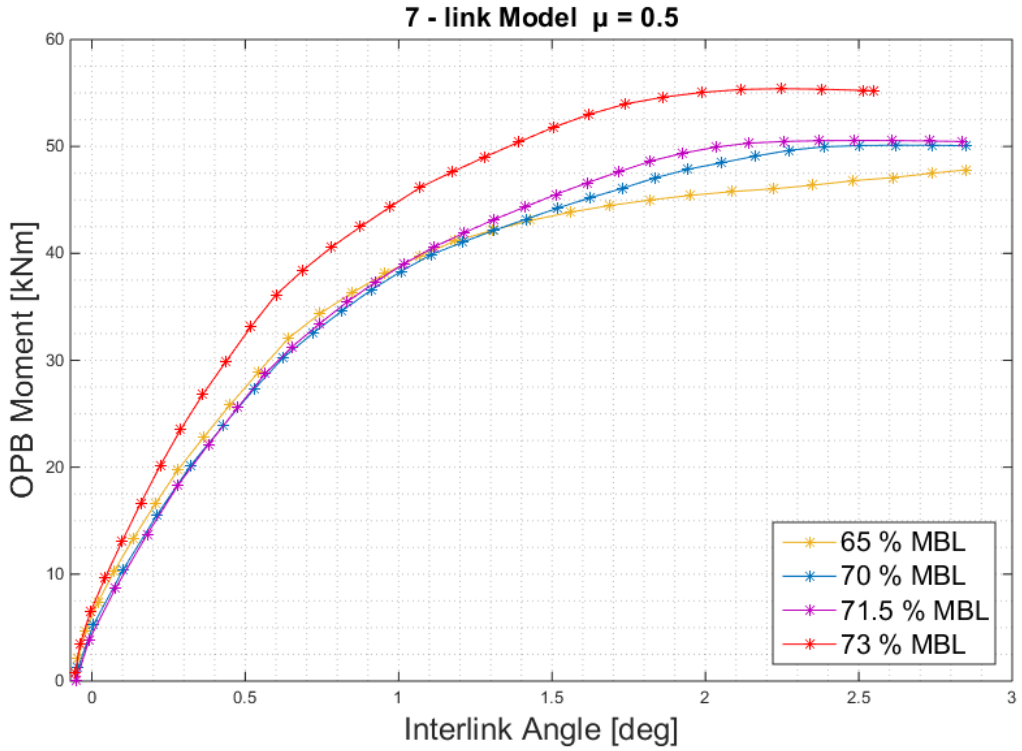

Figure 5.5: Interlink stiffness in air-filled environment

Figure 5.6 illustrates the influence of proof load in submerged conditions.

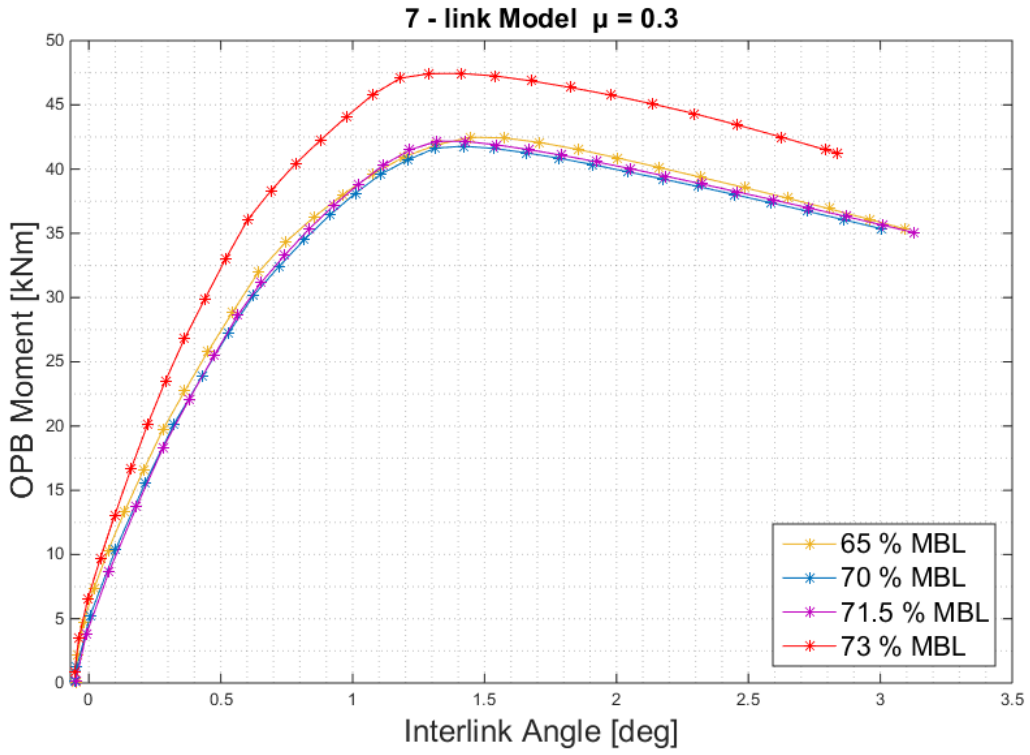

Figure 5.6: Interlink stiffness in submerged operative conditions

Chapter 6

Discussion of Results

That OPB represents a complex problem in the maritime industry was already stated prior to this thesis. The complexity of the phenomenon includes several factors influencing obtained FEA results and OPB analysis in general, including the FEA software, lack of scientific literature, and assumptions from the modelling process. This chapter serves as a reasoning to why the simplified FE-model developed for this thesis is a functioning aid to study OPB. It also discusses eventual sources of errors connected to the finite element modelling and presented results.

6.1 Results from FEA

The FE-analysis had two main phases. The first phase was to apply the proof load to create the deformed contacts surface, unload, and apply a constant operative tensile load. The second phase was to apply a vertical displacement at the final link to create an interlink angle between Link 1 and 2. The two phases are illustrated on the full 7-link model by Figure 6.1.

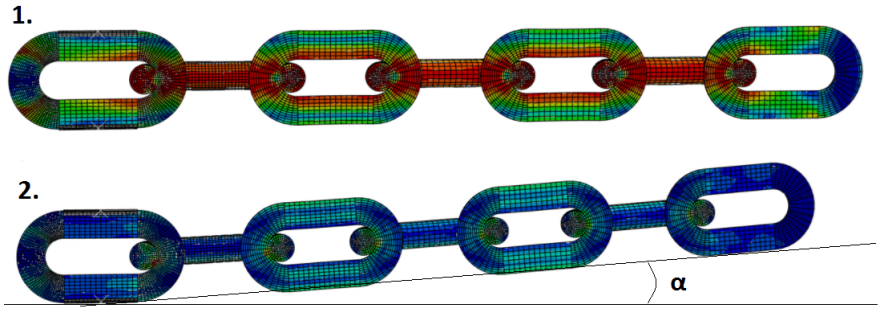

Figure 6.1: Main Phase FEA ABAQUS CAE

6.1.1 Test 1 - Environmental Factors

Test 1 simulated the chain's original full-scale test setup and operative parameters. The results illustrated in Figure 5.1 verify that the model behaves as expected when simulating dry and submerged conditions for the interlink contact surfaces. Characteristic OPB behavior is visualized as the sliding threshold is achieved earlier for submerged operations when the friction coefficient is lower. Both interlink stiffness curves follow each other at small interlink angles, until rolling and sliding motion is commenced for the submerged test.

The early sliding threshold leads to lower OPB stresses, implying that a fully submerged mooring system and hang-off location is beneficial when considering OPB. However, submerged systems are exposed to corrosion and marine growth, in addition to difficulties related to inspection and maintenance of the critical links often placed inside trumpets or hawse pipes. Failure modes connected to the upper chain sections of a mooring line was addressed in Section 2.1, where corrosion and interlink wear are factors found to be influenced by external environmental parameters. This chain section can be located in the splash zone known to be corrosive-aggressive, whereAS general wear between links is not separately included in today's classification standards.

There were some deviations from expectations of OPB interlink stiffness plots. The first was the small negative start angle of -0.05°, which was seen to disappear when testing a 3-link model in Section 4.2.2. It is possible that the final links do not behave as straight beam elements for the original operative conditions, which was the intention and assumption for the model.

Another deviation is how the OPB moment decreases after sliding is commenced for submerged conditions instead of remaining constant. The static tests for seawater and air included from the 2016 JIP, illustrated in Figure 2.27, indicates that the OPB moment rather has a slight increase after sliding threshold is reached. For Test 1, the decreasing OPB moment occurs for the larger interlink angles and can be the consequence of the point of contact moving outside the deformed contact surface.

6.1.2 Test 2 - Operative Pretension

The second test investigated the influence of operative pretension. Test A, the original operational tension load, represented a pretension equal to 12 % MBL whereas Test B and C represented 15 % and 22 % of MBL. The presented interlink stiffness curves in Figure

5.3 and Figure 5.4 illustrate that an increase of tension leads to a subsequent increase of the OPB moment and interlink stiffness for both environmental conditions.

The Guidance Note for combined tension and bending loads by Bureau Veritas was summarized in Section 3.4 and states that OPB should be considered a problem when pretension is 10 % of MBL. As mentioned in Section 2.1.4, Vargas and Jean addressed it as a loading condition occurring for pretension above 15 % MBL in 2005. Pretension is an operational parameter that can and is expected to change at the operation site. Adjusting the line tension during operation should be done to avoid slacking of the lines and to reduce local OPB stress for links located in the chain stopper or other hang-off equipment. Wrongly adjusted line tensions and maintenance plans not followed, have further shown to be contributing factors to mooring line failures over the years (Kvitrud A. for PSA, 2014).

As the pretension is determined from the mooring analysis for individual lines, this makes OPB a single line, single link problem. It was proven in the case study by MARINTEK and studies by ter Brake et al., respectively in 2014 and 2007, that OPB is a problem for the lines operating under the highest tensions, even if these lines has the highest fatigue life. When operations are moved further offshore, the pretension increases in line with the risk of experiencing OPB damage.

The negative start angle observed for the original conditions is no longer present for Test C, implying that the final links behave as straight beam elements when sufficient tension load is applied. This finding is verified by plotting the vertical deflection of Link 2 for all sub-tests in Figure 6.2, where Test C show a linear increase throughout the displacement step.

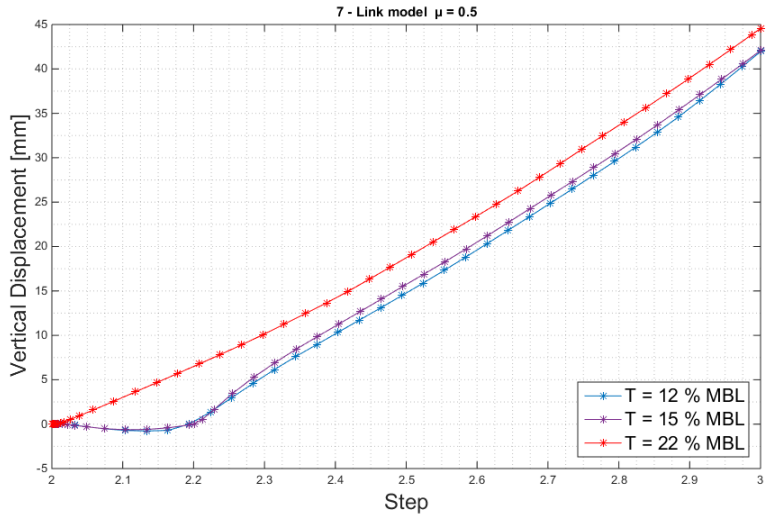

Figure 6.2: Vertical Displacement of Link 2 in an air filled environment

The decreasing OPB moment after sliding motion is commenced in submerged conditions is even more evident when the tension is increased in Test C referring to Figure 5.4. The interlink motion has shifted from rolling to sliding at this point, and the friction has shifted from static to kinetic/dynamic friction. The kinetic sliding friction moment is further a factor dependent on both friction coefficient and axial load.

6.1.3 Test 3 - Proof Load

Test A-D of Test 3, tested proof loads in a range of 65 - 73 % MBL. Originally, the proof load is of magnitude between 65 - 80 % of MBL dependent on material grade, geometry (stud or stud-less), and obtained elongation of the link during manufacturing. Sufficient elongation is achieved when the material reaches yield and shakedown, a plastic phenomenon preventing further elongation by ratchetting from cyclic loads and eventual failure during operation. The phenomena was explained in detail in Section 4.2.1.

Vargas and Jean investigated the influence of applying proof load to offshore chain links in 2005 by comparing experimental results to FEA results, where their main results were included in Section 2.1.5. They concluded that the stress measured from FEA results are too low compared to full-scale measurements if a proof load is not applied, as illustrated in Figure 2.6. If proof load is neglected in simulations, the deformed surface is not present and experienced interlink motion will be *rolling*, leading to low OPB stresses.

Residual stresses left from proof load was also numerically investigated by Bastid and Smith in 2013, highlighting the locations of the chain links where residual stresses were found to be compressive or tensile. The proof load has proven to be beneficial when considering fatigue damage of the links, due to compressive residual stress left at the crown and K_T location. It is, however, critical when evaluating damage from OPB because of tensile residual stress left at the edge of the interlink area. Details of stresses in the interlink area was discussed in Section 2.2.1, highlighting the findings from their paper.

Both environmental conditions visualize expected trends in Test 3 of the parameter study. The results in Figure 5.5 illustrate how Test A-C, representing 65 %, 70 %, and 71.5 %, provide a similar interlink stiffness till 1.2 ° for dry conditions. Up until this point, Test A represented the highest interlink stiffness. After sliding threshold is reached, Test A represents the lowest moments. An increase of 1.5 % MBL in Test C provides slightly higher moments compared to Test B, the original conditions. The tests simulating submerged conditions in Figure 5.6 show no distinctive difference for Test A-C, but it is the lowest proof load of 65 % MBL that represents the highest OPB moments.

Increasing the proof load to 73 % of MBL in Test D illustrate an evidently stiffer interlink stiffness for both dry and submerged conditions. Figure 5.6, representing submerged conditions, show further that the graph trends are nearly identical and the rolling and sliding motion occur at approximately similar interlink angles for all tests. Altering the proof load will result in a stiffer interlink stiffness for lower angles, but the OPB mechanism is identical if the tension remains the same.

A stiffer interlink stiffness is a result of increased length of the contact area at the surface of the links. The increased size of the contact area is visualized by comparing Figure 6.3 and Figure 6.4. This finding is also verified comparing the horizontal displacement of the contact point node of Link 2 in the proof load step in Figure 6.5. Although the difference is only 0.812 mm, it is enough to influence the interlink stiffness.

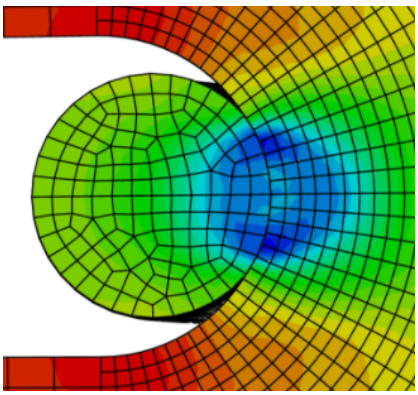

Figure 6.3: Contact area 70 % Proof Load

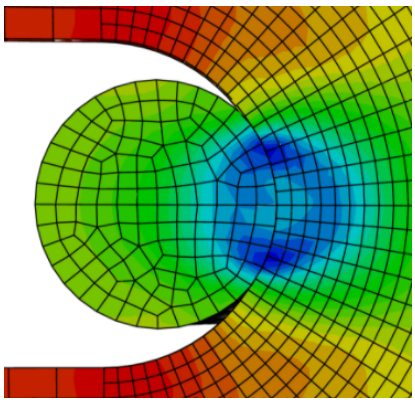

Figure 6.4: Contact area 73 % Proof Load

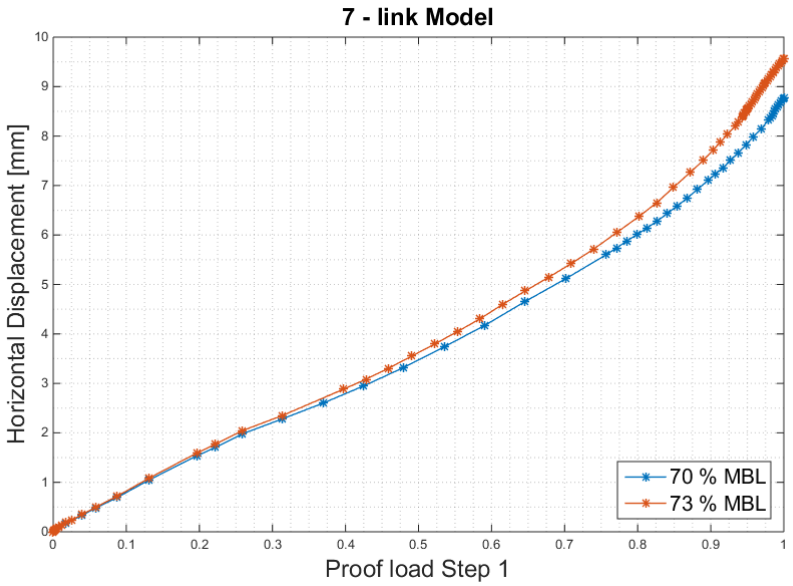

Figure 6.5: Horizontal Displacement of contact node in Link 2 after proof load

6.1.4 Interlink Motion

An offshore mooring chain link can experience three interlink motions. This is sticking (locking), rolling, and sliding motion, where all three were explained in Section 2.1.5 and found present on the presented results in Figure 5.2. The sticking (locking) motion is recognized by a rapid and linear increase of the OPB moment per interlink angle. The dominant force is the friction force, related to a static friction. When the operative tension is increased as in Test 2, the interlink stiffness curve behaves steeper. Increasing the proof load had the same effect, a consequence of a subsequently increased friction force. While the high tensile load locks the links tighter together, increasing the proof load increases the size of the contact area as locking is dependent on the length of contact along the link boundary.

Rolling motion is commenced when the tangential force balancing the tension force exceeds the friction forces. It is observed as the interlink stiffness curve turns non-linear. The two nodes at the contact point between two adjacent links have started to separate at this point. Sliding motion occurs when the contact nodes have separated. Figure 5.2 illustrated the interlink motions for normal operative conditions in submerged tests compared to the vertical displacement of the contact node. It proves that a noticeable separation of the nodes commences as sliding motion occurs.

6.1.5 Comments and Comparisons

Summary of Results

Table 6.1 includes a comparison of the interlink stiffness at $+0.5°$ for the tests illustrating an evident increase from the original operative conditions. This is included to summarize the findings from Chapter 5. Presented values are identical for both environmental conditions as the interlink stiffness curve is identical at $+ 0.5°$.

For original operative conditions, the interlink stiffness is 52.5 kNm/ degree angle at $+0.5°$. Increasing the pretension from 12 % to 15 % results in an interlink stiffness equal to 58 kNm/ degree angle. This is 10.5 % percentage increase from the original conditions. When the pretension is increased to 22 % MBL, representing a very high pretension, it is increased to 62.5 kNm/ degree angle. This is a 19 % percentage increase of interlink stiffness from original conditions.

Increasing the proof load (PL) from 70 % to 73 % lead to an increase of the interlink stiffness at $+ 0.5°$ from 52.5 to 65.5 kNm per degree angle for dry conditions. This

represents a percentage increase of 24.8 %. The percentage increase is summarized in Table 6.1.

Table 6.1: Summary of FEA Results

Test	**T**	**PL**	**Interlink Stiffness at + 0.5 °**	**Increase from Test 1**
Test 1	12 %	70 %	52.5 [kNm/degree angle]	0 %
Test 2-B	15 %	70 %	58.0 [kNm/degree angle]	10.5 %
Test 2-C	22 %	70 %	62.5 [kNm/degree angle]	19 %
Test 3-D	12 %	73 %	65.5 [kNm/degree angle]	24.8 %

Methods from Literature

Different attempts to calculate the OPB moment at sliding threshold is proposed by the industry, all providing the same approach.

Investigation of the Girassol incident (Vargas and Jean, 2005)

$$M_{OPB-Sliding} = r_i \mu_{friction} T \tag{6.1}$$

Bureau Veritas Guidance Note (Bureau Veritas, 2014)

$$M_{threshold} = \frac{d}{2} \mu T \tag{6.2}$$

Static Tests 2016 JIP (Rampi, Dewi, Francois, Gerthoffert and Vargas (2016))

$$\Delta M_{OPB_{Sliding}} = d \mu T \tag{6.3}$$

Calculations by Equation (6.1) for the symmetric 7-link FE-model are compared to measurements from the FEA results Figure 5.1 in Table 6.2. It is observed how the methods fit well for the submerged test results. However, there is an observed deviation for the dry operative conditions, implying that the sliding motion commences too early and a possible poor representation of reality. This observation could be verified with a validation towards the full-scale test results.

Table 6.2: Estimated OPB Moments

Operative Conditions	**Calculated $M_{Sliding}$ from (6.1)**	**FEA $M_{Sliding}$**
Submerged	39.38 [kNm]	$\approx$ 40 [kNm]
Dry	65.23 [kNm]	$\approx$ 50 [kNm]

6.2 FE-Modelling Process

The developed non-linear FE-model represents a simplified model of the actual behavior of offshore mooring chains. The accuracy of the results is dependent on assumptions and simplifications introduced in all modelling steps, from preparing the model to presenting the results. Eventual uncertainties should be kept in mind throughout the entire work process. Sources of error that might lead to a weak approximation of reality are:

- Simplifications and assumptions related to the mathematical model
- Error of discretization
- Numerical error from computations
- Wrong input related to material model and geometry
- Interpretation errors related to results (Moan, 2003)

The following sections presents the observed OPB mechanism compared to the findings in previous literature, assumptions from modelling, and eventual sources of error.

6.2.1 Assumptions from the Modelling Process

Deformed Interlink Contact Area by FEA

Main conclusions from the OPB JIP completed in 2016 was included in Section 2.3, and they concluded that FEA is an effective method to study and understand OPB and the interlink contact stiffness, but will continue to provide under-conservative results. This conclusion was drawn based upon several sources of scatter discovered in the data. The 2016 JIP further found that the interlink stiffness is dependent on if locking occurs within or outside the plastic mating area, resulting in a stiffer interlink stiffness if it were to occur inside.

The convergence test of the developed FEA model in Section 4.2.3 proved that the mating area is to some degree dependent on the mesh size, due to increased size of the contact area from finer mesh. The deformed contact area was found to have an elliptic shape of size $\frac{D}{4}$ in one of the earliest investigations of OPB, the Girassol incident in 2002, mentioned in this thesis in Section 2.1.5. This is illustrated and modified by a cross in Figure 6.6. Figure 6.7 illustrates the contact area of Link 2 after proof load, having approximately the same shape and size.

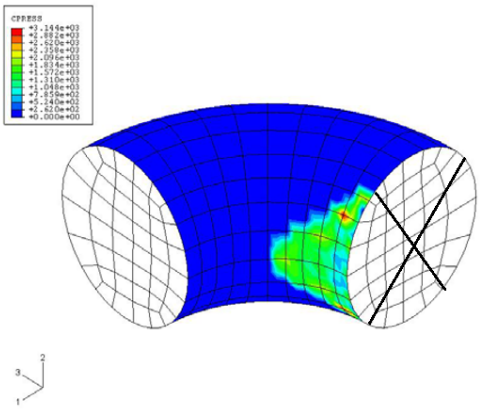

Figure 6.6: Illustration of size of contact area (Jean et al., 2005) (modified by author for comparison)

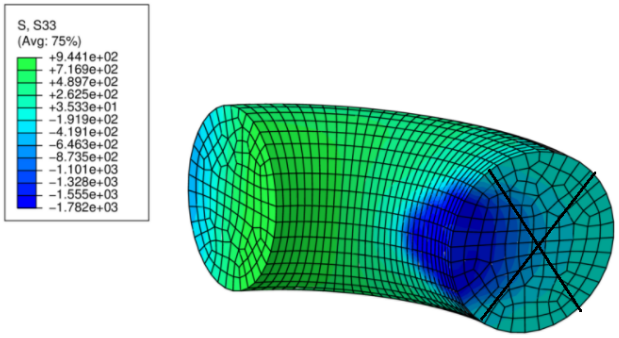

Figure 6.7: Illustration of size of contact area

The same link can experience different up and down curves for the hysteresis loading and rolling can occur for a different range of angles for different links, something that makes the inclusion of OPB in a mooring analysis comprehensive. All possible angle conditions should be included to represent all operative possibilities as also explained in Bureau Veritas' guidance note on OPB from 2014. From static full-scale tests included in the 2016 JIP, it was further noticed that the initial slope was stiffer than the latter as locking occurred within the contact area the first time. The randomness of the locking location makes the interlink stiffness a random variable.

Material Properties and Hardening Model

Defined hardening model influences the formation of the mating surface. The loading and unloading of the proof load is a delicate process, where correct hardening must be applied to obtain a mating area representing the real conditions of the full-scale tests. For this 7-link model, the hardening function is defined as isotropic, implying an equal hardening in tensile and compressive directions. Isotropic hardening was also used by Bastid and Smith in 2013 when investigating the residual stresses left at contact area after proof loading, and by Jean et. al when investigating the Girassol accident in 2005.

The FEA works from the 2016 JIP used a combined kinematic and isotropic hardening model in their new developed material model explained in Section 2.3.3. They found the material law to have great influence on the interlink stiffness as it will decrease with a tougher hardening law. The new material law developed in the JIP could reproduce interlink stiffness, but was still defined as a sub-conservative solution. A combined

hardening rule could also be implemented to the thesis' FE-model as the unloading in compression experiences a reduced yield strength due to the plastic flow in loading. The hardening's impact on the obtained FEA results has not been investigated. The final step after proof load is illustrated by Figure 6.8 showing a geometric elongation of the links.

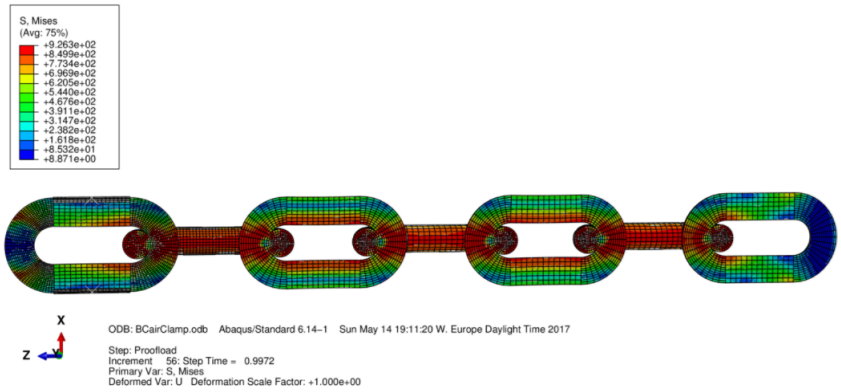

Figure 6.8: Proof load applied to full model ABAQUS CAE

OPB hot spot area

The hot spot area for a chain links subjected to OPB is addressed in several previous OPB researches reviewed for this thesis. Jean et al. investigated the Girassol incident in 2005 and located it by FEA in the bend part of the link, 45 ° from the main plane as illustrated in Figure 2.4. This corresponds to the edge of the interlink area and not at the crown or Kt point as previously found critical for fatigue damage. The same location was further mentioned in the numerical investigations by Bastid and Smith in 2014.

Main findings from the FEA works in the 2016 JIP found the critical area located at an angle $\beta = 50$ ° from top or bottom referring to Figure 2.33. The location of the hot spot area from the thesis' 7-link simulation is illustrated by Figure 6.9 and 6.10, respectively form Test 1 and Test 2 of the parameter study. It proves a good fit with the above-stated assumptions located at the edge of the contact area. It is also seen how the size of the areas with high local stresses are larger when pretension is increased, increasing the risk of crack initiation and failure.

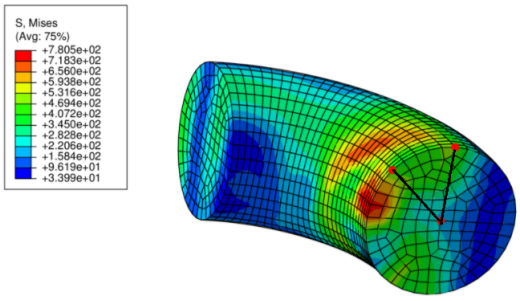

Figure 6.9: 12 % Pretension, measured angle: 50.0 °

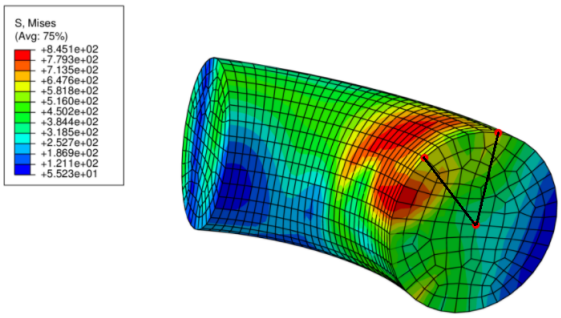

Figure 6.10: 22 % Pretension, measured angle: 49.9 °

The OPB stress concentration factor was found dependent on chain link shape in the 2016 JIP study, and might be altered if the model had experienced more severe non-linear geometry changes from proof load.

Boundary Conditions

The boundary conditions applied to the final model is supposed to be identical to the ones in the full-scale test set-up and was investigated in the modelling process in Section 4.2.2. The comparison of the interlink stiffness for the two different boundary conditions implemented on the thesis model in Figure 4.14 proves that the modelled boundary conditions have an influence on obtained FEA results. The difference in the simulated start angles also indicates the influence of boundary conditions.

The full-scale test boundary conditions represented a chain stopper, where the first link is clamped and restrained from movement or rotation. MARINTEK concluded from their research in 2014 that it was better to have a long stopper arm with bearing to lower the stresses from OPB, rather than direct hang-off connection to a chain stopper. The fatigue life predictions from 2009 connected to the 2016 JIP also suggested this to be used for mooring designs in their fatigue life prediction study. A proposed design was illustrated in Figure 2.24. A long stopper arm was also the applied solution from the review of the Girassol incident investigation (Jean et al., 2005).

It has also been suggestions of designs where the upper mooring chain section is replaced with wire to avoid OPB, but this makes it more difficult to adjust line length during operations. Reviewing the results from Test 1 in Figure 5.1, OPB stresses are found lower for a fully submerged system. OPB is not only a problem at the interface of vessel and mooring line, but can appear for locations of other discontinuities of the line, such as clump weights, buoyancy elements, and sockets. As previously mentioned, submerged

systems introduce difficulties related to both inspection and maintenance.

Mesh and Convergence

FE software has difficulties reproducing the real conditions in the locking area, a factor dependent on friction, material properties, as well as the hardening during loading and unloading of the proof load. This was illustrated and proven in the convergence tests in the modelling process in Section 4.2.3. The first observation is the differences in the stress values measured at contact area and contact point. It was difficult to obtain a converged solution, leaving the mesh as a source of error even if the solution is converged for most of the link diameter. The second finding is the size of the mating area, which is slightly increased for smaller mesh and influencing the interlink stiffness. The third is the friction coefficient. It affects the contact area, in addition to being a linear approximation of the real conditions and affecting convergence. Similar meshes provided a difference in stress values, leading to a possible misjudgment of results.

6.2.2 Sources of Error

Calculations

The calculations of the OPB moment is simplified using beam theory as explained in Section 4.2.4. It was further assumed that Link 2 was kept straight while calculating the interlink angle, and did not experience any excessive bending during the displacement step. The OPB stresses was calculated from Equation (4.7), on background of the same assumption, that the curvature in Link 2 is small. The calculation of the interlink angle takes the elongation of the link under the constant axial force into account, as well the relative rigid vertical displacement of Link 2. The starting angle was -0.05 ° for the original operative interlink stiffness, indicating that the final links do not behave as straight beam elements from the start of the displacement step. However, it is not the smallest angles that are of interest when studying OPB, but the angles where sliding motion commences.

Geometry and Residual stresses

Assumptions regarding the links residual stresses are often included in FEA works. The links are assumed to be stress free from the initial step, neglecting all strain left from manufacturing, including damage and surface defects. During the manufacturing process,

the geometry of the links will change after proof load and the links will no longer be perfect cylinders at contact. The links in the final model experience some deformation by the proof load, but if it is representative to real conditions is not verified. A non-circular geometry will experience more friction and rolling and sliding motion will be initiated later, increasing the OPB moments. The geometry of the links will also change from further corrosion and wear during operations.

Energy Verification

Viscous damping and stabilization was applied in the simulation to lower instabilities at the contact areas in the model. This was validated from an energy verification, where measurements of ALLSD (viscous damping energy) was close to the acceptable limit of 5 % of ALLIE (internal energy) for the final step of the analysis.

The use of linear first order C3D8R elements was verified by checking the level of artificial strain energy (ALLAE) within the model. This verified the level of hourglass control applied for the simulations. The comparison between ALLIE and ALLAE shows that the artificial strain energy is below the acceptable limit of 1 % of ALLIE.

For further development of the simplified FE-model, it would be beneficial to investigate and validate both the applied boundary conditions and element types in the FEA to experimental results. On background of DNV GL's verification of the chain's simulated behavior, the FE-model contributed to a successful parameter study.

General FEA script

In relation to the work with this master's thesis, an attempt was made to make a general Python script to create the FE-model. The script would take in link diameter, tension, proof load, and friction coefficient as changeable parameters, making it easier to study case-dependent mooring systems. The script is included in Appendix B. It creates the model with all relevant boundary conditions and steps, allowing easy adjustments of parameters such as chain geometry and friction coefficient. Some issues remain when attempting to solve this script-based model. Part of the problem appears to be related to the contact pairs, and can be resolved by running the command "find contact pairs" in CAE.

In addition to this, the script has some limitations, basically connected to the change of geometry. The mesh size is per now dependent on inserted diameter, and should therefore

be altered afterwards to fit new link geometries and improve convergence. This is also the case for the pre-selection of elements and nodes for post-processing.

If it is possible to create a general script to simulate OPB with simplified FE-models, has not yet been verified. The created FE-model is sensitive, mostly due to difficulties in the interlink contact areas, and a model with a different geometry will probably need some further work before the simple script-based models provide successful results.

Chapter 7

Conclusion

The failure mode OPB is receiving increased attention in the maritime industry today, but classification rules and safety standards are still missing directions to address the problem. ISOs standards and APIs Recommended Practice urge to use maintenance and link rotation to relieve independent links of localized OPB stress, whereas concerns are expressed in Noble Denton's 2006 JIP how only 50 % of the FPSOs operating at the time could adjust the line tension. In addition to this, 78 % did not have alarm systems installed, unable to tell if a line had failed. Failure of a mooring line can have fatal, economic, and environmental consequences, as it exposes human personnel, environment, and adjacent field installations to unnecessary risk.

This master's thesis investigated the fatigue phenomena out of plane bending of mooring chains by a developing a 7-link finite element model. The model is a reproduction of a full-scale test recently performed by DNV GL. Obtained FEA results were verified by DNV GL, and they concluded that the presented results were replicating the behavior of the chain during testing in a good way. The model was used to investigate the influence of the pretension and proof load magnitude, parameters dependent on the mooring system and link production.

Without the ability to subjectively validate the FEA results against the full-scale test results, reasons to believe that the model is a functioning aid to investigate OPB was proposed and discussed in Chapter 6. Results are presented by plotting the interlink stiffness, expressed as OPB moment per interlink angle between the first two links. The completed parameter study included three tests and proved that different operative and manufacturing conditions have an influence on the OPB interlink stiffness. While the first test proved that the model behaves as expected for dry and submerged conditions, the second and third test gave evidence for the influence of independent system's and component's parameters.

The operative tensile pretension is a parameter that can change on site, either adjusted from ensuing a maintenance plan or unintentionally from environmental loads or human error. By increasing the tension from 12 % (original conditions) to 15 % of MBL, the

interlink stiffness had a percentage increase of 10.5 % at interlink angle + 0.5°.

The magnitude of applied proof load is usually 65-80 % of MBL, and the load is applied to all mooring chain links by the manufacturer. This parameter is dependent on material grade, geometry, and obtained elongation of the link, and leaves behind a permanently deformed contact surface. Proof load is found beneficial in areas known to experience fatigue damage from leaving behind compressive residual stresses at the crown and bend of the link. However, at the edge of the interlink zone, an area of interest when evaluating OPB damage, the residual stresses are tensile. Proof load simulating 65 %, 70 % and 71.5% of MBL provide similar results, whereas an increase to 73 % results in a percentage increase of the interlink stiffness of nearly 25 % at interlink angle + 0.5 °.

Reasons to treat obtained FEA results as under-conservative are related to assumptions and simplifications introduced in the modelling process. There were some deviations from expectations of full-scale test results, mainly the observed decreasing OPB moment after sliding in submerged conditions, expected to remain constant from reviewing static tests. The interlink stiffness is found to be a random variable, dependent on if the locking at contact occur inside or outside the deformed contact surface. It will appear stiffer if locking occurs at the inside, where the contact area size is dependent on mesh size, material law, and proof load magnitude in relation to FEA simulations.

Comparing FEA results of OPB across the industry is difficult as existing literature lack coverage of all operative possibilities. The FEA performed in this thesis indicates how operative and manufacturing parameters have an influence on the interlink stiffness, requiring a gathering of more data for accurate comparisons. As the 2016 OPB JIP and other investigations have concluded with previously, FEA is an effective way to investigate the OPB mechanism and how altering key parameters will affect the results. If it is possible to use simplified models such as the one developed as a conservative method for a mooring analysis is still unknown.

As of today, the quality of maintenance plans, inspections, and alarm systems should be improved as FEA still provides sub-conservative results. Investigating and developing innovative mooring system designs and methods for safe in-water inspections is important to ensure safe operations. Mooring systems represents a critical part of a unit's structural integrity, and its importance, functionality, and response to environmental loads should be known. Not only by the engineers and analyst doing the mooring analysis, but also by the personnel operating the system offshore. Awareness and knowledge of different parameter's influences on the system is the first step to safe operations following the industry's development onto deeper waters.

Chapter 8

Suggestions for Further Work

OPB should be included in future mooring analysis to keep offshore operations safe. This thesis presented and developed a simplified 7-link FEA model, presenting the influence manufacturing and operative parameters have on simulations in dry and submerged conditions. Although the model might provide a valid presentation of chain behavior when subjected to OPB, the introduced assumptions and simplifications in the modelling process still classify the obtained results as sub-conservative.

As mentioned at the end of Chapter 6, a general script was developed to create an FE-model where geometry, tension, proof load, and friction coefficient could be changed. The script creates the model in ABAQUS, with all desired parameters as changeable. However, some issues remain when attempting to solve this script-based model. It would be interesting to do further work on this, to see if a general FEA script is a possible solution to investigate case-dependent OPB situations by FEA.

There are some factors that could be further investigated in relation to the developed FE-model. The OPB JIP from 2016 discovered that the probability of locking appearing inside the deformed area was to some degree random. This was seen from an altering interlink stiffness measured in several displacement cycles for the full-scale static tests. It would be interesting to see if this could be reproduced by FEA to investigate the randomness. However, with seven or more links, the computational time would be much increased.

The non-linear material model included an isotropic hardening model. For later analysis, the influence of using a combined cyclic hardening rule should be implemented and investigated. Another uncertain factor related to the material is the friction model. It is assumed linear and a simplification of what is really happening in the contact area. This too could be further discussed and verified.

Another idea to save computational time is to do proof loading on independent parts and create a new model from already deformed parts. Proof load was applied on all seven links simultaneously for the analysis, which is not representative for reality and how proof load is applied in the manufacturing process. If the model was built by already

deformed parts, it could also be interesting to investigate the possibility of building it from links with a non-circular cross-section representing the true and deformed geometry after proof load. The displacement step could then be run with the deformed model including residual strains and contact surfaces. It could also be interesting to include the manufacturing bending and forming process of the links, to include other defects from production. Further investigations could include the impact of corrosion, surface defects, and wear of the chain links.

If an FE-model is to be used for mooring analysis, the simplified calculations of the OPB moment and interlink angle should be further specified and developed to provide results that are conservative and represent a safe solution.

To save computational time, it could be discussed if a 3-link model would be good enough for the analysis. It resulted in slightly lower interlink stiffness, but should be sufficient if the purpose of the analysis is to investigate the parameter influence. From Bureau Veritas' Guidance Note, the interlink angle is assumed to be present for the 20 first chain links. If a model is built to represent actual on-site conditions, 20 links should have been included.

With more full-scale testing and more FEA works, more data is collected regarding OPB. This increases knowledge and can serve as directions on how to include OPB in future mooring analysis. Simplified models, such as the one created in this thesis, can possibly be used to develop a database of different link sizes, material grades, load, and manufacturing combinations. This can further serve as a library where case-dependent systems can be validated for their mooring analysis. However, the main suggestion from this master's thesis is still to improve quality of maintenance and inspections as well as the alarm systems.

Bibliography

Abaqus Analysis User's Manual (2016), '3.2 Rigid Bodies'. Accessed: 2017-03-22.
URL: *http://abaqus.software.polimi.it/v6.14/books/gsa/default.htm?startat=ch03s02.html*

Akers, R. H. (2014), 'Why good mooring systems go bad - fatigue factors in mooring systems for floating offshore wind turbines'. Accessed: 2016-10-13.
URL: *http://www.mainemarinecomposites.com/uploads/pdfs/WhyGoodMooringSystemsGoBad.pdf*

API (2015), 'Design and analysis of stationkeeping systems for floating structures, API-RP-2SK'.

Bastid, P. and Smith, S. D. (2013), 'Numerical analysis of contact stresses between mooring chain links and potential consequences for fatigue damage', *Proceedings of the* ASME *2013 32nd International Conference on Ocean, Offshore and Arctic Engineering (OMAE2013-11360) Nantes, France* .

Bhattacharjee, S. (2015), 'Design and installation challenges for deepwater mooring systems', *For ExxonMobil* .

Bureau Veritas (2014), 'Fatigue of Top Chain of Mooring Lines due to In-Plane and Out-of-Plane Bendings, Guidance Note NI 604 DT R00 E'.

C. Carra and A. Phadke and D. Laskowski and K.-T. Ma and R. Gordon and G. Kusinski (2015), 'Deepstar mooring study to form basis of new API RP', *Offshore Magazine 09.10.2015* .

Carlberg E., DNV GL (2017), 'Out of plane bending test rig', *Tekna* - DP *og forankring av offshore installasjoner February 2017* .

Das, N. (2016), Models to explain out-of-plane bending mechanism in mooring chain links, Master thesis, Delft University of Technology.

Dhondt, G. (2014), 'Mit - calculix crunchix user's manual version 2.7 - eight-node brick element with reduced integration (c3d8r and f3d8r)'. Accessed: 2017-05-15.
URL: *http://web.mit.edu/calculix*$_v$2.7/$CalculiX$/ccx_2.7/*doc/ccx/node*27.*html*

DNV GL (2013), 'Offshore Standard DNV-OS-E301 Position Mooring'.

DNV GL (2014), Failure investigation of an end link of anchor chain, Technical Report 2014-5150, Rev. 1, Deep Sea Mooring As.

DNV GL (2016), 'DNVGL-RP-C208 Determination of structural capacity by non-linear finite element analysis'.

DNV GL and Kapella, T. (2017), 'Values for material model from private correspondence'.

Groven, G. (2012), Investigation report failure in anchor line no 7 august 2nd, 2012 transocean spitsbergen, Technical Report ACC 2012-0086, Transocean.

IACS (2009), Offshore mooring chain, Technical Report W22 Req.1993/Rev. 5, 2009, International Association of Classification Societies.

Jean, P., Goessens, K. and L'Hostis, D. (2005), 'Failure of chains by bending on deepwater mooring systems', (2005 Offshore Technology Conference (OCT 17238) USA Houston, Texas, USA (OTC 17238)).

Kvitrud A. for PSA (2014), Anchor line failures - Norwegian continental shelf - 2010-2014, Technical Report 992081, Petroleumstilsynet (PSA), F-Konstruksjonssikkerhet.

Langen, I. and Sigbjörnsson, R. (1980), *Dynamisk Analyse av Konstruksjoner*, chapter 6.4 The Master-Slave-Technique.

Lassen, T., Aarsnes, J. and Glomnes, E. (2014), 'Fatigue design methodology for large mooring chains subjected to out-of-plane bending', *Proceedings of the* ASME *2014 33rd International Conference on Ocean, Offshore and Arctic Engineering (OMAE2014-23308) San Francisco, California, USA* .

Lassen, T., Storvoll, E. and Bech, A. (2009), 'Fatigue life predictions of mooring chains subjected to tension and out of plane bending', *Proceedings of the* ASME *2009 28th International Conference on Ocean, Offshore and Arctic Engineering (OMAE2009-79253), Honolulu, Hawaii, USA* .

Ma, K. T., Duggal, A., Smedley, P., L'Hostis, D. and Shu, H. (2013), 'A historical review on integrity issues of permanent mooring systems', *Offshore Technology Conference 2013 (OTC 24025) Houston, Texas, USA* .

Mathisen, J. and Larsen, K. (2004), 'Risk-based inspection planning for mooring chain', *Journal of Offshore Mechanics and Arctic Engineering, Vol. 126* .

Moan, T. (2003), *Finite Element Modelling and Analysis of Marine Structures*, chapter 12 Nonlinear Analysis.

Noble Denton (2006), JIP FPS MOORING INTEGRITY, Technical Report (Research report) 444, Noble Denton Europe Limited.

NORSOK (2010), 'Integrity of offshore structures, N-001'.

NTNU (2010), 'Kildekritikk'. Accessed: 2017-04-25.
URL: *https://innsida.ntnu.no/wiki/-/wiki/Norsk/Finne+kilder*

OPTIMEC Consultants (2017), 'Significance of energies in FE Simulation – part-1'. Accessed: 2017-03-30.
URL: *http://optimec.ca/news/significance-of-energies-in-fe-simulationpart-1/*

Rampi, L., Bignonnet, A., Cunff, C. L., Bourgin, F. and Vargas, P. (2016), 'Chain out of plane bending (OPB) Fatigue Joint Industry Project (JIP) FEA results and multiaxiality study results', *Proceedings of the* ASME *2016 35th International Conference on Ocean, Offshore and Arctic Engineering (OMAE2016-54198) Busan, South Korea* .

Rampi, L., Dewi, F., Francois, M., Gerthoffert, A. and Vargas, P. (2016), 'Chain out of plane bending (OPB) Fatigue Joint Industry Project (JIP) static test program and (OPB) interlink stiffness', *Proceedings of the* ASME *2016 35th International Conference on Ocean, Offshore and Arctic Engineering (OMAE2016-54195) Busan, South Korea* .

Rampi, L., Dewi, F. and Vargas, P. (2015), 'Chain out of plane bending (OPB) Joint Industry Project (JIP) summary and main results', *Offshore Technology Conference 2015 (OTC-25779-MS) Houston, Texas, USA* .

Schijve, J. (2009), *Fatigue of Structures and Materials*, chapter 16 Corrosion Fatigue.

Solnørdal, M., Wästber, S., Heiberg, G. and Hauås-Eide, O. (2009), 'Hydrogen induced stress cracking (HISC) and *DNV*RPF112', *Measurement + Control Vol 42/5* .

Sun, E. Q. (2006), 'Shear locking and hourglassing in msc Nastran, ABAQUS, and ANSYS', *In MSC Software Corporation's 2006 Americas Virtual Product Development Conference: Evolution to Enterprise Simulation (2006), pp. 17-19* .

Teekay Petrojarl (2013), Investigation of mooring line failure petrojarl varg PJV 2012-12-14, Technical Report Synergi case 4006603, Teekay Petrojarl.

ter Brake, E., Van der Cammen, J. and Uittenbogaard, R. (2007), 'Calculation methodology of out of plane bending of mooring chains', *ASME. 2007 26th International Conference on Offshore Mechanics and Arctic Engineering, Volume 4: Materials Technology; Ocean Engineering ():411-419. doi:10.1115/ (OMAE2007-29178). .*

ISO (2013), 'Petroleum and natural gas industries specific requirements for offshore structures part 7: Stationkeeping systems for floating offshore structures and mobile offshore units (19901-7)'.

Statoil (2013), Ankerlinebrudd på NORNE, Dybdestudierapport, Technical Report Synergi nr 1329621, Statoil.

Vargas, P. (2005), 'Out-of-plane bending testing of chain links', *Proceedings of the* ASME *2005 24th International Conference on Ocean, Offshore and Arctic Engineering (OMAE2005-67353) Halkidiki, Greece .*

Vargas, P. M., Hsu, T.-M. and Lee, W. K. (2004), 'Stress concentration factors for stud-less mooring chain links in fairleads', *23rd International Conference on Offshore Mechanics and Arctic Engineering (OMAE2004-51376) Vancouver, British Columbia, Canada .*

Vargas, P. M. and Jean, P. (2005), 'FEA of out-of-plane fatigue mechanism of chain links', (Proceedings of OMAE2005 24th International Conference on Offshore Mechanics and Arctic Engineering: Volume 3 (OMAE2005-67354) Halkidiki, Greece).

Vicinay (2016), 'Vicinay catalogue 2016', *VCSA Catalogue .*

Yaghin, A. L. and Melchers, R. E. (2015), 'Long term inter-link wear of model mooring chains', *Elsevier, Marine Structures 44 (2015) 61e84 .*

Appendix A

Material Model

Table A.1: Material Model R4 - Steel DNV GL (DNV GL and Kapella, 2017)

Stress [MPA]	**Strain**	**Stress [MPA]**	**Strain**
420	3.29E-05	720	0.001493285
440	0.000129719	740	0.001603429
460	0.000226525	760	0.00173361
480	0.00032333	780	0.001911943
500	0.000420136	800	0.002203403
520	0.000516941	820	0.002754994
540	0.000613747	840	0.003892654
560	0.000710553	860	0.006325266
580	0.000807361	880	0.01156657
600	0.000904177	900	0.022792916
620	0.001001012	920	0.04655891
640	0.001097908	940	0.096176016
660	0.001194973	960	0.19826767
680	0.001292506	980	0.405307517
700	0.001391283		

Appendix B

Python FEA OPB Script

```
# -*- coding: mbcs -*-
from part import *
from material import *
from section import *
from assembly import *
from step import *
from interaction import *
from load import *
from mesh import *
from optimization import *
from job import *
from sketch import *
from visualization import *
from connectorBehavior import *

#-------------------------------------------------------------------------
###### OPB FEA Script, Master Thesis Appendix
###### Katarina Berthelsen spring 2017, NTNU, Trondheim
#-------------------------------------------------------------------------
#-------------------------------------------------------------------------
#### This script creates a 7-link FE-model to simulate OPB in ABAQUS CAE
#### for different operative environments.
#### It can be used for several link geometries,
#### but has some limitations:
#-------------------------------------------------------------------------
################ LIMITATIONS TO THE SCRIPT
# Mesh is independent on diameter, and must be altered if geometry is
# much altered.
# History output is independent on diameter and new elements and
# nodes must be defined if new diameter is inserted.
#-------------------------------------------------------------------------

##########################################################################
############### CHANGEABLE PARAMETERS ####################################

diameter=175.0 ######### Chain link nominal diameter [mm]
Straight=2.65*diameter ######### Chain link Straight Part [mm]

TransX = diameter*0.175 ####### Translation parameter [mm]

ProofLoad =  17640000.0/2.0 ######### Applied proof load[N]
Pretension = 3000000.0/2.0 ######## Operational tension[N]
Disp= 290.0 ##### Vertical Displacement of Link 7 [mm]
FrictionCoeff=0.5 ######### Friction coefficient for material
                  ######### interaction properties at displacement step

##########################################################################
############### CREATE PARTS #############################################

############## FixedCrown
#-------------------------------------------------------------------------
mdb.models['Model-1'].ConstrainedSketch(name='__sweep__', sheetSize=1000.0)
mdb.models['Model-1'].sketches['__sweep__'].ArcByCenterEnds(center=(0.0, 0.0),
    direction=CLOCKWISE, point1=(-0.675*diameter, 0.0),
    point2=(0.675*diameter, 0.0))
mdb.models['Model-1'].ConstrainedSketch(name='__profile__', sheetSize=1000.0,
    transform=(0.999999999900762, -1.40881318234538e-05, 0.0, -0.0, 0.0, 1.0,
    -1.40881318234538e-05, -0.999999999900762, -0.0, -118.154663085938,
    0.00166457846924671, 0.0))
mdb.models['Model-1'].sketches['__profile__'].ConstructionLine(point1=(-500.0,
    0.0), point2=(500.0, 0.0))
mdb.models['Model-1'].sketches['__profile__'].ConstructionLine(point1=(0.0,
    -500.0), point2=(0.0, 500.0))
mdb.models['Model-1'].sketches['__profile__'].ArcByCenterEnds(center=(
    -diameter/2.0, 0.0), direction=COUNTERCLOCKWISE, point1=(0.0, 0.0),
    point2=(-diameter, 0.0))
mdb.models['Model-1'].sketches['__profile__'].CoincidentConstraint(
    addUndoState=False, entity1=
    mdb.models['Model-1'].sketches['__profile__'].vertices[2], entity2=
    mdb.models['Model-1'].sketches['__profile__'].geometry[2])
mdb.models['Model-1'].sketches['__profile__'].CoincidentConstraint(
    addUndoState=False, entity1=
    mdb.models['Model-1'].sketches['__profile__'].vertices[0], entity2=
    mdb.models['Model-1'].sketches['__profile__'].geometry[2])
mdb.models['Model-1'].sketches['__profile__'].CoincidentConstraint(
    addUndoState=False, entity1=
    mdb.models['Model-1'].sketches['__profile__'].vertices[1], entity2=
    mdb.models['Model-1'].sketches['__profile__'].geometry[2])
mdb.models['Model-1'].sketches['__profile__'].Line(point1=(-diameter,
    0.0), point2=(0.0, 0.0))
mdb.models['Model-1'].sketches['__profile__'].HorizontalConstraint(
    addUndoState=False, entity=
    mdb.models['Model-1'].sketches['__profile__'].geometry[5])
mdb.models['Model-1'].sketches['__profile__'].PerpendicularConstraint(
    addUndoState=False, entity1=
    mdb.models['Model-1'].sketches['__profile__'].geometry[4], entity2=
    mdb.models['Model-1'].sketches['__profile__'].geometry[5])
mdb.models['Model-1'].Part(dimensionality=THREE_D, name='CrownFix', type=
```

```
    DEFORMABLE_BODY)
mdb.models['Model-1'].parts['CrownFix'].BaseSolidSweep(path=
    mdb.models['Model-1'].sketches['__sweep__'], sketch=
    mdb.models['Model-1'].sketches['__profile__'])
del mdb.models['Model-1'].sketches['__profile__']
del mdb.models['Model-1'].sketches['__sweep__']

############# Copy for Crown Link 1
#-------------------------------------------------------------------------
mdb.models['Model-1'].Part(name='CrownLink1', objectToCopy=
    mdb.models['Model-1'].parts['CrownFix'])

############# Partition for crown
#-------------------------------------------------------------------------
mdb.models['Model-1'].ConstrainedSketch(gridSpacing=8.38, name='__profile__',
    sheetSize=335.26, transform=
    mdb.models['Model-1'].parts['CrownFix'].MakeSketchTransform(
    sketchPlane=mdb.models['Model-1'].parts['CrownFix'].faces[1],
    sketchPlaneSide=SIDE1,
    sketchUpEdge=mdb.models['Model-1'].parts['CrownFix'].edges[3],
    sketchOrientation=RIGHT, origin=(0.0, 0.0, 0.0)))
mdb.models['Model-1'].parts['CrownFix'].projectReferencesOntoSketch(filter=
    COPLANAR_EDGES, sketch=mdb.models['Model-1'].sketches['__profile__'])
mdb.models['Model-1'].sketches['__profile__'].Line(point1=(0.0, (diameter/2.0)),
    point2=(-diameter, -diameter*1.5))
mdb.models['Model-1'].sketches['__profile__'].Line(point1=(0.0, (diameter/2.0)),
    point2=(diameter, -diameter*1.5))
mdb.models['Model-1'].parts['CrownFix'].PartitionFaceBySketchThruAll(faces=
    mdb.models['Model-1'].parts['CrownFix'].faces.getSequenceFromMask((
    '[#f ]', ), ), sketch=mdb.models['Model-1'].sketches['__profile__'],
    sketchPlane=mdb.models['Model-1'].parts['CrownFix'].faces[1],
    sketchPlaneSide=SIDE1, sketchUpEdge=
    mdb.models['Model-1'].parts['CrownFix'].edges[3])
del mdb.models['Model-1'].sketches['__profile__']

############# Crownfull
#-------------------------------------------------------------------------
mdb.models['Model-1'].ConstrainedSketch(name='__sweep__', sheetSize=1000.0)
mdb.models['Model-1'].sketches['__sweep__'].ArcByCenterEnds(center=(0.0, 0.0),
    direction=CLOCKWISE, point1=(-0.675*diameter, 0.0), point2=(0.0, 0.675*diameter))
mdb.models['Model-1'].ConstrainedSketch(name='__profile__', sheetSize=1000.0,
    transform=(1.0, -1.22464679914735e-16, 0.0, -0.0, 0.0, 1.0,
    -1.22464679914735e-16, -1.0, -0.0, -120.0, -1.46957615897682e-14, 0.0))
mdb.models['Model-1'].sketches['__profile__'].ConstructionLine(point1=(-500.0,
    0.0), point2=(500.0, 0.0))
mdb.models['Model-1'].sketches['__profile__'].ConstructionLine(point1=(0.0,
    -500.0), point2=(0.0, 500.0))
mdb.models['Model-1'].sketches['__profile__'].CircleByCenterPerimeter(center=(
    -diameter/2.0, 0.0), point1=(0.0, 0.0))
mdb.models['Model-1'].sketches['__profile__'].CoincidentConstraint(
    addUndoState=False, entity1=
    mdb.models['Model-1'].sketches['__profile__'].vertices[1], entity2=
    mdb.models['Model-1'].sketches['__profile__'].geometry[2])
mdb.models['Model-1'].sketches['__profile__'].CoincidentConstraint(
    addUndoState=False, entity1=
    mdb.models['Model-1'].sketches['__profile__'].vertices[0], entity2=
    mdb.models['Model-1'].sketches['__profile__'].geometry[2])
mdb.models['Model-1'].Part(dimensionality=THREE_D, name='crownfull', type=
    DEFORMABLE_BODY)
mdb.models['Model-1'].parts['crownfull'].BaseSolidSweep(path=
    mdb.models['Model-1'].sketches['__sweep__'], sketch=
    mdb.models['Model-1'].sketches['__profile__'])
del mdb.models['Model-1'].sketches['__profile__']
del mdb.models['Model-1'].sketches['__sweep__']

mdb.models['Model-1'].parts['crownfull'].PartitionCellByPlaneNormalToEdge(cells=
    mdb.models['Model-1'].parts['crownfull'].cells.getSequenceFromMask(('[#1 ]', ),
    ), edge=mdb.models['Model-1'].parts['crownfull'].edges[0], point=
    mdb.models['Model-1'].parts['crownfull'].vertices[0])

################Half Straight
#-------------------------------------------------------------------------
mdb.models['Model-1'].ConstrainedSketch(name='__profile__', sheetSize=200.0)
mdb.models['Model-1'].sketches['__profile__'].ArcByCenterEnds(center=(-diameter,
    0.0), direction=COUNTERCLOCKWISE, point1=(-diameter/2.0, 0.0), point2=(-diameter*1.5, 0.0))
mdb.models['Model-1'].sketches['__profile__'].Line(point1=(-diameter*1.5, 0.0), point2=
    (-diameter/2.0, 0.0))
mdb.models['Model-1'].sketches['__profile__'].HorizontalConstraint(
    addUndoState=False, entity=
    mdb.models['Model-1'].sketches['__profile__'].geometry[3])
mdb.models['Model-1'].sketches['__profile__'].PerpendicularConstraint(
    addUndoState=False, entity1=
    mdb.models['Model-1'].sketches['__profile__'].geometry[2], entity2=
    mdb.models['Model-1'].sketches['__profile__'].geometry[3])
mdb.models['Model-1'].Part(dimensionality=THREE_D, name='HalfStraight', type=
    DEFORMABLE_BODY)
mdb.models['Model-1'].parts['HalfStraight'].BaseSolidExtrude(depth=Straight, sketch=
    mdb.models['Model-1'].sketches['__profile__'])
```

```
del mdb.models['Model-1'].sketches['__profile__']

####################Full Straight
#-------------------------------------------------------------------------
mdb.models['Model-1'].ConstrainedSketch(name='__profile__', sheetSize=200.0)
mdb.models['Model-1'].sketches['__profile__'].CircleByCenterPerimeter(center=(
    -diameter, 0.0), point1=(-diameter/2.0, 0.0))
mdb.models['Model-1'].Part(dimensionality=THREE_D, name='FullStraight', type=
    DEFORMABLE_BODY)
mdb.models['Model-1'].parts['FullStraight'].BaseSolidExtrude(depth=Straight, sketch=
    mdb.models['Model-1'].sketches['__profile__'])
del mdb.models['Model-1'].sketches['__profile__']
mdb.models['Model-1'].parts['FullStraight'].PartitionCellByPlaneNormalToEdge(
    cells=
    mdb.models['Model-1'].parts['FullStraight'].cells.getSequenceFromMask((
    '[#1 ]', ), ), edge=mdb.models['Model-1'].parts['FullStraight'].edges[0],
    point=mdb.models['Model-1'].parts['FullStraight'].vertices[0])


##########################################################################
############### MATERIAL PROPERTIES ######################################

mdb.models['Model-1'].Material(name='ElasticPlastic')
mdb.models['Model-1'].materials['ElasticPlastic'].Elastic(
    table=((206600.0, 0.3), ))
mdb.models['Model-1'].materials['ElasticPlastic'].Plastic(
    table=((420.0, 0.0), (420.0, 3.29138e-05), (440.0, 0.000129719), (460.0,
    0.000226525), (480.0, 0.00032333), (500.0, 0.000420136), (520.0,
    0.000516941), (540.0, 0.000613747), (560.0, 0.000710553), (580.0,
    0.000807361), (600.0, 0.000904177), (620.0, 0.001001012), (640.0,
    0.001097908), (680.0, 0.001292506), (700.0, 0.001391283), (720.0,
    0.001493285), (740.0, 0.001603429), (760.0, 0.00173361), (780.0,
    0.001911943), (800.0, 0.002203403), (820.0, 0.002754944), (840.0,
    0.003892654), (860.0, 0.006325266), (880.0, 0.01156657), (900.0,
    0.022792916), (920.0, 0.04655891), (940.0, 0.096176016), (960.0,
    0.19826767), (980.0, 0.405307517)))
mdb.models['Model-1'].HomogeneousSolidSection(material='ElasticPlastic', name=
    'Section-1', thickness=None)

##########################################################################
############### ASSIGN SECTION PROPERTIES ################################

mdb.models['Model-1'].parts['FullStraight'].Set(cells=
    mdb.models['Model-1'].parts['FullStraight'].cells.getSequenceFromMask((
    '[#3 ]', ), ), name='Set-1')
mdb.models['Model-1'].parts['FullStraight'].SectionAssignment(offset=0.0,
    offsetField='', offsetType=MIDDLE_SURFACE, region=
    mdb.models['Model-1'].parts['FullStraight'].sets['Set-1'], sectionName=
    'Section-1', thicknessAssignment=FROM_SECTION)

mdb.models['Model-1'].parts['HalfStraight'].Set(cells=
    mdb.models['Model-1'].parts['HalfStraight'].cells.getSequenceFromMask((
    '[#1 ]', ), ), name='Set-1')
mdb.models['Model-1'].parts['HalfStraight'].SectionAssignment(offset=0.0,
    offsetField='', offsetType=MIDDLE_SURFACE, region=
    mdb.models['Model-1'].parts['HalfStraight'].sets['Set-1'], sectionName=
    'Section-1', thicknessAssignment=FROM_SECTION)

mdb.models['Model-1'].parts['crownfull'].Set(cells=
    mdb.models['Model-1'].parts['crownfull'].cells.getSequenceFromMask((
    '[#3 ]', ), ), name='Set-1')
mdb.models['Model-1'].parts['crownfull'].SectionAssignment(offset=0.0,
    offsetField='', offsetType=MIDDLE_SURFACE, region=
    mdb.models['Model-1'].parts['crownfull'].sets['Set-1'], sectionName=
    'Section-1', thicknessAssignment=FROM_SECTION)

mdb.models['Model-1'].parts['CrownFix'].Set(cells=
    mdb.models['Model-1'].parts['CrownFix'].cells.getSequenceFromMask((
    '[#1 ]', ), ), name='Set-1')
mdb.models['Model-1'].parts['CrownFix'].SectionAssignment(offset=0.0,
    offsetField='', offsetType=MIDDLE_SURFACE, region=
    mdb.models['Model-1'].parts['CrownFix'].sets['Set-1'], sectionName=
    'Section-1', thicknessAssignment=FROM_SECTION)

mdb.models['Model-1'].parts['CrownLink1'].Set(cells=
    mdb.models['Model-1'].parts['CrownLink1'].cells.getSequenceFromMask(('[#1 ]', ),
    ), name='Set-1')
mdb.models['Model-1'].parts['CrownLink1'].SectionAssignment(offset=0.0, offsetField=
    '', offsetType=MIDDLE_SURFACE, region=
    mdb.models['Model-1'].parts['CrownLink1'].sets['Set-1'], sectionName='Section-1',
    thicknessAssignment=FROM_SECTION)

################################# Copy for coarser end links
#-------------------------------------------------------------------------
mdb.models['Model-1'].Part(name='Crown-End', objectToCopy=
    mdb.models['Model-1'].parts['CrownLink1'])
mdb.models['Model-1'].Part(name='crownfull-End', objectToCopy=
    mdb.models['Model-1'].parts['crownfull'])
```

```
mdb.models['Model-1'].Part(name='FullStraight-End', objectToCopy=
    mdb.models['Model-1'].parts['FullStraight'])
mdb.models['Model-1'].Part(name='HalfStraight-End', objectToCopy=
    mdb.models['Model-1'].parts['HalfStraight'])

##########################################################################
############### MODEL ASSEMBLY ###########################################

############## Fixed link 1
#--------------------------------------------------------------------
mdb.models['Model-1'].rootAssembly.DatumCsysByDefault(CARTESIAN)
mdb.models['Model-1'].rootAssembly.Instance(dependent=ON, name='CrownFix-1',
    part=mdb.models['Model-1'].parts['CrownFix'])

mdb.models['Model-1'].rootAssembly.rotate(angle=180.0, axisDirection=(0.0, 1.0,
    0.0), axisPoint=(0.0, 0.0, 0.0), instanceList=('CrownFix-1', ))
mdb.models['Model-1'].rootAssembly.rotate(angle=90.0, axisDirection=(1.0, 0.0,
    0.0), axisPoint=(0.0, 0.0, 0.0), instanceList=('CrownFix-1', ))

mdb.models['Model-1'].rootAssembly.Instance(dependent=ON, name='HalfStraight-1'
    , part=mdb.models['Model-1'].parts['HalfStraight'])
mdb.models['Model-1'].rootAssembly.Surface(name='m_Surf-1', side1Faces=
    mdb.models['Model-1'].rootAssembly.instances['HalfStraight-1'].faces.getSequenceFromMask(
    ('[#4 ]', ), ))
mdb.models['Model-1'].rootAssembly.Surface(name='s_Surf-1', side1Faces=
    mdb.models['Model-1'].rootAssembly.instances['CrownFix-1'].faces.getSequenceFromMask(
    ('[#40 ]', ), ))
mdb.models['Model-1'].Tie(adjust=ON, constraintEnforcement=SURFACE_TO_SURFACE,
    master=mdb.models['Model-1'].rootAssembly.surfaces['m_Surf-1'], name=
    'Link1-1', positionToleranceMethod=COMPUTED, slave=
    mdb.models['Model-1'].rootAssembly.surfaces['s_Surf-1'], thickness=ON,
    tieRotations=ON)
mdb.models['Model-1'].rootAssembly.translate(instanceList=('HalfStraight-1', ),
    vector=(-TransX, 0.0, -Straight))
#--------------------------------------------------------------------
mdb.models['Model-1'].rootAssembly.Instance(dependent=ON, name='HalfStraight-2'
    , part=mdb.models['Model-1'].parts['HalfStraight'])
mdb.models['Model-1'].rootAssembly.Surface(name='m_Surf-3', side1Faces=
    mdb.models['Model-1'].rootAssembly.instances['HalfStraight-2'].faces.getSequenceFromMask(
    ('[#4 ]', ), ))
mdb.models['Model-1'].rootAssembly.Surface(name='s_Surf-3', side1Faces=
    mdb.models['Model-1'].rootAssembly.instances['CrownFix-1'].faces.getSequenceFromMask(
    ('[#80 ]', ), ))
mdb.models['Model-1'].Tie(adjust=ON, constraintEnforcement=SURFACE_TO_SURFACE,
    master=mdb.models['Model-1'].rootAssembly.surfaces['m_Surf-3'], name=
    'Link1-2', positionToleranceMethod=COMPUTED, slave=
    mdb.models['Model-1'].rootAssembly.surfaces['s_Surf-3'], thickness=ON,
    tieRotations=ON)
mdb.models['Model-1'].rootAssembly.translate(instanceList=('HalfStraight-2', ),
    vector=((diameter*2.0) + TransX, 0.0, -Straight))
#--------------------------------------------------------------------
mdb.models['Model-1'].rootAssembly.Instance(dependent=ON, name='CrownLink1-1', part=
    mdb.models['Model-1'].parts['CrownLink1'])
mdb.models['Model-1'].rootAssembly.rotate(angle=180.0, axisDirection=(0.0, 1.0,
    0.0), axisPoint=(0.0, 0.0, 0.0), instanceList=('CrownLink1-1', ))
mdb.models['Model-1'].rootAssembly.Surface(name='m_Surf-5', side1Faces=
    mdb.models['Model-1'].rootAssembly.instances['CrownLink1-1'].faces.getSequenceFromMask(
    ('[#4 ]', ), ))
mdb.models['Model-1'].rootAssembly.Surface(name='s_Surf-5', side1Faces=
    mdb.models['Model-1'].rootAssembly.instances['HalfStraight-2'].faces.getSequenceFromMask(
    ('[#8 ]', ), ))
mdb.models['Model-1'].Tie(adjust=ON, constraintEnforcement=SURFACE_TO_SURFACE,
    master=mdb.models['Model-1'].rootAssembly.surfaces['m_Surf-5'], name=
    'Link1-3', positionToleranceMethod=COMPUTED, slave=
    mdb.models['Model-1'].rootAssembly.surfaces['s_Surf-5'], thickness=ON,
    tieRotations=ON)
mdb.models['Model-1'].rootAssembly.Surface(name='m_Surf-7', side1Faces=
    mdb.models['Model-1'].rootAssembly.instances['CrownLink1-1'].faces.getSequenceFromMask(
    ('[#8 ]', ), ))
mdb.models['Model-1'].rootAssembly.Surface(name='s_Surf-7', side1Faces=
    mdb.models['Model-1'].rootAssembly.instances['HalfStraight-1'].faces.getSequenceFromMask(
    ('[#8 ]', ), ))
mdb.models['Model-1'].Tie(adjust=ON, constraintEnforcement=SURFACE_TO_SURFACE,
    master=mdb.models['Model-1'].rootAssembly.surfaces['m_Surf-7'], name=
    'Link1-4', positionToleranceMethod=COMPUTED, slave=
    mdb.models['Model-1'].rootAssembly.surfaces['s_Surf-7'], thickness=ON,
    tieRotations=ON)
#--------------------------------------------------------------------
mdb.models['Model-1'].rootAssembly.rotate(angle=180.0, axisDirection=(0.0, 1.0,
    0.0), axisPoint=(0.0, 0.0, 0.0), instanceList=('CrownLink1-1', ))
mdb.models['Model-1'].rootAssembly.rotate(angle=270.0, axisDirection=(1.0, 0.0,
    0.0), axisPoint=(0.0, 0.0, 0.0), instanceList=('CrownLink1-1', ))

mdb.models['Model-1'].rootAssembly.translate(instanceList=('CrownLink1-1', ),
    vector=(0.0, 0.0, -Straight))
```

```
###############2nd link
#-------------------------------------------------------------------------
mdb.models['Model-1'].rootAssembly.Instance(dependent=ON, name='crownfull-1',
    part=mdb.models['Model-1'].parts['crownfull'])
mdb.models['Model-1'].rootAssembly.rotate(angle=90.0, axisDirection=(1.0, 0.0,
    0.0), axisPoint=(0.0, 0.0, 0.0), instanceList=('crownfull-1', ))
mdb.models['Model-1'].rootAssembly.rotate(angle=270.0, axisDirection=(0.0, 0.0,
    1.0), axisPoint=(0.0, 0.0, 0.0), instanceList=('crownfull-1', ))
mdb.models['Model-1'].rootAssembly.translate(instanceList=('crownfull-1', ),
    vector=(0.0, 0.0, -(Straight + (1.35*diameter))))
#-------------------------------------------------------------------------

mdb.models['Model-1'].rootAssembly.Instance(dependent=ON, name='FullStraight-1'
    , part=mdb.models['Model-1'].parts['FullStraight'])
mdb.models['Model-1'].rootAssembly.rotate(angle=270.0, axisDirection=(0.0, 0.0,
    1.0), axisPoint=(0.0, 0.0, 0.0), instanceList=('FullStraight-1', ))
mdb.models['Model-1'].rootAssembly.Surface(name='m_Surf-9', side1Faces=
    mdb.models['Model-1'].rootAssembly.instances['FullStraight-1'].faces.getSequenceFromMask(
    ('[#24 ]', ), ))
mdb.models['Model-1'].rootAssembly.Surface(name='s_Surf-9', side1Faces=
    mdb.models['Model-1'].rootAssembly.instances['crownfull-1'].faces.getSequenceFromMask(
    ('[#44 ]', ), ))
mdb.models['Model-1'].Tie(adjust=ON, constraintEnforcement=SURFACE_TO_SURFACE,
    master=mdb.models['Model-1'].rootAssembly.surfaces['m_Surf-9'], name=
    'Link2-1', positionToleranceMethod=COMPUTED, slave=
    mdb.models['Model-1'].rootAssembly.surfaces['s_Surf-9'], thickness=ON,
    tieRotations=ON)
mdb.models['Model-1'].rootAssembly.translate(instanceList=('FullStraight-1', ),
    vector=(0.0, TransX, -((Straight*2.0) + diameter + 2.0*TransX)))
#-------------------------------------------------------------------------
mdb.models['Model-1'].rootAssembly.Instance(dependent=ON, name='crownfull-End-4',
    part=mdb.models['Model-1'].parts['crownfull-End'])
mdb.models['Model-1'].rootAssembly.rotate(angle=270.0, axisDirection=(0.0, 0.0,
    1.0), axisPoint=(0.0, 0.0, 0.0), instanceList=('crownfull-End-4', ))
mdb.models['Model-1'].rootAssembly.rotate(angle=90.0, axisDirection=(0.0, 1.0,
    0.0), axisPoint=(0.0, 0.0, 0.0), instanceList=('crownfull-End-4', ))
mdb.models['Model-1'].rootAssembly.Surface(name='m_Surf-11', side1Faces=
    mdb.models['Model-1'].rootAssembly.instances['FullStraight-1'].faces.getSequenceFromMask(
    ('[#42 ]', ), ))
mdb.models['Model-1'].rootAssembly.Surface(name='s_Surf-11', side1Faces=
    mdb.models['Model-1'].rootAssembly.instances['crownfull-End-4'].faces.getSequenceFromMask(
    ('[#44 ]', ), ))
mdb.models['Model-1'].Tie(adjust=ON, constraintEnforcement=SURFACE_TO_SURFACE,
    master=mdb.models['Model-1'].rootAssembly.surfaces['m_Surf-11'], name=
    'Link2-2', positionToleranceMethod=COMPUTED, slave=
    mdb.models['Model-1'].rootAssembly.surfaces['s_Surf-11'], thickness=ON,
    tieRotations=ON)
mdb.models['Model-1'].rootAssembly.translate(instanceList=('crownfull-End-4', ),
    vector=(0.0, 0.0 , -((Straight*2.0) + diameter + (2.0*TransX))))

##################3rd link
#-------------------------------------------------------------------------
mdb.models['Model-1'].rootAssembly.Instance(dependent=ON, name='Crown-End-5', part=
    mdb.models['Model-1'].parts['Crown-End'])
mdb.models['Model-1'].rootAssembly.Surface(name='m_Surf-13', side1Faces=
    mdb.models['Model-1'].rootAssembly.instances['Crown-End-5'].faces.getSequenceFromMask(
    ('[#8 ]', ), ))
mdb.models['Model-1'].rootAssembly.rotate(angle=180.0, axisDirection=(0.0, 1.0,
    0.0), axisPoint=(0.0, 0.0, 0.0), instanceList=('Crown-End-5', ))
mdb.models['Model-1'].rootAssembly.rotate(angle=90.0, axisDirection=(1.0, 0.0,
    0.0), axisPoint=(0.0, 0.0, 0.0), instanceList=('Crown-End-5', ))
mdb.models['Model-1'].rootAssembly.translate(instanceList=('Crown-End-5', ),
    vector=(0.0, 0.0, -(2.0*Straight + 2.35*diameter + 2.0*TransX)))
#-------------------------------------------------------------------------
mdb.models['Model-1'].rootAssembly.Instance(dependent=ON, name='HalfStraight-3'
    , part=mdb.models['Model-1'].parts['HalfStraight'])
mdb.models['Model-1'].rootAssembly.Surface(name='m_Surf-13', side1Faces=    ###Tie
    mdb.models['Model-1'].rootAssembly.instances['HalfStraight-3'].faces.getSequenceFromMask(
    ('[#4 ]', ), ))
mdb.models['Model-1'].rootAssembly.Surface(name='s_Surf-13', side1Faces=
    mdb.models['Model-1'].rootAssembly.instances['Crown-End-5'].faces.getSequenceFromMask(
    ('[#4 ]', ), ))
mdb.models['Model-1'].Tie(adjust=ON, constraintEnforcement=SURFACE_TO_SURFACE,
    master=mdb.models['Model-1'].rootAssembly.surfaces['m_Surf-13'], name=
    'Link3-1', positionToleranceMethod=COMPUTED, slave=
    mdb.models['Model-1'].rootAssembly.surfaces['s_Surf-13'], thickness=ON,
    tieRotations=ON)
mdb.models['Model-1'].rootAssembly.translate(instanceList=('HalfStraight-3', ),
    vector=(-( TransX), 0.0, -(3.0*Straight + 2.35*diameter + 2.0*TransX)))
mdb.models['Model-1'].rootAssembly.Instance(dependent=ON, name='HalfStraight-4'
    , part=mdb.models['Model-1'].parts['HalfStraight'])
#-------------------------------------------------------------------------
mdb.models['Model-1'].rootAssembly.Surface(name='m_Surf-15', side1Faces=
    mdb.models['Model-1'].rootAssembly.instances['HalfStraight-4'].faces.getSequenceFromMask(
    ('[#4 ]', ), ))
mdb.models['Model-1'].rootAssembly.Surface(name='s_Surf-15', side1Faces=
    mdb.models['Model-1'].rootAssembly.instances['Crown-End-5'].faces.getSequenceFromMask(
    ('[#8 ]', ), ))
```

```
mdb.models['Model-1'].Tie(adjust=ON, constraintEnforcement=SURFACE_TO_SURFACE,
    master=mdb.models['Model-1'].rootAssembly.surfaces['m_Surf-15'], name=
    'Link3-2', positionToleranceMethod=COMPUTED, slave=
    mdb.models['Model-1'].rootAssembly.surfaces['s_Surf-15'], thickness=ON,
    tieRotations=ON)
mdb.models['Model-1'].rootAssembly.translate(instanceList=('HalfStraight-4', ),
    vector=(diameter*2.0 + TransX, 0.0, -(3.0*Straight + 2.35*diameter + 2.0*TransX)))

mdb.models['Model-1'].rootAssembly.Instance(dependent=ON, name='Crown-End-4', part=
    mdb.models['Model-1'].parts['Crown-End'])

mdb.models['Model-1'].rootAssembly.rotate(angle=270.0, axisDirection=(1.0, 0.0,
    0.0), axisPoint=(0.0, 0.0, 0.0), instanceList=('Crown-End-4', ))

mdb.models['Model-1'].rootAssembly.Surface(name='m_Surf-17', side1Faces=
    mdb.models['Model-1'].rootAssembly.instances['Crown-End-4'].faces.getSequenceFromMask(
    ('[#4 ]', ), ))
mdb.models['Model-1'].rootAssembly.Surface(name='s_Surf-17', side1Faces=
    mdb.models['Model-1'].rootAssembly.instances['HalfStraight-4'].faces.getSequenceFromMask(
    ('[#8 ]', ), ))
mdb.models['Model-1'].Tie(adjust=ON, constraintEnforcement=SURFACE_TO_SURFACE,
    master=mdb.models['Model-1'].rootAssembly.surfaces['m_Surf-17'], name=
    'Link3-3', positionToleranceMethod=COMPUTED, slave=
    mdb.models['Model-1'].rootAssembly.surfaces['s_Surf-17'], thickness=ON,
    tieRotations=ON)
mdb.models['Model-1'].rootAssembly.Surface(name='m_Surf-19', side1Faces=
    mdb.models['Model-1'].rootAssembly.instances['Crown-End-4'].faces.getSequenceFromMask(
    ('[#8 ]', ), ))
mdb.models['Model-1'].rootAssembly.Surface(name='s_Surf-19', side1Faces=
    mdb.models['Model-1'].rootAssembly.instances['HalfStraight-3'].faces.getSequenceFromMask(
    ('[#8 ]', ), ))
mdb.models['Model-1'].Tie(adjust=ON, constraintEnforcement=SURFACE_TO_SURFACE,
    master=mdb.models['Model-1'].rootAssembly.surfaces['m_Surf-19'], name=
    'Link3-4', positionToleranceMethod=COMPUTED, slave=
    mdb.models['Model-1'].rootAssembly.surfaces['s_Surf-19'], thickness=ON,
    tieRotations=ON)
mdb.models['Model-1'].rootAssembly.translate(instanceList=('Crown-End-4', ),
    vector=(0.0, 0.0, -(3.0*Straight + 2.35*diameter +2.0*TransX)))

#################### 4th link
#-----------------------------------------------------------------------
mdb.models['Model-1'].rootAssembly.Instance(dependent=ON, name='crownfull-End-1',
    part=mdb.models['Model-1'].parts['crownfull-End'])
mdb.models['Model-1'].rootAssembly.rotate(angle=270.0, axisDirection=(0.0, 0.0,
    1.0), axisPoint=(0.0, 0.0, 0.0), instanceList=('crownfull-End-1', ))
mdb.models['Model-1'].rootAssembly.rotate(angle=270.0, axisDirection=(0.0, 1.0,
    0.0), axisPoint=(0.0, 0.0, 0.0), instanceList=('crownfull-End-1', ))
mdb.models['Model-1'].rootAssembly.translate(instanceList=('crownfull-End-1', ),
    vector=(0.0, 0.0, -(2.0*Straight + 2.0*TransX + (6.35*diameter))))
#-----------------------------------------------------------------------
mdb.models['Model-1'].rootAssembly.Instance(dependent=ON, name='FullStraight-End-1'
    , part=mdb.models['Model-1'].parts['FullStraight-End'])
mdb.models['Model-1'].rootAssembly.rotate(angle=270.0, axisDirection=(0.0, 0.0,
    1.0), axisPoint=(0.0, 0.0, 0.0), instanceList=('FullStraight-End-1', ))
mdb.models['Model-1'].rootAssembly.Surface(name='m_Surf-20', side1Faces=
    mdb.models['Model-1'].rootAssembly.instances['FullStraight-End-1'].faces.getSequenceFromMask(
    ('[#24 ]', ), ))
mdb.models['Model-1'].rootAssembly.Surface(name='s_Surf-20', side1Faces=
    mdb.models['Model-1'].rootAssembly.instances['crownfull-End-1'].faces.getSequenceFromMask(
    ('[#44 ]', ), ))
mdb.models['Model-1'].Tie(adjust=ON, constraintEnforcement=SURFACE_TO_SURFACE,
    master=mdb.models['Model-1'].rootAssembly.surfaces['m_Surf-20'], name=
    'Link4-1', positionToleranceMethod=COMPUTED, slave=
    mdb.models['Model-1'].rootAssembly.surfaces['s_Surf-20'], thickness=ON,
    tieRotations=ON)
mdb.models['Model-1'].rootAssembly.translate(instanceList=('FullStraight-End-1', ),
    vector=(0.0, TransX, - (5.5*Straight + 13.125)))
#-----------------------------------------------------------------------
mdb.models['Model-1'].rootAssembly.Instance(dependent=ON, name='crownfull-End-2',
    part=mdb.models['Model-1'].parts['crownfull-End'])

mdb.models['Model-1'].rootAssembly.rotate(angle=270.0, axisDirection=(0.0, 0.0,
    1.0), axisPoint=(0.0, 0.0, 0.0), instanceList=('crownfull-End-2', ))
mdb.models['Model-1'].rootAssembly.rotate(angle=90.0, axisDirection=(0.0, 1.0,
    0.0), axisPoint=(0.0, 0.0, 0.0), instanceList=('crownfull-End-2', ))
mdb.models['Model-1'].rootAssembly.Surface(name='m_Surf-21', side1Faces=
    mdb.models['Model-1'].rootAssembly.instances['FullStraight-End-1'].faces.getSequenceFromMask(
    ('[#42 ]', ), ))
mdb.models['Model-1'].rootAssembly.Surface(name='s_Surf-21', side1Faces=
    mdb.models['Model-1'].rootAssembly.instances['crownfull-End-2'].faces.getSequenceFromMask(
    ('[#44 ]', ), ))
mdb.models['Model-1'].Tie(adjust=ON, constraintEnforcement=SURFACE_TO_SURFACE,
    master=mdb.models['Model-1'].rootAssembly.surfaces['m_Surf-21'], name=
    'Link4-2', positionToleranceMethod=COMPUTED, slave=
    mdb.models['Model-1'].rootAssembly.surfaces['s_Surf-21'], thickness=ON,
    tieRotations=ON)
mdb.models['Model-1'].rootAssembly.translate(instanceList=('crownfull-End-2', ),
    vector=(0.0, 0.0 , -((Straight*4.0) +4.0*diameter + 8.75)))
```

```
################### 5th link
#-------------------------------------------------------------------------
mdb.models['Model-1'].rootAssembly.Instance(dependent=ON, name='Crown-End-1', part=
    mdb.models['Model-1'].parts['Crown-End'])
mdb.models['Model-1'].rootAssembly.Surface(name='m_Surf-22', side1Faces=
    mdb.models['Model-1'].rootAssembly.instances['Crown-End-1'].faces.getSequenceFromMask(
    ('[#8 ]', ), ))
mdb.models['Model-1'].rootAssembly.rotate(angle=180.0, axisDirection=(0.0, 1.0,
    0.0), axisPoint=(0.0, 0.0, 0.0), instanceList=('Crown-End-1', ))
mdb.models['Model-1'].rootAssembly.rotate(angle=90.0, axisDirection=(1.0, 0.0,
    0.0), axisPoint=(0.0, 0.0, 0.0), instanceList=('Crown-End-1', ))
mdb.models['Model-1'].rootAssembly.translate(instanceList=('Crown-End-1', ),
    vector=(0.0, 0.0, -(4.0*Straight + 5.4*diameter)))
#-------------------------------------------------------------------------
mdb.models['Model-1'].rootAssembly.Instance(dependent=ON, name='HalfStraight-End-1'
    , part=mdb.models['Model-1'].parts['HalfStraight-End'])
mdb.models['Model-1'].rootAssembly.Surface(name='m_Surf-22', side1Faces=
    mdb.models['Model-1'].rootAssembly.instances['HalfStraight-End-1'].faces.getSequenceFromMask(
    ('[#4 ]', ), ))
mdb.models['Model-1'].rootAssembly.Surface(name='s_Surf-22', side1Faces=
    mdb.models['Model-1'].rootAssembly.instances['Crown-End-1'].faces.getSequenceFromMask(
    ('[#4 ]', ), ))
mdb.models['Model-1'].Tie(adjust=ON, constraintEnforcement=SURFACE_TO_SURFACE,
    master=mdb.models['Model-1'].rootAssembly.surfaces['m_Surf-22'], name=
    'Link5-1', positionToleranceMethod=COMPUTED, slave=
    mdb.models['Model-1'].rootAssembly.surfaces['s_Surf-22'], thickness=ON,
    tieRotations=ON)
mdb.models['Model-1'].rootAssembly.translate(instanceList=('HalfStraight-End-1', ),
    vector=(-TransX, 0.0, -(5.0*Straight + 5.4*diameter)))
#-------------------------------------------------------------------------
mdb.models['Model-1'].rootAssembly.Instance(dependent=ON, name='HalfStraight-End-2'
    , part=mdb.models['Model-1'].parts['HalfStraight-End'])

mdb.models['Model-1'].rootAssembly.Surface(name='m_Surf-23', side1Faces=
    mdb.models['Model-1'].rootAssembly.instances['HalfStraight-End-2'].faces.getSequenceFromMask(
    ('[#4 ]', ), ))
mdb.models['Model-1'].rootAssembly.Surface(name='s_Surf-23', side1Faces=
    mdb.models['Model-1'].rootAssembly.instances['Crown-End-1'].faces.getSequenceFromMask(
    ('[#8 ]', ), ))
mdb.models['Model-1'].Tie(adjust=ON, constraintEnforcement=SURFACE_TO_SURFACE,
    master=mdb.models['Model-1'].rootAssembly.surfaces['m_Surf-23'], name=
    'Link5-2', positionToleranceMethod=COMPUTED, slave=
    mdb.models['Model-1'].rootAssembly.surfaces['s_Surf-23'], thickness=ON,
    tieRotations=ON)
mdb.models['Model-1'].rootAssembly.translate(instanceList=('HalfStraight-End-2', ),
    vector=(diameter*2.0 + TransX, 0.0, -(5.0*Straight + 5.4*diameter)))

mdb.models['Model-1'].rootAssembly.Instance(dependent=ON, name='Crown-End-2', part=
    mdb.models['Model-1'].parts['Crown-End'])
mdb.models['Model-1'].rootAssembly.rotate(angle=270.0, axisDirection=(1.0, 0.0,
    0.0), axisPoint=(0.0, 0.0, 0.0), instanceList=('Crown-End-2', ))
#-------------------------------------------------------------------------
mdb.models['Model-1'].rootAssembly.Surface(name='m_Surf-24', side1Faces=
    mdb.models['Model-1'].rootAssembly.instances['Crown-End-2'].faces.getSequenceFromMask(
    ('[#4 ]', ), ))
mdb.models['Model-1'].rootAssembly.Surface(name='s_Surf-24', side1Faces=
    mdb.models['Model-1'].rootAssembly.instances['HalfStraight-End-2'].faces.getSequenceFromMask(
    ('[#8 ]', ), ))
mdb.models['Model-1'].Tie(adjust=ON, constraintEnforcement=SURFACE_TO_SURFACE,
    master=mdb.models['Model-1'].rootAssembly.surfaces['m_Surf-24'], name=
    'Link5-3', positionToleranceMethod=COMPUTED, slave=
    mdb.models['Model-1'].rootAssembly.surfaces['s_Surf-24'], thickness=ON,
    tieRotations=ON)
mdb.models['Model-1'].rootAssembly.Surface(name='m_Surf-25', side1Faces=
    mdb.models['Model-1'].rootAssembly.instances['Crown-End-2'].faces.getSequenceFromMask(
    ('[#8 ]', ), ))
mdb.models['Model-1'].rootAssembly.Surface(name='s_Surf-25', side1Faces=
    mdb.models['Model-1'].rootAssembly.instances['HalfStraight-End-1'].faces.getSequenceFromMask(
    ('[#8 ]', ), ))
mdb.models['Model-1'].Tie(adjust=ON, constraintEnforcement=SURFACE_TO_SURFACE,
    master=mdb.models['Model-1'].rootAssembly.surfaces['m_Surf-25'], name=
    'Link5-4', positionToleranceMethod=COMPUTED, slave=
    mdb.models['Model-1'].rootAssembly.surfaces['s_Surf-25'], thickness=ON,
    tieRotations=ON)
mdb.models['Model-1'].rootAssembly.translate(instanceList=('Crown-End-2', ),
    vector=(0.0, 0.0, -(5.0*Straight + 5.4*diameter)))

################### 6th link
#-------------------------------------------------------------------------
mdb.models['Model-1'].rootAssembly.Instance(dependent=ON, name='crownfull-End-3',
    part=mdb.models['Model-1'].parts['crownfull-End'])
mdb.models['Model-1'].rootAssembly.rotate(angle=270.0, axisDirection=(0.0, 0.0,
    1.0), axisPoint=(0.0, 0.0, 0.0), instanceList=('crownfull-End-3', ))
mdb.models['Model-1'].rootAssembly.rotate(angle=270.0, axisDirection=(0.0, 1.0,
    0.0), axisPoint=(0.0, 0.0, 0.0), instanceList=('crownfull-End-3', ))
mdb.models['Model-1'].rootAssembly.translate(instanceList=('crownfull-End-3', ),
    vector=(0.0, 0.0, -(5.0*Straight + 6.75*diameter)))
```

```
#-------------------------------------------------------------------------
mdb.models['Model-1'].rootAssembly.Instance(dependent=ON, name='FullStraight-End-2'
    , part=mdb.models['Model-1'].parts['FullStraight-End'])
mdb.models['Model-1'].rootAssembly.rotate(angle=270.0, axisDirection=(0.0, 0.0,
    1.0), axisPoint=(0.0, 0.0, 0.0), instanceList=('FullStraight-End-2', ))
mdb.models['Model-1'].rootAssembly.Surface(name='m_Surf-26', side1Faces=
    mdb.models['Model-1'].rootAssembly.instances['FullStraight-End-2'].faces.getSequenceFromMask(
    ('[#24 ]', ), ))
mdb.models['Model-1'].rootAssembly.Surface(name='s_Surf-26', side1Faces=
    mdb.models['Model-1'].rootAssembly.instances['crownfull-End-3'].faces.getSequenceFromMask(
    ('[#44 ]', ), ))
mdb.models['Model-1'].Tie(adjust=ON, constraintEnforcement=SURFACE_TO_SURFACE,
    master=mdb.models['Model-1'].rootAssembly.surfaces['m_Surf-26'], name=
    'Link6-1', positionToleranceMethod=COMPUTED, slave=
    mdb.models['Model-1'].rootAssembly.surfaces['s_Surf-26'], thickness=ON,
    tieRotations=ON)
mdb.models['Model-1'].rootAssembly.translate(instanceList=('FullStraight-End-2', ),
    vector=(0.0, TransX, -((Straight*6.0) + 6.75*diameter)))
#-------------------------------------------------------------------------
mdb.models['Model-1'].rootAssembly.Instance(dependent=ON, name='crownfull-End-5',
    part=mdb.models['Model-1'].parts['crownfull-End'])

mdb.models['Model-1'].rootAssembly.rotate(angle=270.0, axisDirection=(0.0, 0.0,
    1.0), axisPoint=(0.0, 0.0, 0.0), instanceList=('crownfull-End-5', ))
mdb.models['Model-1'].rootAssembly.rotate(angle=90.0, axisDirection=(0.0, 1.0,
    0.0), axisPoint=(0.0, 0.0, 0.0), instanceList=('crownfull-End-5', ))
mdb.models['Model-1'].rootAssembly.Surface(name='m_Surf-27', side1Faces=
    mdb.models['Model-1'].rootAssembly.instances['FullStraight-End-2'].faces.getSequenceFromMask(
    ('[#42 ]', ), ))
mdb.models['Model-1'].rootAssembly.Surface(name='s_Surf-27', side1Faces=
    mdb.models['Model-1'].rootAssembly.instances['crownfull-End-5'].faces.getSequenceFromMask(
    ('[#44 ]', ), ))
mdb.models['Model-1'].Tie(adjust=ON, constraintEnforcement=SURFACE_TO_SURFACE,
    master=mdb.models['Model-1'].rootAssembly.surfaces['m_Surf-27'], name=
    'Link6-2', positionToleranceMethod=COMPUTED, slave=
    mdb.models['Model-1'].rootAssembly.surfaces['s_Surf-27'], thickness=ON,
    tieRotations=ON)
mdb.models['Model-1'].rootAssembly.translate(instanceList=('crownfull-End-5', ),
    vector=(0.0, 0.0 , -((Straight*6.0) +6.75*diameter)))

################### 7th link
#-------------------------------------------------------------------------
mdb.models['Model-1'].rootAssembly.Instance(dependent=ON, name='Crown-End-3', part=
    mdb.models['Model-1'].parts['Crown-End'])
mdb.models['Model-1'].rootAssembly.Surface(name='m_Surf-28', side1Faces=
    mdb.models['Model-1'].rootAssembly.instances['Crown-End-3'].faces.getSequenceFromMask(
    ('[#8 ]', ), ))

mdb.models['Model-1'].rootAssembly.rotate(angle=180.0, axisDirection=(0.0, 1.0,
    0.0), axisPoint=(0.0, 0.0, 0.0), instanceList=('Crown-End-3', ))
mdb.models['Model-1'].rootAssembly.rotate(angle=90.0, axisDirection=(1.0, 0.0,
    0.0), axisPoint=(0.0, 0.0, 0.0), instanceList=('Crown-End-3', ))
mdb.models['Model-1'].rootAssembly.translate(instanceList=('Crown-End-3', ),
    vector=(0.0, 0.0, -(6.5*Straight + 6.775*diameter)))
#-------------------------------------------------------------------------
mdb.models['Model-1'].rootAssembly.Instance(dependent=ON, name='HalfStraight-End-3'
    , part=mdb.models['Model-1'].parts['HalfStraight-End'])
mdb.models['Model-1'].rootAssembly.Surface(name='m_Surf-28', side1Faces=
    mdb.models['Model-1'].rootAssembly.instances['HalfStraight-End-3'].faces.getSequenceFromMask(
    ('[#4 ]', ), ))
mdb.models['Model-1'].rootAssembly.Surface(name='s_Surf-28', side1Faces=
    mdb.models['Model-1'].rootAssembly.instances['Crown-End-3'].faces.getSequenceFromMask(
    ('[#4 ]', ), ))
mdb.models['Model-1'].Tie(adjust=ON, constraintEnforcement=SURFACE_TO_SURFACE,
    master=mdb.models['Model-1'].rootAssembly.surfaces['m_Surf-28'], name=
    'Link7-1', positionToleranceMethod=COMPUTED, slave=
    mdb.models['Model-1'].rootAssembly.surfaces['s_Surf-28'], thickness=ON,
    tieRotations=ON)
mdb.models['Model-1'].rootAssembly.translate(instanceList=('HalfStraight-End-3', ),
    vector=(-TransX, 0.0, -(7.0*Straight + 8.1*diameter)))
#-------------------------------------------------------------------------
mdb.models['Model-1'].rootAssembly.Instance(dependent=ON, name='HalfStraight-End-4'
    , part=mdb.models['Model-1'].parts['HalfStraight-End'])

mdb.models['Model-1'].rootAssembly.Surface(name='m_Surf-29', side1Faces=
    mdb.models['Model-1'].rootAssembly.instances['HalfStraight-End-4'].faces.getSequenceFromMask(
    ('[#4 ]', ), ))
mdb.models['Model-1'].rootAssembly.Surface(name='s_Surf-29', side1Faces=
    mdb.models['Model-1'].rootAssembly.instances['Crown-End-3'].faces.getSequenceFromMask(
    ('[#8 ]', ), ))
mdb.models['Model-1'].Tie(adjust=ON, constraintEnforcement=SURFACE_TO_SURFACE,
    master=mdb.models['Model-1'].rootAssembly.surfaces['m_Surf-29'], name=
    'Link7-2', positionToleranceMethod=COMPUTED, slave=
    mdb.models['Model-1'].rootAssembly.surfaces['s_Surf-29'], thickness=ON,
    tieRotations=ON)
mdb.models['Model-1'].rootAssembly.translate(instanceList=('HalfStraight-End-4', ),
    vector=(diameter*2.0 + TransX, 0.0, -(7.0*Straight + 8.1*diameter)))
```

```
mdb.models['Model-1'].rootAssembly.Instance(dependent=ON, name='Crown-End-6', part=
    mdb.models['Model-1'].parts['Crown-End'])

mdb.models['Model-1'].rootAssembly.rotate(angle=270.0, axisDirection=(1.0, 0.0,
    0.0), axisPoint=(0.0, 0.0, 0.0), instanceList=('Crown-End-6', ))
#-------------------------------------------------------------------
mdb.models['Model-1'].rootAssembly.Surface(name='m_Surf-30', side1Faces=
    mdb.models['Model-1'].rootAssembly.instances['Crown-End-6'].faces.getSequenceFromMask(
    ('[#4 ]', ), ))
mdb.models['Model-1'].rootAssembly.Surface(name='s_Surf-30', side1Faces=
    mdb.models['Model-1'].rootAssembly.instances['HalfStraight-End-4'].faces.getSequenceFromMask(
    ('[#8 ]', ), ))
mdb.models['Model-1'].Tie(adjust=ON, constraintEnforcement=SURFACE_TO_SURFACE,
    master=mdb.models['Model-1'].rootAssembly.surfaces['m_Surf-30'], name=
    'Link7-3', positionToleranceMethod=COMPUTED, slave=
    mdb.models['Model-1'].rootAssembly.surfaces['s_Surf-30'], thickness=ON,
    tieRotations=ON)

mdb.models['Model-1'].rootAssembly.Surface(name='m_Surf-31', side1Faces=
    mdb.models['Model-1'].rootAssembly.instances['Crown-End-6'].faces.getSequenceFromMask(
    ('[#8 ]', ), ))
mdb.models['Model-1'].rootAssembly.Surface(name='s_Surf-31', side1Faces=
    mdb.models['Model-1'].rootAssembly.instances['HalfStraight-End-3'].faces.getSequenceFromMask(
    ('[#8 ]', ), ))
mdb.models['Model-1'].Tie(adjust=ON, constraintEnforcement=SURFACE_TO_SURFACE,
    master=mdb.models['Model-1'].rootAssembly.surfaces['m_Surf-31'], name=
    'Link7-4', positionToleranceMethod=COMPUTED, slave=
    mdb.models['Model-1'].rootAssembly.surfaces['s_Surf-31'], thickness=ON,
    tieRotations=ON)
mdb.models['Model-1'].rootAssembly.translate(instanceList=('Crown-End-6', ),
    vector=(0.0, 0.0, -(7.0*Straight + 8.1*diameter)))


##########################################################################
############### CONTACT ##################################################

mdb.models['Model-1'].ContactProperty('IntProp-1')
mdb.models['Model-1'].interactionProperties['IntProp-1'].TangentialBehavior(
    dependencies=0, directionality=ISOTROPIC, elasticSlipStiffness=None,
    formulation=PENALTY, fraction=0.005, maximumElasticSlip=FRACTION,
    pressureDependency=OFF, shearStressLimit=None, slipRateDependency=OFF,
    table=((0.5, ), ), temperatureDependency=OFF)
#-------------------------------------------------------------------
mdb.models['Model-1'].rootAssembly.Surface(name='m_Surf-32', side1Faces=
    mdb.models['Model-1'].rootAssembly.instances['crownfull-1'].faces.getSequenceFromMask(
    ('[#18 ]', ), ))
mdb.models['Model-1'].rootAssembly.Surface(name='s_Surf-32', side1Faces=
    mdb.models['Model-1'].rootAssembly.instances['CrownLink1-1'].faces.getSequenceFromMask(
    ('[#1 ]', ), ))
mdb.models['Model-1'].SurfaceToSurfaceContactStd(adjustMethod=OVERCLOSED,
    clearanceRegion=None, createStepName='Initial', datumAxis=None,
    initialClearance=OMIT, interactionProperty='IntProp-1', master=
    mdb.models['Model-1'].rootAssembly.surfaces['m_Surf-32'], name='Int-1',
    slave=mdb.models['Model-1'].rootAssembly.surfaces['s_Surf-32'], sliding=
    FINITE, thickness=ON, tied=OFF)
mdb.models['Model-1'].interactionProperties['IntProp-1'].tangentialBehavior.setValues(
    dependencies=0, directionality=ISOTROPIC, elasticSlipStiffness=None,
    formulation=PENALTY, fraction=0.005, maximumElasticSlip=FRACTION,
    pressureDependency=OFF, shearStressLimit=None, slipRateDependency=OFF,
    table=((0.5, ), ), temperatureDependency=OFF)
mdb.models['Model-1'].interactionProperties['IntProp-1'].NormalBehavior(
    allowSeparation=ON, constraintEnforcementMethod=DEFAULT,
    pressureOverclosure=HARD)
#-------------------------------------------------------------------
mdb.models['Model-1'].rootAssembly.Surface(name='m_Surf-33', side1Faces=
    mdb.models['Model-1'].rootAssembly.instances['crownfull-End-4'].faces.getSequenceFromMask(
    ('[#18 ]', ), ))
mdb.models['Model-1'].rootAssembly.Surface(name='s_Surf-33', side1Faces=
    mdb.models['Model-1'].rootAssembly.instances['Crown-End-5'].faces.getSequenceFromMask(
    ('[#1 ]', ), ))
mdb.models['Model-1'].SurfaceToSurfaceContactStd(adjustMethod=OVERCLOSED,
    clearanceRegion=None, createStepName='Initial', datumAxis=None,
    initialClearance=OMIT, interactionProperty='IntProp-1', master=
    mdb.models['Model-1'].rootAssembly.surfaces['m_Surf-33'], name='Int-2',
    slave=mdb.models['Model-1'].rootAssembly.surfaces['s_Surf-33'], sliding=
    FINITE, thickness=ON, tied=OFF)
#-------------------------------------------------------------------
mdb.models['Model-1'].rootAssembly.Surface(name='m_Surf-49', side1Faces=
    mdb.models['Model-1'].rootAssembly.instances['crownfull-End-1'].faces.getSequenceFromMask(
    ('[#18 ]', ), ))
mdb.models['Model-1'].rootAssembly.Surface(name='s_Surf-49', side1Faces=
    mdb.models['Model-1'].rootAssembly.instances['Crown-End-4'].faces.getSequenceFromMask(
    ('[#1 ]', ), ))
mdb.models['Model-1'].SurfaceToSurfaceContactStd(adjustMethod=OVERCLOSED,
    clearanceRegion=None, createStepName='Initial', datumAxis=None,
    initialClearance=OMIT, interactionProperty='IntProp-1', master=
    mdb.models['Model-1'].rootAssembly.surfaces['m_Surf-49'], name='Int-3',
    slave=mdb.models['Model-1'].rootAssembly.surfaces['s_Surf-49'], sliding=
```

```
    FINITE, thickness=ON)
mdb.models['Model-1'].rootAssembly.Surface(name='m_Surf-51', side1Faces=
    mdb.models['Model-1'].rootAssembly.instances['crownfull-End-2'].faces.getSequenceFromMask(
    ('[#18 ]', ), ))
mdb.models['Model-1'].rootAssembly.Surface(name='s_Surf-51', side1Faces=
    mdb.models['Model-1'].rootAssembly.instances['Crown-End-1'].faces.getSequenceFromMask(
    ('[#1 ]', ), ))
mdb.models['Model-1'].SurfaceToSurfaceContactStd(adjustMethod=OVERCLOSED,
    clearanceRegion=None, createStepName='Initial', datumAxis=None,
    initialClearance=OMIT, interactionProperty='IntProp-1', master=
    mdb.models['Model-1'].rootAssembly.surfaces['m_Surf-51'], name='Int-4',
    slave=mdb.models['Model-1'].rootAssembly.surfaces['s_Surf-51'], sliding=
    FINITE, thickness=ON, tied=OFF)
mdb.models['Model-1'].interactions['Int-3'].setValues(adjustMethod=OVERCLOSED,
    bondingSet=None, contactTracking=TWO_CONFIG, enforcement=SURFACE_TO_SURFACE
    , initialClearance=OMIT, sliding=FINITE, thickness=ON, tied=OFF)
mdb.models['Model-1'].rootAssembly.Surface(name='m_Surf-53', side1Faces=
    mdb.models['Model-1'].rootAssembly.instances['crownfull-End-3'].faces.getSequenceFromMask(
    ('[#18 ]', ), ))
mdb.models['Model-1'].rootAssembly.Surface(name='s_Surf-53', side1Faces=
    mdb.models['Model-1'].rootAssembly.instances['Crown-End-2'].faces.getSequenceFromMask(
    ('[#1 ]', ), ))
mdb.models['Model-1'].SurfaceToSurfaceContactStd(adjustMethod=OVERCLOSED,
    clearanceRegion=None, createStepName='Initial', datumAxis=None,
    initialClearance=OMIT, interactionProperty='IntProp-1', master=
    mdb.models['Model-1'].rootAssembly.surfaces['m_Surf-53'], name='Int-5',
    slave=mdb.models['Model-1'].rootAssembly.surfaces['s_Surf-53'], sliding=
    FINITE, thickness=ON, tied=OFF)
mdb.models['Model-1'].rootAssembly.Surface(name='m_Surf-55', side1Faces=
    mdb.models['Model-1'].rootAssembly.instances['crownfull-End-5'].faces.getSequenceFromMask(
    ('[#18 ]', ), ))
mdb.models['Model-1'].rootAssembly.Surface(name='s_Surf-55', side1Faces=
    mdb.models['Model-1'].rootAssembly.instances['Crown-End-3'].faces.getSequenceFromMask(
    ('[#1 ]', ), ))
mdb.models['Model-1'].SurfaceToSurfaceContactStd(adjustMethod=OVERCLOSED,
    clearanceRegion=None, createStepName='Initial', datumAxis=None,
    initialClearance=OMIT, interactionProperty='IntProp-1', master=
    mdb.models['Model-1'].rootAssembly.surfaces['m_Surf-55'], name='Int-6',
    slave=mdb.models['Model-1'].rootAssembly.surfaces['s_Surf-55'], sliding=
    FINITE, thickness=ON, tied=OFF)

##########################################################################
############### STEPS ####################################################
#--------------------------------------------------------------------------
### Step 1 Proof Load
mdb.models['Model-1'].StaticStep(adaptiveDampingRatio=0.05,
    continueDampingFactors=False, initialInc=0.0001, maxNumInc=3000, minInc=
    1e-08, name='Proofload', nlgeom=ON, previous='Initial',
    stabilizationMagnitude=0.02, stabilizationMethod=
    DISSIPATED_ENERGY_FRACTION)
#--------------------------------------------------------------------------
### Step 2 Pretension Operational Load
mdb.models['Model-1'].StaticStep(adaptiveDampingRatio=0.05,
    continueDampingFactors=False, name='WorkLoad', previous='Proofload',
    stabilizationMagnitude=0.002, stabilizationMethod=
    DISSIPATED_ENERGY_FRACTION)
mdb.models['Model-1'].steps['WorkLoad'].setValues(initialInc=0.0001)
#--------------------------------------------------------------------------
### Step 3 Displacement
mdb.models['Model-1'].StaticStep(adaptiveDampingRatio=0.05,
    continueDampingFactors=False, initialInc=0.0001, maxNumInc=3000, minInc=
    1e-08, name='Displacement', previous='WorkLoad', stabilizationMagnitude=
    0.002, stabilizationMethod=DISSIPATED_ENERGY_FRACTION)
#--------------------------------------------------------------------------

##########################################################################
############### BOUNDARY CONDITIONS ######################################

################# Fixed end
#--------------------------------------------------------------------------
mdb.models['Model-1'].rootAssembly.Set(faces=
    mdb.models['Model-1'].rootAssembly.instances['CrownFix-1'].faces.getSequenceFromMask(
    ('[#8 ]', ), ), name='Set-4')
mdb.models['Model-1'].DisplacementBC(amplitude=UNSET, createStepName='Initial',
    distributionType=UNIFORM, fieldName='', localCsys=None, name='Fixed',
    region=mdb.models['Model-1'].rootAssembly.sets['Set-4'], u1=SET, u2=SET,
    u3=SET, ur1=UNSET, ur2=UNSET, ur3=UNSET)

################### Symmetry
#--------------------------------------------------------------------------
mdb.models['Model-1'].rootAssembly.Set(faces=
    mdb.models['Model-1'].rootAssembly.instances['CrownFix-1'].faces.getSequenceFromMask(
    mask=('[#23 ]', ), )+\
    mdb.models['Model-1'].rootAssembly.instances['HalfStraight-1'].faces.getSequenceFromMask(
    mask=('[#2 ]', ), )+\
    mdb.models['Model-1'].rootAssembly.instances['HalfStraight-2'].faces.getSequenceFromMask(
    mask=('[#2 ]', ), )+\
    mdb.models['Model-1'].rootAssembly.instances['CrownLink1-1'].faces.getSequenceFromMask(
```

```
    mask=('[#2 ]', ), )+\
    mdb.models['Model-1'].rootAssembly.instances['crownfull-1'].faces.getSequenceFromMask(
    mask=('[#22 ]', ), )+\
    mdb.models['Model-1'].rootAssembly.instances['crownfull-End-4'].faces.getSequenceFromMask(
    mask=('[#22 ]', ), )+\
    mdb.models['Model-1'].rootAssembly.instances['Crown-End-5'].faces.getSequenceFromMask(
    mask=('[#2 ]', ), )+\
    mdb.models['Model-1'].rootAssembly.instances['HalfStraight-3'].faces.getSequenceFromMask(
    mask=('[#2 ]', ), )+\
    mdb.models['Model-1'].rootAssembly.instances['HalfStraight-4'].faces.getSequenceFromMask(
    mask=('[#2 ]', ), )+\
    mdb.models['Model-1'].rootAssembly.instances['crownfull-End-1'].faces.getSequenceFromMask(
    mask=('[#22 ]', ), )+\
    mdb.models['Model-1'].rootAssembly.instances['Crown-End-4'].faces.getSequenceFromMask(
    mask=('[#2 ]', ), )+\
    mdb.models['Model-1'].rootAssembly.instances['Crown-End-1'].faces.getSequenceFromMask(
    mask=('[#2 ]', ), )+\
    mdb.models['Model-1'].rootAssembly.instances['crownfull-End-2'].faces.getSequenceFromMask(
    mask=('[#22 ]', ), )+\
    mdb.models['Model-1'].rootAssembly.instances['HalfStraight-End-1'].faces.getSequenceFromMask(
    mask=('[#2 ]', ), )+\
    mdb.models['Model-1'].rootAssembly.instances['HalfStraight-End-2'].faces.getSequenceFromMask(
    mask=('[#2 ]', ), )+\
    mdb.models['Model-1'].rootAssembly.instances['Crown-End-2'].faces.getSequenceFromMask(
    mask=('[#2 ]', ), )+\
    mdb.models['Model-1'].rootAssembly.instances['crownfull-End-3'].faces.getSequenceFromMask(
    mask=('[#22 ]', ), )+\
    mdb.models['Model-1'].rootAssembly.instances['crownfull-End-5'].faces.getSequenceFromMask(
    mask=('[#22 ]', ), )+\
    mdb.models['Model-1'].rootAssembly.instances['Crown-End-3'].faces.getSequenceFromMask(
    mask=('[#2 ]', ), )+\
    mdb.models['Model-1'].rootAssembly.instances['HalfStraight-End-4'].faces.getSequenceFromMask(
    mask=('[#2 ]', ), )+\
    mdb.models['Model-1'].rootAssembly.instances['HalfStraight-End-3'].faces.getSequenceFromMask(
    mask=('[#2 ]', ), )+\
    mdb.models['Model-1'].rootAssembly.instances['Crown-End-6'].faces.getSequenceFromMask(
    mask=('[#23 ]', ), ), name='Set-5')
mdb.models['Model-1'].YsymmBC(createStepName='Initial', localCsys=None, name=
    'Symmetry', region=mdb.models['Model-1'].rootAssembly.sets['Set-5'])

############################### Partition for history node output
#-------------------------------------------------------------------------
mdb.models['Model-1'].parts['CrownLink1'].PartitionEdgeByPoint(edge=
    mdb.models['Model-1'].parts['CrownLink1'].edges[1], point=
    mdb.models['Model-1'].parts['CrownLink1'].InterestingPoint(
    mdb.models['Model-1'].parts['CrownLink1'].edges[1], MIDDLE))
#-------------------------------------------------------------------------
mdb.models['Model-1'].parts['CrownFix'].PartitionEdgeByPoint(edge=
    mdb.models['Model-1'].parts['CrownFix'].edges[12], point=
    mdb.models['Model-1'].parts['CrownFix'].InterestingPoint(
    mdb.models['Model-1'].parts['CrownFix'].edges[12], MIDDLE))
#-------------------------------------------------------------------------


################## Create Clamped boundary conditions
#-------------------------------------------------------------------------
mdb.models['Model-1'].ConstrainedSketch(name='__profile__', sheetSize=200.0)
mdb.models['Model-1'].sketches['__profile__'].Arc3Points(point1=(-0.5714285714*diameter, 0.0),
    point2=(0.1357142857*diameter, 0.0), point3=(-0.2179695783*diameter, 0.1465969413*diameter))
mdb.models['Model-1'].Part(dimensionality=THREE_D, name='shell', type=
    DEFORMABLE_BODY)
mdb.models['Model-1'].parts['shell'].BaseShellExtrude(depth=Straight, sketch=
    mdb.models['Model-1'].sketches['__profile__'])
del mdb.models['Model-1'].sketches['__profile__']
#-------------------------------------------------------------------------
######### Assign section
mdb.models['Model-1'].HomogeneousShellSection(idealization=NO_IDEALIZATION,
    integrationRule=SIMPSON, material='ElasticPlastic', name='Section-2',
    numIntPts=5, poissonDefinition=DEFAULT, preIntegrate=OFF, temperature=
    GRADIENT, thickness=10.0, thicknessField='', thicknessModulus=None,
    thicknessType=UNIFORM, useDensity=OFF)
mdb.models['Model-1'].parts['shell'].Set(faces=
    mdb.models['Model-1'].parts['shell'].faces.getSequenceFromMask(('[#1 ]', ),
    ), name='Set-1')
mdb.models['Model-1'].parts['shell'].SectionAssignment(offset=0.0, offsetField=
    '', offsetType=MIDDLE_SURFACE, region=
    mdb.models['Model-1'].parts['shell'].sets['Set-1'], sectionName='Section-2'
    , thicknessAssignment=FROM_SECTION)
#-------------------------------------------------------------------------
######## Move
mdb.models['Model-1'].rootAssembly.Instance(dependent=ON, name='shell-1', part=
    mdb.models['Model-1'].parts['shell'])

mdb.models['Model-1'].rootAssembly.rotate(angle=270.0, axisDirection=(0.0, 0.0,
    1.0), axisPoint=(0.0, 0.0, 0.0), instanceList=('shell-1', ))
mdb.models['Model-1'].rootAssembly.translate(instanceList=('shell-1', ),
    vector=(1.528403046*diameter, -0.2178571429*diameter, -2.65*diameter))
mdb.models['Model-1'].rootAssembly.Instance(dependent=ON, name='shell-2', part=
```

```
    mdb.models['Model-1'].parts['shell'])
mdb.models['Model-1'].rootAssembly.rotate(angle=90.0, axisDirection=(0.0, 0.0,
    1.0), axisPoint=(0.0, 0.0, 0.0), instanceList=('shell-2', ))
mdb.models['Model-1'].rootAssembly.translate(instanceList=('shell-2', ),
    vector=(-1.528403046*diameter, 0.2178571429*diameter, -2.65*diameter))
#-------------------------------------------------------------------------
################ Interaction
mdb.models['Model-1'].rootAssembly.Surface(name='m_Surf-59', side1Faces=
    mdb.models['Model-1'].rootAssembly.instances['shell-1'].faces.getSequenceFromMask(
    ('[#1 ]', ), ))
mdb.models['Model-1'].rootAssembly.Surface(name='s_Surf-59', side1Faces=
    mdb.models['Model-1'].rootAssembly.instances['HalfStraight-2'].faces.getSequenceFromMask(
    ('[#1 ]', ), ))
mdb.models['Model-1'].SurfaceToSurfaceContactStd(adjustMethod=OVERCLOSED,
    clearanceRegion=None, createStepName='Proofload', datumAxis=None,
    initialClearance=OMIT, interactionProperty='IntProp-1', master=
    mdb.models['Model-1'].rootAssembly.surfaces['m_Surf-59'], name='Clamp1',
    slave=mdb.models['Model-1'].rootAssembly.surfaces['s_Surf-59'], sliding=
    FINITE, thickness=ON, tied=OFF)
mdb.models['Model-1'].rootAssembly.Surface(name='m_Surf-61', side1Faces=
    mdb.models['Model-1'].rootAssembly.instances['shell-2'].faces.getSequenceFromMask(
    ('[#1 ]', ), ))
mdb.models['Model-1'].rootAssembly.Surface(name='s_Surf-61', side1Faces=
    mdb.models['Model-1'].rootAssembly.instances['HalfStraight-1'].faces.getSequenceFromMask(
    ('[#1 ]', ), ))
mdb.models['Model-1'].SurfaceToSurfaceContactStd(adjustMethod=OVERCLOSED,
    clearanceRegion=None, createStepName='Proofload', datumAxis=None,
    initialClearance=OMIT, interactionProperty='IntProp-1', master=
    mdb.models['Model-1'].rootAssembly.surfaces['m_Surf-61'], name='Clamp2',
    slave=mdb.models['Model-1'].rootAssembly.surfaces['s_Surf-61'], sliding=
    FINITE, thickness=ON, tied=OFF)

mdb.models['Model-1'].rootAssembly.ReferencePoint(point=
    mdb.models['Model-1'].rootAssembly.instances['HalfStraight-2'].InterestingPoint(
    mdb.models['Model-1'].rootAssembly.instances['HalfStraight-2'].edges[1],
    MIDDLE))
mdb.models['Model-1'].rootAssembly.ReferencePoint(point=
    mdb.models['Model-1'].rootAssembly.instances['HalfStraight-1'].InterestingPoint(
    mdb.models['Model-1'].rootAssembly.instances['HalfStraight-1'].edges[3],
    MIDDLE))

mdb.models['Model-1'].rootAssembly.Set(name='Set-9', referencePoints=(
    mdb.models['Model-1'].rootAssembly.referencePoints[121],
    mdb.models['Model-1'].rootAssembly.referencePoints[122]))
mdb.models['Model-1'].DisplacementBC(amplitude=UNSET, createStepName=
    'Proofload', distributionType=UNIFORM, fieldName='', fixed=OFF, localCsys=
    None, name='Clamping', region=
    mdb.models['Model-1'].rootAssembly.sets['Set-9'], u1=UNSET, u2=0.0, u3=0.0,
    ur1=0.0, ur2=0.0, ur3=0.0)
mdb.models['Model-1'].rootAssembly.Set(name='Set-10', referencePoints=(
    mdb.models['Model-1'].rootAssembly.referencePoints[121], ))
mdb.models['Model-1'].ConcentratedForce(cf1=-10.0, createStepName='Proofload',
    distributionType=UNIFORM, field='', localCsys=None, name='Clamp1', region=
    mdb.models['Model-1'].rootAssembly.sets['Set-10'])
mdb.models['Model-1'].loads['Clamp1'].deactivate('Displacement')
mdb.models['Model-1'].rootAssembly.Set(name='Set-11', referencePoints=(
    mdb.models['Model-1'].rootAssembly.referencePoints[122], ))
mdb.models['Model-1'].ConcentratedForce(cf1=10.0, createStepName='Proofload',
    distributionType=UNIFORM, field='', localCsys=None, name='Clamp2', region=
    mdb.models['Model-1'].rootAssembly.sets['Set-11'])
mdb.models['Model-1'].loads['Clamp2'].deactivate('Displacement')
mdb.models['Model-1'].boundaryConditions['Clamping'].deactivate('Displacement')
mdb.models['Model-1'].rootAssembly.Set(name='Set-12', referencePoints=(
    mdb.models['Model-1'].rootAssembly.referencePoints[121],
    mdb.models['Model-1'].rootAssembly.referencePoints[122]))
mdb.models['Model-1'].DisplacementBC(amplitude=UNSET, createStepName=
    'Displacement', distributionType=UNIFORM, fieldName='', fixed=ON,
    localCsys=None, name='BC-6', region=
    mdb.models['Model-1'].rootAssembly.sets['Set-12'], u1=SET, u2=SET, u3=SET,
    ur1=SET, ur2=SET, ur3=SET)
mdb.models['Model-1'].boundaryConditions.changeKey(fromName='BC-6', toName=
    'ClampFix')
#-------------------------------------------------------------------------
############ Mesh clamped parts
mdb.models['Model-1'].parts['shell'].seedPart(deviationFactor=0.1,
    minSizeFactor=0.1, size=25.0)
mdb.models['Model-1'].parts['shell'].generateMesh()
mdb.models['Model-1'].rootAssembly.regenerate()
#-------------------------------------------------------------------------
######## Set as rigid bodies
mdb.models['Model-1'].rootAssembly.Set(faces=
    mdb.models['Model-1'].rootAssembly.instances['shell-1'].faces.getSequenceFromMask(
    ('[#1 ]', ), ), name='b_Set-8')
mdb.models['Model-1'].RigidBody(bodyRegion=
    mdb.models['Model-1'].rootAssembly.sets['b_Set-8'], name='Clamp1',
    refPointRegion=Region(referencePoints=(
    mdb.models['Model-1'].rootAssembly.referencePoints[121], )))
mdb.models['Model-1'].rootAssembly.Set(faces=
```

```
    mdb.models['Model-1'].rootAssembly.instances['shell-2'].faces.getSequenceFromMask(
    ('[#1 ]', ), ), name='b_Set-10')
mdb.models['Model-1'].RigidBody(bodyRegion=
    mdb.models['Model-1'].rootAssembly.sets['b_Set-10'], name='Clamp2',
    refPointRegion=Region(referencePoints=(
    mdb.models['Model-1'].rootAssembly.referencePoints[122], )))
mdb.models['Model-1'].rootAssembly.regenerate()

##########################################################################
############### TENSILE LOAD ##############################################

############# MPC point
#--------------------------------------------------------------------------
mdb.models['Model-1'].rootAssembly.ReferencePoint(point=
    mdb.models['Model-1'].rootAssembly.instances['Crown-End-6'].InterestingPoint(
    mdb.models['Model-1'].rootAssembly.instances['Crown-End-6'].edges[1],
    CENTER))
############# MPC Interaction Constraint
#--------------------------------------------------------------------------
mdb.models['Model-1'].rootAssembly.Set(name='m_Set-11', referencePoints=(
    mdb.models['Model-1'].rootAssembly.referencePoints[131], ))
mdb.models['Model-1'].rootAssembly.Set(faces=
    mdb.models['Model-1'].rootAssembly.instances['Crown-End-6'].faces.getSequenceFromMask(
    ('[#1 ]', ), ), name='s_Set-11')
mdb.models['Model-1'].MultipointConstraint(controlPoint=
    mdb.models['Model-1'].rootAssembly.sets['m_Set-11'], csys=None, mpcType=
    BEAM_MPC, name='MPC-Load', surface=
    mdb.models['Model-1'].rootAssembly.sets['s_Set-11'], userMode=DOF_MODE_MPC,
    userType=0)

############ Tension Load
#--------------------------------------------------------------------------
mdb.models['Model-1'].rootAssembly.Set(name='Set-20', referencePoints=(
    mdb.models['Model-1'].rootAssembly.referencePoints[131], ))
mdb.models['Model-1'].ConcentratedForce(cf3=-ProofLoad, createStepName=
    'Proofload', distributionType=UNIFORM, field='', follower=ON, localCsys=
    None, name='Tension', region=
    mdb.models['Model-1'].rootAssembly.sets['Set-20'])
mdb.models['Model-1'].loads['Tension'].setValuesInStep(cf3=-Pretension,
    stepName='WorkLoad')

##########################################################################
############### MESH ######################################################
#--------------------------------------------------------------------------
################################################ FULL STRAIGHT

mdb.models['Model-1'].parts['FullStraight'].seedPart(deviationFactor=0.1,
    minSizeFactor=0.1, size=20.0)
mdb.models['Model-1'].parts['FullStraight'].generateMesh()

################################################ CROWN Link 1
#--------------------------------------------------------------------------
mdb.models['Model-1'].parts['CrownLink1'].seedPart(deviationFactor=0.1,
    minSizeFactor=0.1, size=17.0)

mdb.models['Model-1'].parts['CrownLink1'].seedEdgeByNumber(constraint=FINER,
    edges=mdb.models['Model-1'].parts['CrownLink1'].edges.getSequenceFromMask((
    '[#60 ]', ), ), number=16)
mdb.models['Model-1'].parts['CrownLink1'].seedEdgeByNumber(constraint=FINER,
    edges=mdb.models['Model-1'].parts['CrownLink1'].edges.getSequenceFromMask((
    '[#9 ]', ), ), number=30)
mdb.models['Model-1'].parts['CrownLink1'].seedEdgeByNumber(constraint=FINER,
    edges=mdb.models['Model-1'].parts['CrownLink1'].edges.getSequenceFromMask((
    '[#10 ]', ), ), number=25)

mdb.models['Model-1'].parts['CrownLink1'].generateMesh()

################################################ HALF STRAIGHT
#--------------------------------------------------------------------------
mdb.models['Model-1'].parts['HalfStraight'].seedPart(deviationFactor=0.1,
    minSizeFactor=0.1, size=35.0)
mdb.models['Model-1'].parts['HalfStraight'].seedEdgeByNumber(constraint=FINER,
    edges=
    mdb.models['Model-1'].parts['HalfStraight'].edges.getSequenceFromMask((
    '[#1 ]', ), ), number=14)
mdb.models['Model-1'].parts['HalfStraight'].seedEdgeByNumber(constraint=FINER,
    edges=
    mdb.models['Model-1'].parts['HalfStraight'].edges.getSequenceFromMask((
    '[#2 ]', ), ), number=14)
mdb.models['Model-1'].parts['HalfStraight'].seedEdgeByNumber(constraint=FINER,
    edges=
    mdb.models['Model-1'].parts['HalfStraight'].edges.getSequenceFromMask((
    '[#10 ]', ), ), number=8)
mdb.models['Model-1'].parts['HalfStraight'].generateMesh()

################################################ FIXED CROWN
#--------------------------------------------------------------------------
mdb.models['Model-1'].parts['CrownFix'].seedPart(deviationFactor=0.1,
```

```
    minSizeFactor=0.1, size=40.0)

mdb.models['Model-1'].parts['CrownFix'].seedEdgeByNumber(constraint=FINER,
    edges=mdb.models['Model-1'].parts['CrownFix'].edges.getSequenceFromMask((
    '[#828 ]', ), ), number=16)
mdb.models['Model-1'].parts['CrownFix'].seedEdgeByNumber(constraint=FINER,
    edges=mdb.models['Model-1'].parts['CrownFix'].edges.getSequenceFromMask((
    '[#44 ]', ), ), number=16)
mdb.models['Model-1'].parts['CrownFix'].seedEdgeByNumber(constraint=FINER,
    edges=mdb.models['Model-1'].parts['CrownFix'].edges.getSequenceFromMask((
    '[#4200 ]', ), ), number=10)
mdb.models['Model-1'].parts['CrownFix'].seedEdgeByNumber(constraint=FINER,
    edges=mdb.models['Model-1'].parts['CrownFix'].edges.getSequenceFromMask((
    '[#500 ]', ), ), number=16)
mdb.models['Model-1'].parts['CrownFix'].seedEdgeByNumber(constraint=FINER,
    edges=mdb.models['Model-1'].parts['CrownFix'].edges.getSequenceFromMask((
    '[#82 ]', ), ), number=20)
mdb.models['Model-1'].parts['CrownFix'].seedEdgeByNumber(constraint=FINER,
    edges=mdb.models['Model-1'].parts['CrownFix'].edges.getSequenceFromMask((
    '[#3000 ]', ), ), number=2)
mdb.models['Model-1'].parts['CrownFix'].generateMesh()

################################################### Full Crown
#--------------------------------------------------------------------
mdb.models['Model-1'].parts['crownfull'].seedPart(deviationFactor=0.1,
    minSizeFactor=0.1, size=41.0)
mdb.models['Model-1'].parts['crownfull'].seedEdgeByNumber(constraint=FINER,
    edges=mdb.models['Model-1'].parts['crownfull'].edges.getSequenceFromMask((
    '[#50 ]', ), ), number=17)
mdb.models['Model-1'].parts['crownfull'].seedEdgeByNumber(constraint=FINER,
    edges=mdb.models['Model-1'].parts['crownfull'].edges.getSequenceFromMask((
    '[#1 ]', ), ), number=17)
mdb.models['Model-1'].parts['crownfull'].seedEdgeByBias(biasMethod=SINGLE,
    constraint=FINER, end2Edges=
    mdb.models['Model-1'].parts['crownfull'].edges.getSequenceFromMask((
    '[#8 ]', ), ), maxSize=17.0, minSize=13.0)

mdb.models['Model-1'].parts['crownfull'].generateMesh()

################################################### CROWN END
#--------------------------------------------------------------------
mdb.models['Model-1'].parts['Crown-End'].seedPart(deviationFactor=0.1,
    minSizeFactor=0.1, size=40.0)
mdb.models['Model-1'].parts['Crown-End'].seedEdgeByNumber(constraint=FINER,
    edges=mdb.models['Model-1'].parts['Crown-End'].edges.getSequenceFromMask((
    '[#30 ]', ), ), number=12)
mdb.models['Model-1'].parts['Crown-End'].seedEdgeByNumber(constraint=FINER,
    edges=mdb.models['Model-1'].parts['Crown-End'].edges.getSequenceFromMask((
    '[#5 ]', ), ), number=16)
mdb.models['Model-1'].parts['Crown-End'].seedEdgeByNumber(constraint=FINER,
    edges=mdb.models['Model-1'].parts['Crown-End'].edges.getSequenceFromMask((
    '[#8 ]', ), ), number=20)
mdb.models['Model-1'].parts['Crown-End'].generateMesh()

############################################### FULL CROWN END
#--------------------------------------------------------------------
mdb.models['Model-1'].parts['crownfull-End'].seedPart(deviationFactor=0.1,
    minSizeFactor=0.1, size=40.0)
mdb.models['Model-1'].parts['crownfull-End'].seedEdgeByNumber(constraint=FINER,
    edges=
    mdb.models['Model-1'].parts['crownfull-End'].edges.getSequenceFromMask((
    '[#2 ]', ), ), number=16)
mdb.models['Model-1'].parts['crownfull-End'].seedEdgeByNumber(constraint=FINER,
    edges=
    mdb.models['Model-1'].parts['crownfull-End'].edges.getSequenceFromMask((
    '[#50 ]', ), ), number=16)
mdb.models['Model-1'].parts['crownfull-End'].seedEdgeByNumber(constraint=FINER,
    edges=
    mdb.models['Model-1'].parts['crownfull-End'].edges.getSequenceFromMask((
    '[#1 ]', ), ), number=16)
mdb.models['Model-1'].parts['crownfull-End'].generateMesh()

############################################## FULL STRAIGHT END
#--------------------------------------------------------------------
mdb.models['Model-1'].parts['FullStraight-End'].seedPart(deviationFactor=0.1,
    minSizeFactor=0.1, size=35.0)
mdb.models['Model-1'].parts['FullStraight-End'].seedEdgeByNumber(constraint=
    FINER, edges=
    mdb.models['Model-1'].parts['FullStraight-End'].edges.getSequenceFromMask((
    '[#a0 ]', ), ), number=10)
mdb.models['Model-1'].parts['FullStraight-End'].generateMesh()

############################################### HALF STRAIGHT END
#--------------------------------------------------------------------
mdb.models['Model-1'].parts['HalfStraight-End'].seedPart(deviationFactor=0.1,
    minSizeFactor=0.1, size=35.0)
mdb.models['Model-1'].parts['HalfStraight-End'].generateMesh()
mdb.models['Model-1'].rootAssembly.regenerate()
```

```
##########################################################################
############### LOAD EDIT ################################################

##### Deactivate Clamp Forces
mdb.models['Model-1'].loads['Clamp1'].deactivate('Displacement')
mdb.models['Model-1'].loads['Clamp2'].deactivate('Displacement')
mdb.models['Model-1'].boundaryConditions['Clamping'].deactivate('Displacement')
##### Fix Clamps for constrained BC
mdb.models['Model-1'].rootAssembly.Set(name='Set-15', referencePoints=(
    mdb.models['Model-1'].rootAssembly.referencePoints[121],
    mdb.models['Model-1'].rootAssembly.referencePoints[122]))
mdb.models['Model-1'].DisplacementBC(amplitude=UNSET, createStepName=
    'Displacement', distributionType=UNIFORM, fieldName='', fixed=ON,
    localCsys=None, name='FixBC', region=
    mdb.models['Model-1'].rootAssembly.sets['Set-15'], u1=SET, u2=SET, u3=SET,
    ur1=SET, ur2=SET, ur3=SET)

##########################################################################
############### DISPLACEMENT #############################################

mdb.models['Model-1'].rootAssembly.Set(name='Set-16', referencePoints=(
    mdb.models['Model-1'].rootAssembly.referencePoints[131], ))
mdb.models['Model-1'].DisplacementBC(amplitude=UNSET, createStepName='Initial',
    distributionType=UNIFORM, fieldName='', localCsys=None, name='Displacement'
    , region=mdb.models['Model-1'].rootAssembly.sets['Set-16'], u1=SET, u2=
    UNSET, u3=UNSET, ur1=UNSET, ur2=UNSET, ur3=UNSET)
mdb.models['Model-1'].boundaryConditions['Displacement'].setValuesInStep(
    stepName='Displacement', u1=Disp)

##########################################################################
############### FRICTION OPERATIVE ENVIRONMENT ###########################
#--------------------------------------------------------------------------
mdb.models['Model-1'].ContactProperty('OpEnvironment')
mdb.models['Model-1'].interactionProperties['OpEnvironment'].TangentialBehavior(
    dependencies=0, directionality=ISOTROPIC, elasticSlipStiffness=None,
    formulation=PENALTY, fraction=0.005, maximumElasticSlip=FRACTION,
    pressureDependency=OFF, shearStressLimit=None, slipRateDependency=OFF,
    table=((FrictionCoeff, ), ), temperatureDependency=OFF)
mdb.models['Model-1'].interactionProperties['OpEnvironment'].tangentialBehavior.setValues(
    dependencies=0, directionality=ISOTROPIC, elasticSlipStiffness=None,
    formulation=PENALTY, fraction=0.005, maximumElasticSlip=FRACTION,
    pressureDependency=OFF, shearStressLimit=None, slipRateDependency=OFF,
    table=((FrictionCoeff, ), ), temperatureDependency=OFF)
mdb.models['Model-1'].interactionProperties['OpEnvironment'].NormalBehavior(
    allowSeparation=ON, constraintEnforcementMethod=DEFAULT,
    pressureOverclosure=HARD)
mdb.models['Model-1'].interactions['Int-1'].setValuesInStep(
    interactionProperty='OpEnvironment', stepName='Displacement')

##########################################################################
############### HISTORY OUTPUT ###########################################
#--------------------------------------------------------------------------
mdb.models['Model-1'].rootAssembly.Set(name='NodeDisplacementOutput', nodes=
    mdb.models['Model-1'].rootAssembly.instances['crownfull-1'].nodes.getSequenceFromMask(
    mask=('[#4 #0:2 #100 ]', ), )+\
    mdb.models['Model-1'].rootAssembly.instances['crownfull-End-4'].nodes.getSequenceFromMask(
    mask=('[#0:2 #80 ]', ), ))
#--------------------------------------------------------------------------
mdb.models['Model-1'].HistoryOutputRequest(createStepName='Proofload', name=
    'NodeDisplacement', rebar=EXCLUDE, region=
    mdb.models['Model-1'].rootAssembly.sets['NodeDisplacementOutput'],
    sectionPoints=DEFAULT, variables=('U1', 'U2', 'U3'))
#--------------------------------------------------------------------------
mdb.models['Model-1'].rootAssembly.Set(elements=
    mdb.models['Model-1'].rootAssembly.instances['FullStraight-1'].elements.getSequenceFromMask(
    mask=('[#0:15 #20000000 #0:33 #10000 ]', ), ), name='ElementStressOutput')
#--------------------------------------------------------------------------
mdb.models['Model-1'].HistoryOutputRequest(createStepName='Proofload', name=
    'ElementHistory', rebar=EXCLUDE, region=
    mdb.models['Model-1'].rootAssembly.sets['ElementStressOutput'], sectionPoints=DEFAULT,
    variables=('S11', 'S22', 'S33', 'S12', 'S13', 'S23', 'SP', 'TRESC',
    'PRESS', 'INV3', 'MISES', 'EE11', 'EE22', 'EE33', 'EE12', 'EE13', 'EE23',
    'EEP', 'IE11', 'IE22', 'IE33', 'IE12', 'IE13', 'IE23', 'IEP'))

##########################################################################
############### ADDITIONAL CONTACT PAIRS #################################

# There were some problems when creating the script, generating unconnected
# regions. Some of these can be avoided by using the manual command “Find contact pairs”.
```